Politecnico di Torino

Master of Science in Energy and Nuclear Engineering
Academic Year 2023/2024
Session Degree December 2024

Photovoltaic energy analysis using satellite data and nearly weather station

Supervisors:
Prof. Filippo Spertino
Ing. Gabriele Malgaroli
Prof. José Vicente Muñoz Diez
Prof. Slawomir Gulkowski

Candidate:
Francesco Ninni

Acknowledgements

Prima di immergermi nella trattazione, voglio dedicare qualche riga a tutte le persone che mi hanno accompagnato in questo viaggio, sia personale che professionale. Se oggi sono qui, lo devo anche a voi.

Un grazie di cuore al mio relatore, il Professor Filippo Spertino, per avermi dato l'opportunità di lavorare su una tesi così stimolante e per avermi guidato nel mondo dell'energia fotovoltaica. Le nozioni apprese nei suoi corsi e durante la stesura della tesi non sono state solo utili, ma mi hanno aperto nuovi orizzonti in un campo che mi appassiona profondamente.

Un ringraziamento speciale va a Gabriele, il mio correlatore. È stata una fortuna enorme averti al mio fianco durante questo percorso. Lavorare con te è stato un piacere immenso: grazie per tutte le ore passate in videochiamata, io dalla Spagna e tu dall'Italia, a confrontarci sulle soluzioni migliori e sui prossimi passi da seguire. La tua pazienza, umiltà e competenza sono qualità rare, e auguro a chiunque di avere un correlatore come te.

I would also like to thank my Spanish supervisor, Vicente. Deciding to come to Jaén, Spain, to write my thesis was a choice I would make a thousand times over. Thank you for your incredible hospitality, which made me feel at home from the very first moment. I am truly grateful for all the knowledge you have shared with me and for teaching me that it's possible to work with a smile. You've always been there for me and have come to my aid during the most difficult moments. ¡Ya echo de menos esas tostadas con café con leche de cada mañana!

A big thank you also goes to Professor Slawomir Gulkowski for assisting me with sending the necessary data. I hope this work can be useful for some future study regarding the system.

Un capitolo a parte lo meritano due persone speciali: mamma e papà. Se sono arrivato fin qui, è solo grazie a voi. Siete stati il mio supporto, il mio faro, la mia certezza in ogni momento. Avete sempre creduto in me, persino quando io stesso facevo fatica a farlo, e mi avete dato la forza per superare le difficoltà. La vostra perseveranza e la vostra forza nel superare le difficoltà della vita sono qualcosa di enorme, e vi ringrazio per avermi insegnato ad andare sempre avanti, a capire che, in un modo o nell'altro, c'è sempre una soluzione alle cose e che non bisogna mai abbattersi. Grazie per avermi permesso di vivere tutte queste esperienze, di partire

per nuove avventure e di scoprire il mondo. Fare i genitori non è sicuramente facile, ma voi ci riuscite in un modo straordinario.

Grazie a mia sorella Wawa, la mia spalla nei momenti difficili, la certezza che c'è sempre qualcuno al mio fianco su cui posso contare. Grazie anche ad Andre e grazie a mio nipote Enni per essere il bambino più dolce e bello che io conosca.

Un pensiero speciale va alle mie nonne. Grazie a Nonna Francesca, che anche quando non capivo nulla di quello che studiavo, mi diceva convinta che fossi "Einstein". E grazie a Nonna Maria, che con il suo sorriso contagioso mi ha insegnato ad affrontare la vita con leggerezza e serenità.

Un grande abbraccio va alla mia famiglia allargata: zii, cugini e tutti i 3000 membri che rendono unica la nostra grande famiglia. Grazie per esserci sempre stati nei momenti importanti e per dimostrare che, nonostante tutto, la famiglia è il nostro porto sicuro.

E ora, gli amici.

Un grazie di cuore ai "Buchi di c**o" di Cambiano. Siamo cresciuti insieme, ognuno seguendo strade diverse, ma sempre con un legame forte che ci tiene uniti. Grazie per tutte le risate, le discussioni, i consigli (anche quando poi facevamo il contrario), le ore in aula studio, i viaggi e le vacanze. Spero che, qualsiasi cosa ci riservi il futuro, questo gruppo rimanga così com'è. Un altro grazie enorme va al gruppo "Berlino Flex". Ci tenevo a dirvi che siete veramente un gruppo di criminali... e per favore, rimanete sempre così. Fin dal primo viaggio insieme, nato quasi per caso, abbiamo trovato un'intesa spettacolare che voglio che vada avanti per sempre. Grazie per tutti i viaggi, le serate, le giornate di studio, le patenti, le risate e per la vostra ospitalità che vi contraddistingue da sempre. Grazie a Nanzo, che non appartiene a nessuno di questi gruppi ma che per me è sempre stata una costante, fin dai tempi delle superiori. Sono certo che continueremo a condividere tanto anche in futuro. Un grazie speciale agli amici di Jaén: questa esperienza resterà per sempre nel cuore. E a tutti coloro non nominati, ma con cui ho condiviso momenti indimenticabili, grazie di cuore.

E, infine, un grazie a me stesso. Non per aver fatto qualcosa di straordinario, ma per aver imparato a superare i momenti di difficoltà e per non aver mai mollato, anche quando sembrava più facile farlo. Sono grato per le esperienze vissute, per le persone che ho incontrato lungo il cammino e per tutto quello che ho imparato, un passo alla volta.

Abstract

This master thesis, authored by the undersigned, is a collaborative effort involving Politecnico di Torino, Universidad de Jaén, and Lublin University of Technology. The study focuses on a 1.4 MWp photovoltaic (PV) plant situated near Bordziłówka, Poland, approximately 77 km from Lublin. Installed in 2014, the plant faces challenging meteorological conditions, including frequent snowfalls and other extreme conditions which lead to inaccurate data readings.

The aim of this study is to find an alternative method to evaluate whether the energy production of the plant aligns with predictions based on solar irradiance and temperature conditions. For this comparison, data measured from the plant (such as solar irradiance, temperature, and instantaneous power) will be analyzed and compared to data from a weather station located in Włodawa, approximately 44.8 km away. Additionally, this study will incorporate datasets from PVGIS and SOLCAST to fill gaps in the weather station and PV plant data. PVGIS provides validated solar radiation and temperature data specific to the geographic location, while SOLCAST offers high-resolution solar forecasting data. These datasets enhance accuracy and facilitate comprehensive comparisons.

The research is structured around two primary objectives. The first involves an in-depth study of various models for transposing solar irradiance measured on a horizontal plane to an inclined plane, allowing for a more accurate assessment of the potential energy production given the orientation of the plant's panels. The second objective, building on the transposed irradiance data, applies further models to predict energy production by comparing the predicted DC energy output with the actual DC production recorded at the PV plant. Through this comparison, the study identifies discrepancies, evaluates the plant's performance under varying meteorological conditions, and assesses the accuracy of using this weather station as a reliable reference for estimating energy production.

Contents

List of Figures

List of Tables

Chapter 1

1 Overview of photovoltaic technology

1.1 Photovoltaic Technology

1.1.1 Solar radiation

Only a small portion of the energy that the Sun emits onto Earth is visible to us on a daily basis. As can be seen in the image below with the "VIS" designation, visible light, which is a tiny portion of electromagnetic radiation, is produced by sunlight within a specific wavelength range.

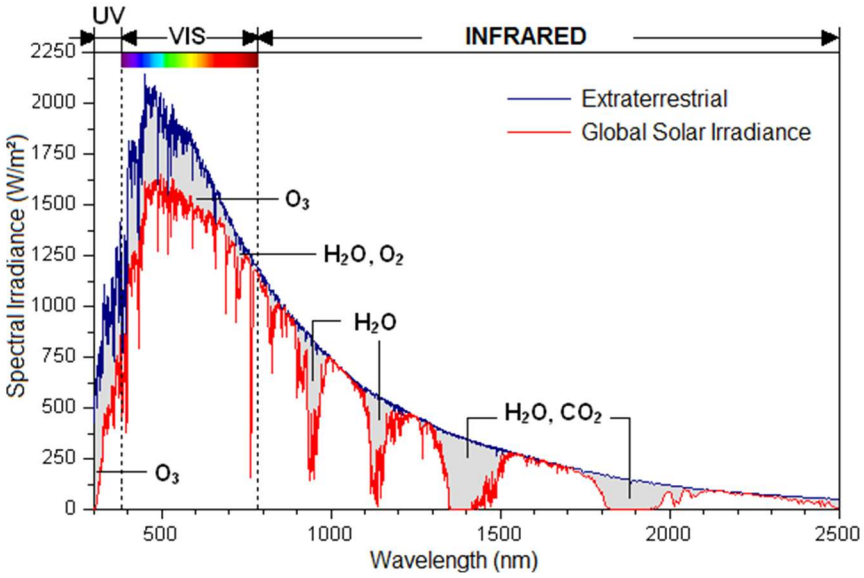

Figure 1-1: Solar spectrum [1].

In more detail, the photoelectric effect—the release of electrons from specific metals and semiconductors when struck by light—has allowed scientists to determine the values of the indistinguishable energy elements that make up the total energy of light. This has been made possible by the experiments conducted by Planck and Einstein.

The wavelength (λ), or more accurately its energy (E), is the primary characteristic that defines a photon. The following equation establishes the relationship between these two:

$$E_{ph} = {}^{hc}/_{\lambda} \tag{1-1}$$

Where:

- h = 6.626 x 10^{-34} $\frac{m^2 \cdot kg}{s}$ - Planck's constant.
- c = 2.998 x 10^8 m/s – speed of light.
- λ – wavelength [μs].

Instead of using Joules [J], electron-Volts [eV] are frequently used to indicate energy when working with particles such as protons or electrons. Because of this, the preceding equation can be expressed as follows:

$$E_{ph} = {}^{1.24}/_{\lambda} \tag{1-2}$$

Where *h* and *c* are multiplied and their value is converted to [eV] to get 1.24. Understanding the relationships between solar energy, solar cells, and the ensuing energy conversion process is made easier with the help of this formulation. The photon flux, which is defined as follows, is a second quantity that is used to calculate the generated electrons and, consequently, the current generated from a solar cell.

$$\Phi = {}^{\#photons}/_{sec \cdot m^2} \tag{1-3}$$

The power density of photons at a specific wavelength can be estimated using these two equations; this is more helpful when assessing the productivity of photovoltaic cells, which is measured in W/m^2[2].

When analysing how incident sunlight interacts with a photovoltaic converter, it is important to take into account a few critical features of the incident solar energy. These are the following:

- The incident light's spectral content.
- The Sun's radiant power density.
- The angle at which a photovoltaic module is struck by incident solar radiation.
- The Sun's radiant energy on a specific surface throughout the course of a day or year.

Furthermore, as was said at the beginning of this chapter, the radiation at Earth's surface fluctuates because of the following factors:

- Atmospheric effects include absorption, scattering, and reflection.
- Variations in solar radiation impinge on Earth's atmosphere.
- Location's latitude.
- Variations in the atmosphere locally.
- The time of year and the season.

More specifically, irradiance G $[W/m^2]$ is the total power received by a unitary area from a radiating source. A portion of the solar radiation that enters the Earth's atmosphere is either absorbed by clouds, carbon dioxide, ozone, and air molecules (diffused irradiance) or lost to scattering and reflection in space. On the other hand, direct irradiance refers to sunlight that reaches the Earth's surface without being scattered. The final element is a portion of the irradiance that, because of a feature known as *albedo*, gets reflected once it reaches the Earth's surface. Thus, it is now possible to condense all of these ideas into the following balance:

$$G_g = G_b + G_d + G_a \tag{1-4}$$

With:

- G_g - global irradiance $[W/m^2]$.
- G_b - direct irradiance $[W/m^2]$.
- G_d - diffuse irradiance $[W/m^2]$.
- G_a - reflected irradiance $[W/m^2]$.

The Air Mass (AM), which is the relative length of the solar beam's direct passage through the atmosphere, is another variable that measures the decrease in light strength as it travels through the atmosphere and is absorbed by air and particles. The formula for it is:

$$AM = {}^{1}/_{cos\theta_z} \tag{1-5}$$

where, as the following figure more clearly illustrates, θ_z is the zenith angle between the irradiance and the perpendicular to the ground:

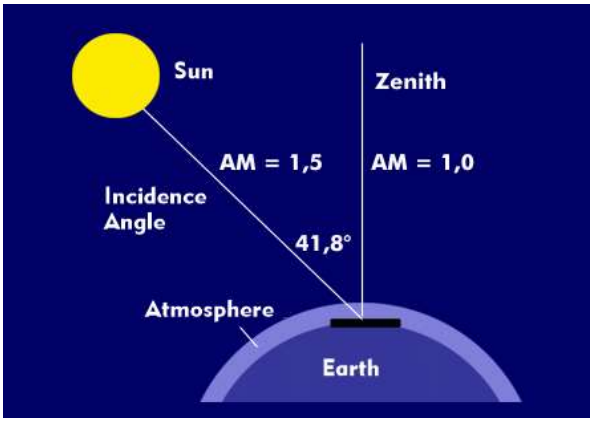

Figure 1-2: Air Mass simplified scheme [3].

A photovoltaic module's power incidence is determined not only by the power in the sun but also by the tilt angle—the angle at which the module faces the sun—with the PV module's highest power density occurring when it is perpendicular to the sun. The azimuth, or coplanar angle between a line pointing towards the sun (celestial body) and a line pointing due south (in the northern hemisphere) as viewed from a stationary point, provides another angular attribute. Depending on the season and latitude, this angle changes during the day [2].

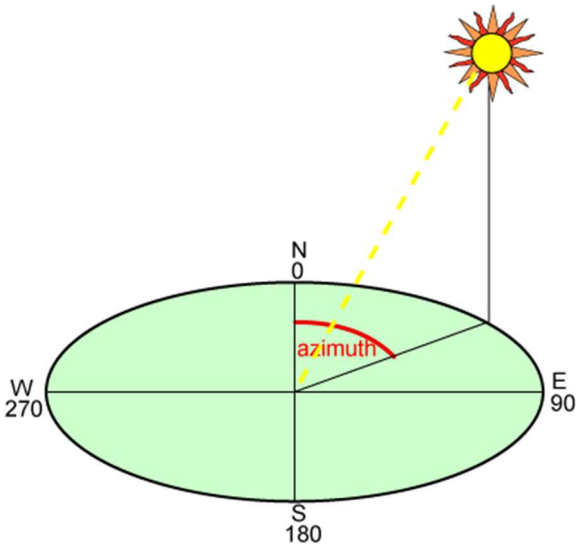

Figure 1-3: Azimuth angle [4].

1.1.2 Energy bands and material classification

The fundamental component of a photovoltaic module is the solar cell, and the material that makes up the cell directly affects how the cell behaves. For this reason, an outline of energy bands and material classification will be provided in the lines that follow in order to examine the conversion process that occurs inside the cell.

The first is that electrons behave differently depending on whether they are blocked in a crystal lattice or free, and as a result, their energy is directly related to this factor and affected by the presence of neighbouring electrons. They can only occupy specific, quantized levels of energy as a result.

A valence band electron can stay near to the atom it belongs to and has a more stable, lower energy value. Alternatively, if it is in the conduction band, it can exit the atom's structure, resulting in the electrical conduction phenomena; the prohibited band, on the other hand, lies between these final two and is associated with the *energy gap*.

The important thing to remember is that this energy gap essentially represents the amount of energy required for an electron to move from the valence band into the conduction band, or what is known as the conduction phenomenon.

As a result, materials can be divided into three primary groups based on the energy gap value [eV]:

- *Conductors*: valence and conduction bands partially or completely overlap; the energy gap is very small. Because of this, electrons are easily able to migrate and aid in the conduction process. This group includes metals.
- *Insulating materials*: because of their huge energy gap, electrons in these materials need more energy to enter the conduction band.
- *Semiconductors*: their energy gap lies in the middle of that of insulators and conductors.

The prior ideas are summed up in the following image:

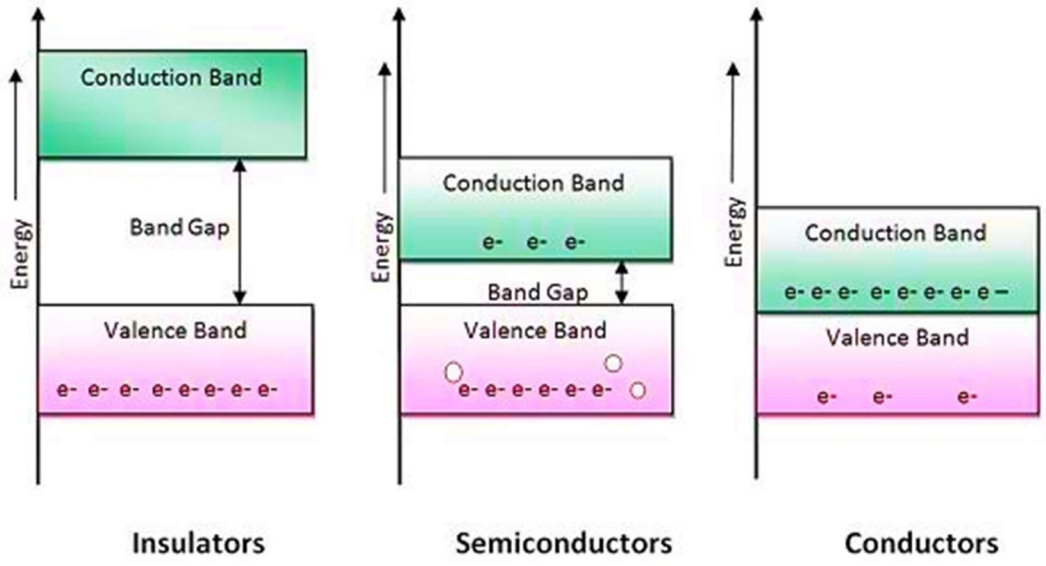

Figure 1-4: Comparison among energy gap values for the three different types of materials[5].

The best materials for photovoltaic applications are semiconductors because they can regulate voltage and current well and are sensitive to changes in temperature, light, magnetic fields, and doping (the latter of which will be covered

in the paragraph that follows). The energy gap typical values for the primary semiconductors are shown in the following table.

Material	Energy gap [eV]
Crystalline Silicon (c-Si)	1.12
Amorphous Silicon (a-Si)	1.75
Germanium (Ge)	0.67
Gallium Arsenide (GaAs)	1.42
Indium Phosphide (InP)	1.34
Copper Indium Diselenide (CuInSe)	1.1
Cadmium Telluride (CdTe)	1.45
Cadmium Sulfide (CdS)	2.4

Table 1-1 - Typical values of energy gap of some semiconductors[6].

Since their valence band is saturated in their native state, semiconductors are poor conductors because electrons find it difficult to transition from the valence band to the conduction band. Doping is a method that can enhance their conductivity and performance because of this. The function of silicon and its role in photovoltaic applications will be discussed in the following subparagraph.

1.1.3 The Function of P-N Junction and Silicon

Silicon (Si) is the finest compromise in terms of materials. As one of the most prevalent elements in nature, it is a member of the periodic table's IV group. Consequently, it forms a basis for integrated circuit chips and is now the most advanced technology used in photovoltaic applications.

Silicon's atomic structure gives it a 1.12 eV band gap. It is tetravalent because its four valence electrons form chemical connections with nearby atoms. As the accompanying graphic more clearly illustrates, it indicates that each atom shares eight electrons with the four atoms around it.

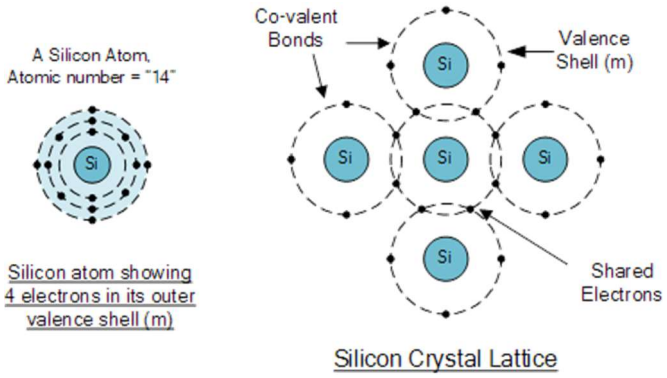

Figure 1-5: Silicon atomic structure[7].

An electron can travel from the valence band to the conduction band by a process known as the *photovoltaic effect*, which is fueled by sun light. Specifically, a photon's energy that makes up solar radiation needs to be greater than the corresponding material's band gap when impacted by that radiation.

$$E_{ph} = {}^{hc}/_{\lambda} \geq E_{gap} \tag{1-6}$$

Where:

- E_{ph} - photon energy [J].
- E_{gap} - energy gap [J].
- h = 6.626 x 10^{-34} $\frac{m^2 \cdot kg}{s}$ - Planck's constant.
- c = 2.998 x 10^8 m/s – speed of light.
- λ – wavelength [μm].

Using the relationship mentioned above as a guide, a photon can be absorbed and an electron can move from the valence band to the conduction band when it

hits a semiconductor. As a result of the absorption process, an electron-hole couple is created in the valence band. In the absence of outside interference, the electron and hole eventually return to their initial positions in the valence band, losing any remaining energy as thermal energy and preventing any more energy conversion.

Through the process of "doping," the electron and hole balance in a silicon crystal lattice can be altered. This technique creates "N-type" (negatively charged) semiconductor materials, which are often made of atoms with one extra valence electron than silicon and typically fall into the V group of the periodic table, such as phosphorous.

Since only four electrons from each atom are required to form the covalent bonds surrounding the silicon atoms, the fifth electron introduced with the dopant has nothing to bond with and is free to move, making it easy for it to access the conduction band. This is why small amounts of the aforementioned atoms are particularly effective at allowing an electric current to flow within the Silicon crystal lattice. Because of this, the donor's energy level is near the conduction band, which lowers the band gap overall and, as a result, the energy required for electrons to move from the valence band to the conduction band.

On the other hand, "P-type" (positively charged) semiconductor materials have one fewer valence electron. Similar to boron, they are members of the III group of the periodic table and only have three valence electrons that interact with silicon atoms. This leaves a hole in the atoms since there aren't enough electrons to make the four covalent bonds that surround them.

In this instance, a positive charge is produced by the absence of electrons, making the valence band electrons mobile. Accepting electrons from neighbouring atoms allows holes to conduct electricity because it causes the atoms to move in the opposite direction of the electrons' movement. This is beneficial since the energy level of the acceptor is near the valence band, again lowering the energy gap, because the injected hole can already be occupied at low energy by a valence band electron.

Because one type of carrier is always present in greater quantities than the other in doped materials, the P-N junction theory—where P- and N- summarize the above ideas—better captures the fundamentals of the cell's dark-condition behaviour by simulating it as a semiconductor diode.

In terms of crystalline silicon cells, an N-type layer is placed on top of a P-type layer to form a diode. Bidirectional diffusion occurs when these two layers come into contact: holes, which are acceptors of the P-type region, diffuse towards the N-

type layer and a local negative charge originates in the P-type layer, while electrons, which are donors, diffuse from the N-type region to the P-type one.

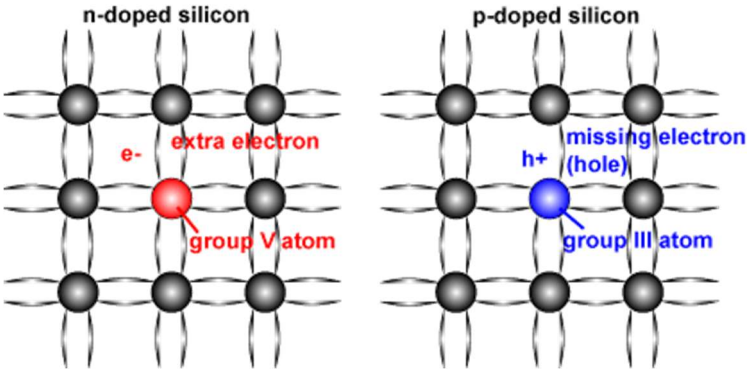

Figure 1-6: Atomic structure of N-type and P-type materials[2].

The *depletion area*, often referred to as the *space-charge region*, is created at the junction interface between the two layers as carriers move from a more concentrated region to a less concentrated one. In this instance, there are no mobile charges contained, but positive charges are found on the N-side and negative charges are on the P-side. An equilibrium condition is reached, and the fixed charges of the doped layers create a *junction field* that acts as a kind of electric barrier, preventing additional mobile carrier flow.

The equilibrium remains unaltered when considering an open-circuit configuration: the *diffusion current* equals the current produced by the electric field (*drift current*).

Two methods exist for altering this balance: *forward bias* and *reverse bias*. When the first scenario is taken into account, the P-type side receives an external positive voltage, which lowers the barrier.

Diffusion current is the term for this kind of important current that flows through the diode. In comparison to the preceding scenario, the flowing current is substantially less when the voltage is supplied to the N-type side because this increases the potential barrier, which impedes the diffusion process. This one is directed by the potential barrier and is known as *reverse saturation current*[8].

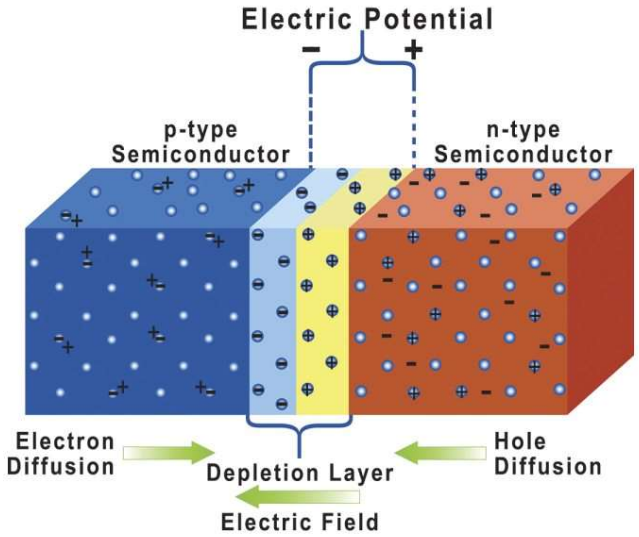

Figure 1-7: P-N junction layout[9].

1.1.4 Equivalent circuit and I-V curve

After researching the relationships between solar radiation and the photovoltaic effect of semiconductor materials, an analogous circuit can be defined to better understand the electrical behaviour of a solar cell.

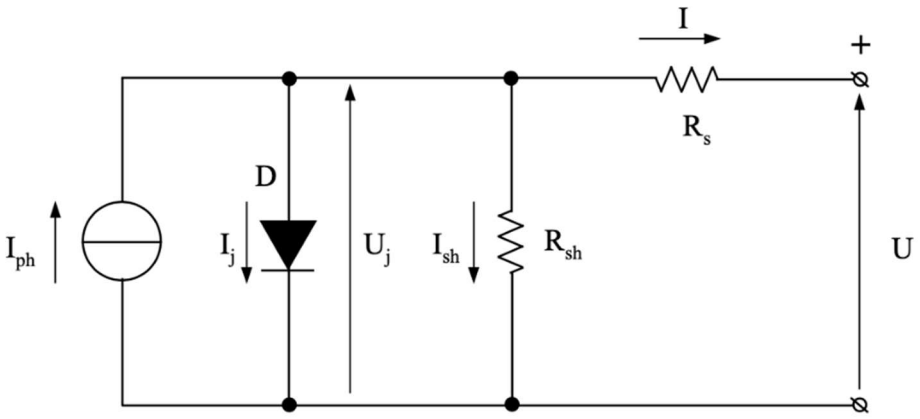

Figure 1-8: Equivalent circuit of a solar cell[8].

The left part of the above picture depicts an ideal current source and explains how the photovoltaic current, I_{ph}, is generated. This current is proportional to the irradiance. An anti-parallel configuration is used to link a diode in order to mimic the rectified behaviour of the P-N junction. The power losses caused by the second channel for the generated current are indicated by the parallel connections of the shunt resistance R_{sh}. As a result, higher shunt resistance values are associated with lower power losses. The second is the series resistance R_s, which is the total of all the losses resulting from the current flowing between electrodes and their contacts, namely fingers, and the resistance between silicon and metal contacts. The second is the series resistance R_s, which is the total of all the losses resulting from the current flowing through electrodes and their contacts, specifically fingers and busbars, and the resistance between Silicon and metal contacts. Lower series resistance values are better in this case since they produce less power losses.

Just a simplified version of the analogous circuit is presented in this thesis, utilising analytical equations to highlight the essential elements required to comprehend the subject matter.

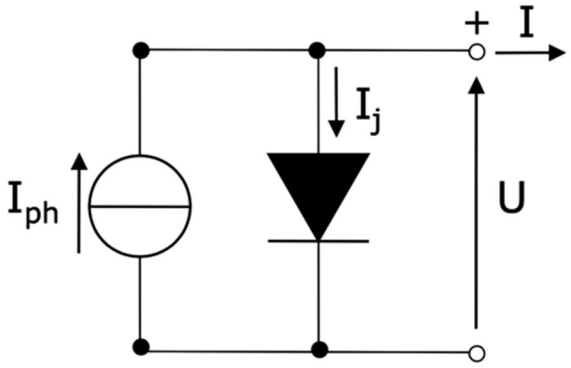

Figure 1-9: Simplified equivalent circuit of a solar cell[8].

Since the shunt and series resistance are absent from this simplified circuit, the PV current and voltage formulas can be found using Kirchhoff's voltage and current equations.

$$I = I_{ph} - I_j \tag{1-7}$$

$$V = V_j \tag{1-8}$$

Assuming constant values for temperature and irradiation, the I-V characteristic curve can be computed by evaluating these parameters. This curve, which shows the relationship between voltage and current, is crucial for determining how well photovoltaic systems operate and how well they use solar energy. Furthermore, it provides vital information regarding a cell's power output, as it can be determined using the formula:

$$P = V \cdot I \tag{1-9}$$

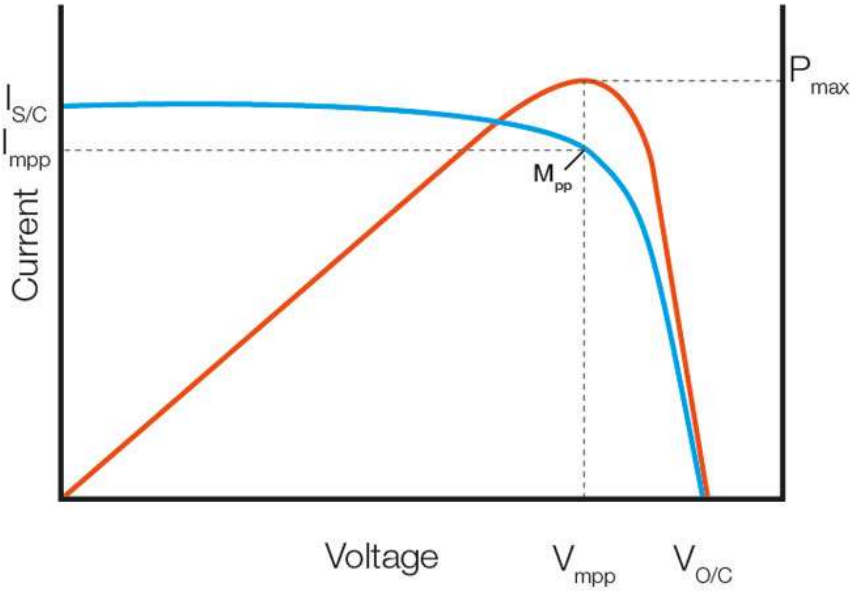

Figure 1-10: I-V characteristic curve[10].

This curve highlights a number of important solar cell properties, such as:

- The Maximum Power Point (MPP) of the I-V curve represents the maximum power that the cell can generate. IMPP and VMPP are the corresponding current and voltage, indicated by the subscript MPP.
- I_{sc} - When a cell is shorted out, the highest current flow that happens is the short-circuit current; in this scenario, the voltage is zero.
- V_{oc} - Open-circuit voltage. Open-circuit voltage. When there is no load on the cell, no current flowing through it, and the voltage is at its maximum, this voltage is at its highest value.

The *Fill Factor* can be obtained from the I-V curve and is defined as follows. It is a parameter that describes the proximity between the region corresponding to the cell's maximal power and the one produced by the short-circuit current and the open-circuit voltage.

$$FF = {(I_{mpp} \cdot V_{mpp})}\Big/{(I_{sc} \cdot V_{oc})} \tag{1-10}$$

The maximum power generated is in the numerator, and the product of the open-circuit voltage and the short-circuit current is in the denominator. Increased Fill Factor values indicate a behaviour closer to the ideal, which enhances the performance of the cell. The combined effect of the resistances shown in Figure 1-8 and diode operation is what causes this departure from the ideal situation. Values typically range from 0.7 to 0.85[8].

It is important to remember that the II and IV quadrants are also included in the solar cell's I-V characteristic curve. Because of the negative values of voltage in the fourth quadrant and negative current in the second, the solar cell reacts differently in this situation and acts like a load.

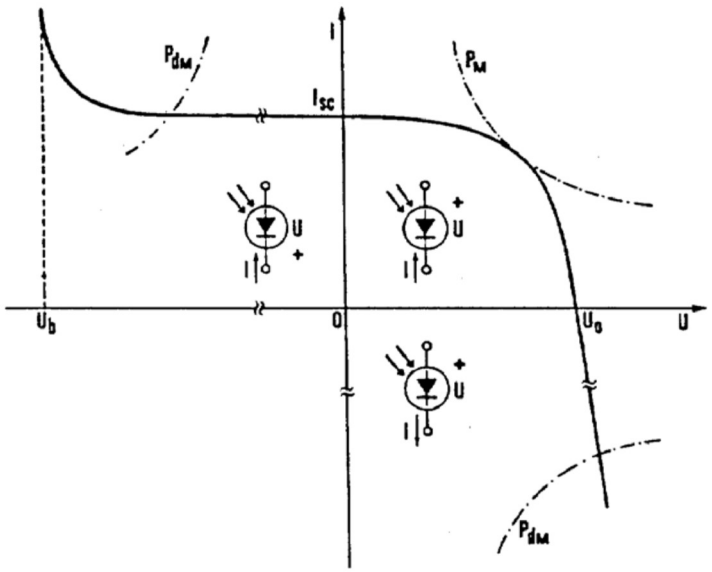

Figure 1-11: Complete solar cell I-V curve[8].

Only when the operating point of a solar cell is situated above the temperature limits can it function as a load. If not, the heat generated by the dissipated power will surpass the threshold value of 85 °C, potentially resulting in damage. Moreover, the breakdown voltage U_b acts as a primary constraint, rapidly causing the solar cell to fail if the voltage reversal reaches this magnitude. The majority of silicon cells can experience failure at voltages between 10 V and 30 V[11].

1.1.5 Temperature and Irradiance Dependence

Two essential elements that must be looked into are the sun irradiance and the operating temperature of photovoltaic cells. The following figure shows how, at constant temperature, irradiance modifies the characteristic curve.

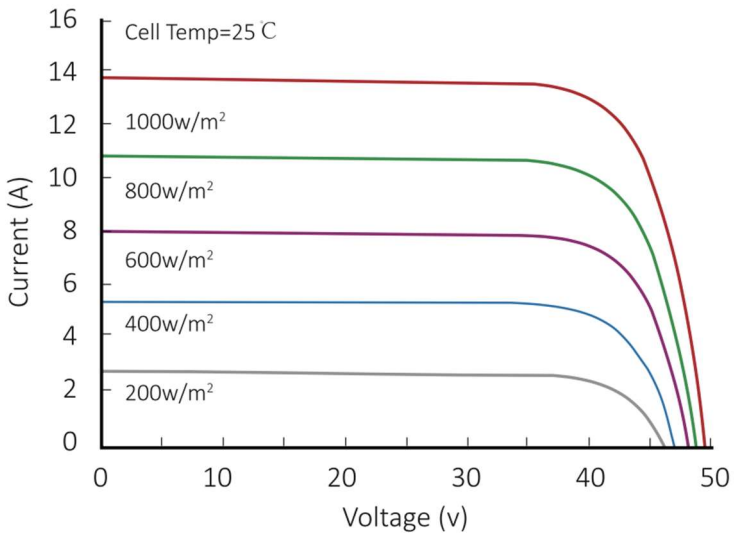

Figure 1-12: Irradiance effect on I-V curve for LONGI LR5-72HBD-530M panel[12].

Due to the close relationship between solar radiation and photogenerated current, a fall in irradiance is correlated with a decrease in short-circuit current. The open-circuit voltage is practically constant until very low levels of G (less than 200 W/m^2) are attained, at which point it declines logarithmically as the irradiance

decreases. This dependency stated in the preceding paragraphs is thought to be expressed by the following equation:

$$I_{sc}(G, T_C) = I_{sc,STC} \cdot \frac{G}{G_{STC}} \cdot [1 + \alpha \cdot (T_c - T_{STC})] \quad (1\text{-}11)$$

Where:

- $I_{sc,STC}$ - Short-circuit current in STC (A).
- G - Incident irradiance on the cell (W/m^2).
- G_{STC} - Incident irradiance in STC – 1000 W/m^2.
- α - Thermal coefficient for I_{sc} (°C^{-1}).
- T_c - Solar cell temperature (°C).
- T_{STC} - Ambient temperature in STC – 25°C.

Another crucial detail to note is the time constant of these fluctuations on the I-V characteristic curve. The current response occurs when the irradiance varies in around 10-20 μs. The temperature dependency of solar cells is intimately related to their semiconductor characteristics, as shown in the picture below. An increase in temperature causes semiconductor materials' energy gap to contract, lowering the open circuit voltage. The short-circuit current is also somewhat increased as a result of this band gap reduction.

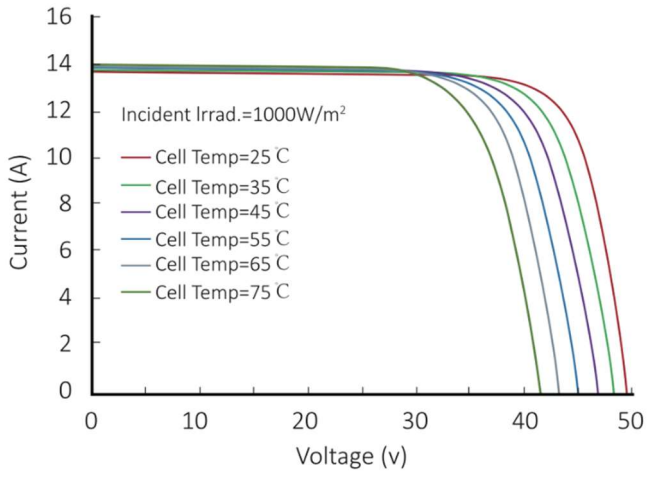

Figure 1-13: Temperature effect on I-V curve for LONGI LR5-72HBD-530M panel[12].

An analytical equation can be used to model this impact, just as it can be for the irradiance dependency example. However, because the short-circuit current change with temperature is small, the formula links the open circuit voltage to the single cell temperature.

$$V_{oc}(T_C) = V_{oc,STC} \cdot [1 + \beta \cdot (T_c - T_{STC})] \quad (1\text{-}12)$$

The variables taken into account in the equation are:

- $V_{oc,STC}$ - Open-circuit voltage in STC (V).
- β - Thermal coefficient for V_{oc} (°C^{-1}).
- T_c - Solar cell temperature (°C).
- T_{STC} - Ambient temperature in STC – 25°C.

Since this value is generated by multiplying voltage by current, it is evident to state that temperature and irradiance both directly affect a solar cell's capacity to produce power. To emphasise the idea, the following formula summarises the direct relationship between the maximum power output, irradiance, and temperature:

$$P_{max}(G, T_C) = P_{max,STC} \cdot \frac{G}{G_{STC}} \cdot [1 + \gamma \cdot (T_c - T_{STC})] \quad (1\text{-}13)$$

Where:

- $P_{max,STC}$ - Maximum power in STC (A).
- G - Incident irradiance on the cell (W/m^2).
- G_{STC} - Incident irradiance in STC – 1000 W/m^2.
- γ - Thermal coefficient for P_{max} (°C^{-1}).
- T_c - Solar cell temperature (°C).
- T_{STC} - Ambient temperature in STC – 25°C.

1.1.6 Efficiency of solar cell conversion

Efficiency is a crucial parameter that evaluates a solar cell's ability to transform solar radiation into electrical power. The ratio of maximal power output to incident solar power can be used to characterise it.

$$\eta_{cell} = \frac{P_{max}}{P_{solar}} = \frac{I_{mpp} \cdot V_{mpp}}{G \cdot A} = \frac{FF \cdot I_{sc} \cdot V_{oc}}{G \cdot A} \quad (1\text{-}14)$$

Where:

- I_{mpp} - Maximum power point current (A).
- V_{mpp} - Maximum power point voltage (V).
- G - Incident irradiance on the cell (W/m^2).
- A - Area of the solar cell (m^2).
- FF - Fill Factor (-).
- I_{sc} - Short-circuit current (A).
- V_{oc} - Open-circuit voltage (V).

Efficiency ratings for commercially available cells are usually 20%, with major variation based on cell type. Multiple loss sources that can be reduced but not entirely eliminated are the cause of these low values[8]:

1) An excess or shortage of incident photon energy. It is feasible to identify two scenarios: the first is when the energy is more than what is needed to bridge the semiconductor's bandgap. The surplus of energy is discharged as heat. Nevertheless, photons nevertheless have a comparable effect even when they are unable to form an electron-hole pair because they lack the energy to overcome the bandgap. Their energy is thus totally transformed into heat. Roughly 45% of the losses worldwide are caused by these two inescapable events.

2) Before reaching the solar cell or interacting with the frontal contacts, some photons are reflected. Reducing the contact area and using antireflection coatings can help reduce this type of loss, which accounts for up to 10% of all global losses.

3) In the P-N junction depletion zone, some electron-hole pairs might rejoin right before being broken apart by an electric field. Heat is the result of this global energy loss due to recombination. It represents roughly 2% of total losses.

4) The diode, the shunt resistance, and the series resistance in the circuit that is equal to a solar cell dissipate some of the energy produced before it can exit the circuit. The Fill Factor option takes this energy loss into account, and it can have values as high as 20%.

1.2 Photovoltaic cell connection

One PV cell's open-circuit voltage is only about 1 V, or somewhat less, which means that the power provided is not enough to meet the demands of commercial loads. Therefore, many cells are connected in series or parallel to produce useful amounts of power output.

A higher short-circuit current can be obtained by connecting more cells in parallel, whereas a higher open-circuit voltage can be obtained by connecting them in series. In both cases, the increase is closely correlated with the number of connected cells.

Mismatch is a condition that arises when solar cells with different I-V curves are coupled, and this solution might possibly become a significant source of losses. The primary factors causing variation in the I-V curve are tolerances, manufacturing defects, and shading phenomena. An interconnected group of cells' electrical response is defined by the cell with the worst electrical properties. For this reason, in order to avoid the bottleneck phenomena, it is imperative that the considered set of cells have almost equal electrical properties. We'll look at these behaviours in the ensuing paragraphs.

1.2.1 Mismatch for cells connected in series

The PV system's overall open-circuit voltage can be raised by connecting solar cells in series, which can be summed up as follows:

$$V_{oc} = \sum_i^{N_s} V_{oc,i} \quad (1\text{-}15)$$

$$I_{sc} \cong \left(I_{sc,i}\right)_{min} \quad (1\text{-}16)$$

The equivalent I-V curve for the whole number of solar cells linked in series (N_s) has an open-circuit voltage equal to the sum of the individual cells and a short-circuit current comparable to the cell with the lowest current.

When there is a mismatch, the cell with the lowest short-circuit current in relation to the others acts as an extremely high resistance resistor (up to ten or hundreds of ohms), therefore this restriction on the I_{sc} could be detrimental. The weakest cell, which exhibits inverted voltage, thereby dissipates the current produced by the cells that are normally operating. As a result, hotspots expand and may harm the cell. More precisely, the cell quickly breaks when the breakdown voltage U_b—a threshold value for voltage reversal—is achieved. In the event of a single shaded cell, damage must be produced by connecting many cells with N_s of 30–50 V, as silicon cells normally have a breakdown voltage of 20–30 V and a voltage value between 0.6 and 0.7 V per cell. The most dangerous type of mismatch for a solar cell is this one, which can happen often.

To prevent the functioning as a load for a shaded cell, a diode is linked in anti-parallel to bypass the weakest cell and recover the current generated by the regular running cell. By employing this technique, the power generated by all the other functioning cells in a series of cells is removed without resulting in additional losses, and the lowest-performing cell in the series no longer has the short-circuit current. It is important to remember that it is expensive to implement this kind of security strategy on a per-cell basis. For this reason, the bypass diode is connected to a number of cells, typically in groups of 18–24–36[13].

1.2.2 Mismatch for cells connected in parallel

In a photovoltaic system, connecting many solar cells in parallel can be a viable means of increasing the short-circuit current. This can have the following effects on the overall short-circuit current and open-circuit voltage:

$$I_{sc} = \sum_i^{N_p} I_{sc,i} \quad (1\text{-}17)$$

$$V_{oc} \cong \left(V_{oc,i}\right)_{min} \quad (1\text{-}18)$$

In the case of a short-circuit current, it is defined by the total current of all the cells linked in parallel (N_p), as opposed to a series connection where the open-circuit voltage is limited by a defective or shaded cell.

Since the weakest cell will function as a load with a reverse current (IV quadrant in figure 1-11), equivalent to the current produced by the other cells when they are operating normally, the worst case scenario in the event of a mismatch is an open circuit. If the thermal limit is exceeded, the weak cell temperature rises as a result of current dissipation, which may result in a hotspot and damage to the cell structure.

Similar to the preceding instance, current reversal can be stopped if a diode is connected to each string of cells' current output. This blocking diode, which is normally closed to permit the current generated under normal operating conditions to exit the cell, stops the reversed current when there is a mismatch. This prevented dissipation losses in the shaded cell and allowed the other functional cells to gather electricity. The blocking diode is used to a series of connected cells as opposed to a single cell, just as the bypass diode. This type of connection is less common than series connections[13].

1.3 Photovoltaic modules

The majority of PV plants in use today were constructed utilising monofacial PV panels, the most developed technology at the time. The features and functionality of this technology will be covered in the paragraph that follows.

1.3.1 PV module: a well-established technology

The basic parts of a photovoltaic module, the solar cells, are driven by light from the sun and when connected, can generate electricity. A module may consist of 36–96 series-linked cells that are created.

Cell modules that are well-isolated from outside elements including wind, dust, humidity, and other things that can interfere with the module's functionality are built using a range of manufacturing techniques. A well-isolated module also ensures a thermal equilibrium, which is typically kept between 45 and 75 °C. As was previously noted, silicon modules made of crystalline silicon (c-Si) comprise the most advanced technology. There is a difference between monocrystalline silicon cells (m-Si) and polycrystalline silicon cells (p-Si). The round shape of m-Si cells can result in a smaller conversion area that is useful, but the crystal growth method makes this feasible. This means that some of the material that would otherwise be thrown away can be recycled by processing these to take on a square shape that crosses their boundaries. Nonetheless, the square shape of p-Si cells already aids in making greater use of the module surface.

The electrically welded cells that make up a photovoltaic module's core have an efficiency ranging from 6 to 23%. These cells are encapsulated securely between two layers: a high transmittance glass on the front, which is required to be transparent to light, and either glass or a polymeric composed of PET, Tedlar, or Mylar on the rear. With time, the layers are fused together by the thermoplastic polymer (Ethylene Vinyl Acetate, or EVA) enclosing the module to produce a structure that is waterproof, insulated, and compact. The fact that it cannot tolerate temperatures higher than 85 °C is its lone disadvantage. Lastly, an aluminium frame protects the module's structural integrity. A junction box with bypass diodes and connectors is situated at the back of the module. Since it acts as a connection between the module and the external circuit, it needs to have both sufficient and the module's own insulation. This figure illustrates each of these attributes [8].

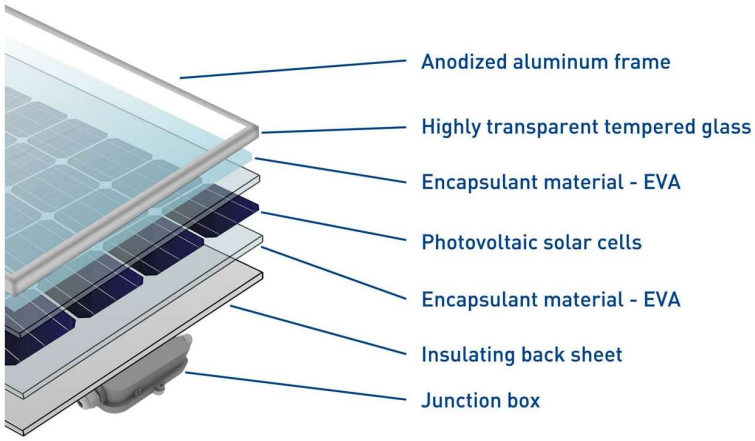

Figure 1-14: Design of a PV module[14].

Other cell types include thin-film technologies (whose efficiency ranges from 6–18%) and multi-junction and concentration cells (whose highest efficiency is 44%, with a potential limit of 70%). These are in addition to the m-Si and p-Si cells that have been mentioned thus far.

1.4 Standard Test Conditions and PV module temperature evaluation

A PV module's global conversion efficiency is determined under Standard Test Conditions (STC), which are specified by G=1000 W/m^2, AM = 1.5 (simulated using suitable flash lights), and cell temperature of 25 °C. This is a crucial point to note. As mentioned earlier, the module efficiency varies from 7% to 23% based on the type of cell.

Known as peak power (W_p) or maximum power output at STC, these values are defined by their normal range of 10 W_p to 400 W_p. Other electric characteristics defined in STC include the open-circuit voltage U_{oc}, the short-circuit current I_{sc}, and the current and voltage in the maximum power point, denoted as I_{mpp} and U_{mpp}.

1.4.1 NOCT Temperature

The characteristics that have been presented thus far are Standard Test Conditions, as previously said; the term itself implies that these conditions are manufactured in a lab. In addition to the preceding values, there is also the Nominal Operating Cell Temperature (NOCT). This temperature, which is defined as the thermal equilibrium (CEI EN 60904-3) for a PV module operating in open circuit and subjected to G=800 W/m^2, T_a=20 °C ambient temperature, and 1 m/s wind speed, is one of the primary parameters that the manufacturer of the module must supply.

The NOCT parameter makes it possible to predict the cell's temperature under a variety of operating scenarios. Its temperature range is 42 to 50 °C. Given that the

irradiance G has a linear relationship with the temperature difference between T_{PV} and T_a, the cell temperature can be calculated using the following formula[6]:

$$T_{PV} = T_a + \frac{NOCT-20}{G_{NOCT}} \cdot G \quad (1\text{-}19)$$

Where:

- T_{PV} - module temperature (°C).
- T_a - ambient temperature (°C).
- $NOCT$ - Nominal Operating Cell Temperature (°C) given by module's manufacturer.
- G - measured irradiance (W/m^2).
- G_{NOCT} - NOCT irradiance defined as 800 W/m^2.

1.5 Photovoltaic plant: main components

Since multiple modules are required for optimal solar energy utilisation, the additional components that are added make up the balance of the system (BOS). The PV system, or more specifically, the photovoltaic system, is the whole facility. It includes everything required to convert solar energy into AC electricity reliably and safely. In some cases, it can also be combined with a storage system.

In contrast to stand-alone systems, which can function independently of the grid, most PV systems are grid-connected, enabling them to communicate with the electrical grid.

PV systems fall into two primary types based on installed power:

- Community-scale plants: they are small-scale residential and commercial energy systems, typically with capacities from a few tens to several hundred kilowatts. These plants are deployed in rooftop configurations or integrated systems within buildings.

- Utility-scale plants: usually operated by energy companies, they are enormous industrial facilities capable of generating power on a utility or grid scale. A few hundred to several thousand megawatts of installed

capacity are available; more recent installations have already surpassed the one gigawatt installed power benchmark. These installations are also referred to as solar farms. They lack stand-alone designs, but they are linked to the electrical grid.

In Figure 1-15, an example of a classic PV plant layout is depicted [6][15]:

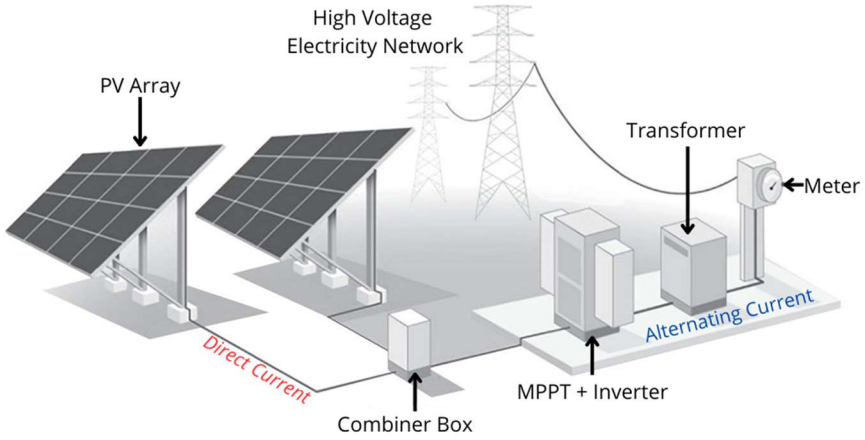

Figure 1-15: A classical PV plant layout[16].

1.5.1 Photovoltaic generator

Since a single module's power nowadays ranges from 350 to 500 W, connecting many modules is necessary to get the right installed capacity values. The kind of connection that is being used helps to identify these groups of panels. The term "string" refers to the series-linked modules; further strings join to form arrays, which are then combined to form the PV field.

Utility-scale photovoltaic arrays are frequently installed on iron foundations that are firmly fixed in the earth. These structures need to be built properly since they have to endure the tremendous mechanical loads brought on by wind.

1.5.2 Combiner box

The cables that are used to connect several strings or arrays together are kept in a type of enclosure called a combiner box. It is located on either the DC or AC side of the plant and is used to better manage the connections between the various components of a PV system[17].

1.5.3 PCU – Power Conditioning Unit

Since medium- to high-voltage electrical networks are usually connected to large photovoltaic facilities, the power conditioning unit (PCU) is a crucial component for regulating the electricity generated by the PV modules for grid injection. The most important components of the PCU, which cooperate to maximise the plant's power production, are as follows:

- Inverter

The inverter, a DC/AC converter, is crucial in photovoltaic systems since solar modules generate DC electricity while the grid produces AC electricity. The waveform of the output voltage (AC side), especially when power is injected into the network, is a crucial feature of this type of device since it must adhere to strict regulations on the quality of the electricity generated. This type of waveform is produced by inverters through the use of transistors as switch-controlled components and a technique called pulse width modulation (PWM). The most important attribute of an inverter is its DC-AC efficiency, which can be calculated by dividing its AC power (P_{AC}) by its DC power (P_{DC}). In equation:

$$\eta_{DC-A} = \frac{P_{AC}}{P_{DC}} \tag{1-21}$$

Inverters typically have high conversion efficiencies, with values greater than 90%, even at low load percentages. Another important factor to consider is the minimum input voltage of inverters used in solar applications. These inverters are designed to wait for the voltage generated by the PV modules (DC side) to reach a specific level before turning on. An example of an inverter's efficiency curve may be seen in the accompanying figure.

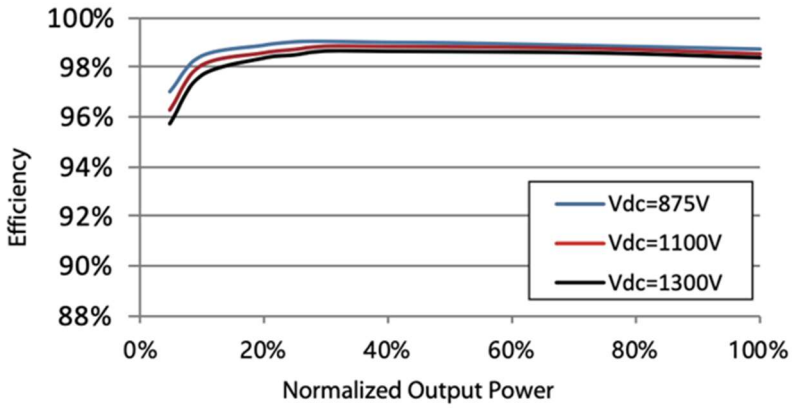

Figure 1-16: Inverter efficiency curve for Sungrow SG3125 HV-MV-30 inverter[18].

- Filters

The inverter generates a waveform that is not quite sinusoidal when the PWM approach is utilised to transform the DC electricity generated by the modules into AC electricity. This flaw in the converted power is known as Total Harmonic Distortion (THD) or Electromagnetic Interference (EMI); to address this problem, an LC filter is installed on the AC side of the inverter. An extra EMI filter is required in the event that there is electromagnetic interference on the DC side as well[6][19].

- MPPT

Maximum Power Point Tracker (MPPT), a DC/DC converter, allows solar panel efficiency to be maximised. The maximum power point of solar modules is susceptible to fluctuations throughout the day owing to changes in temperature and irradiance because it is fixed at a specific voltage and current for various ambient conditions. By modifying the operating point on the I-V curve, the MPPT matches the maximum power point. Depending on the demands of the grid or the load, the MPPT can adjust the amount of electricity that is harvested from the PV modules. For instance, a PV plant linked to the high voltage grid can use the MPPT to lower the power injected if requested to do so by the Transmission System Operator (TSO).

- Transformer

The transformer is a crucial component in utility-scale applications because it raises the voltage to the necessary level for grid matching by receiving the AC electricity that the inverter has converted as input. A high-voltage grid connection can cause the input voltage to rise to hundreds of kV.

1.5.4 Protection devices

Even while PV systems are simple to operate, they are prone to mistakes that could impair their ability to generate electricity or, more dangerously, damage the integrity of the system. Conventional international standards provide certain protective measures to ensure safe operations in the event of hazardous situations. Both on the DC and AC sides of the system, devices like switches, circuit breakers, fuses, bypass and blocking diodes—discussed in paragraphs 1.2.1 and 1.2.2—must be installed in line with these protocols. The part that houses the majority of these devices is called switchgear[8][20].

1.6 PV system data acquisition devices

If one of the plant's modules malfunctions, the production of electricity could be reduced or stopped, which would result in significant losses in terms of asset value and efficiency. As a result, it's critical in a PV power plant to respond to a defect as quickly as feasible. For these reasons, PVs' dependability, enhanced performance, and ease of maintenance depend on their continuous measurement and monitoring of data, including voltage, current, temperature, and solar irradiation.

Information about solar panels is gathered for maintenance and repair purposes by local and remote photovoltaic monitoring systems. The primary issues with PV systems, such as soiling, shadowing, snow deposition, and the panels' capacity to absorb solar radiation, are also connected to the need for data collection and monitoring in these systems.

Soiling on PV modules can cause a daily loss of power of up to 1%. Soiling is a site-specific phenomenon that varies geographically. Even under the best of

cleaning conditions, pollution in PV modules reduces the amount of solar electricity generated overall by at least 3–4%. A monitoring system will be required to determine the factors impacting PV production, taking into account extra problems such as cracks. In order to lower operating costs by minimising maintenance and system downtime, it is imperative that the DAQ system and monitoring enhance the ability to detect any issues. Additionally, the monitoring system reduces the amount of manual controls, which lowers the danger to safety.

PV systems have a range of DAQ and monitoring applications because the goal of any data acquisition system is to gather data, process it as needed, and record the results for appropriate storage, presentation, or further processing [21]. PV array level measuring is a standard operation, but DAQ is often implemented at the PV module level. Whether data is transferred wirelessly or through wires is another crucial question.

As is well knowledge, current-voltage (I-V) and power-voltage (P-V) curves are used to represent the electrical attributes of PV modules. Tracking the voltage and current levels is essential for determining the PV module's power production. The amount of energy produced is dependent on several environmental factors, including temperature, humidity, and solar radiation levels. The weather has a direct impact on PV system performance.

The International Electrotechnical Commission (IEC) has published guidelines for data gathering and assessment for photovoltaic facilities in their 61724 guidance (1998). For meteorological parameters, it is required to monitor the temperature and solar irradiance of the surrounding air; measurements of wind, precipitation, and humidity are optional. There are multiple sections in the IEC 61724:

- The methodologies, instruments, and processes for PV system performance monitoring are covered by IEC 61724-1.
- IEC TS 61724-2 and IEC TS 61724-3 are primarily concerned with performance analysis utilising monitoring data.

As per varying precision levels and uses, the standard additionally delineates three categories of monitoring systems:

- High (Class A).
- Class C: basic, and Class B: medium; these are better suited for smaller systems. A maximum sampling period of one minute should apply to these classes, while maximum recording intervals of fifteen minutes for Class B and sixty minutes for Class C are required.

After data collection is complete, data filters could be needed. IEC 61724 standards include further guidelines for filtering monitored variables: irradiance should be filtered between 6 W/m2 and 1500 W/m2, and ambient temperature should be filtered between -30 °C and 50 °C[22].

The graphic below displays a DAQ layout sample.

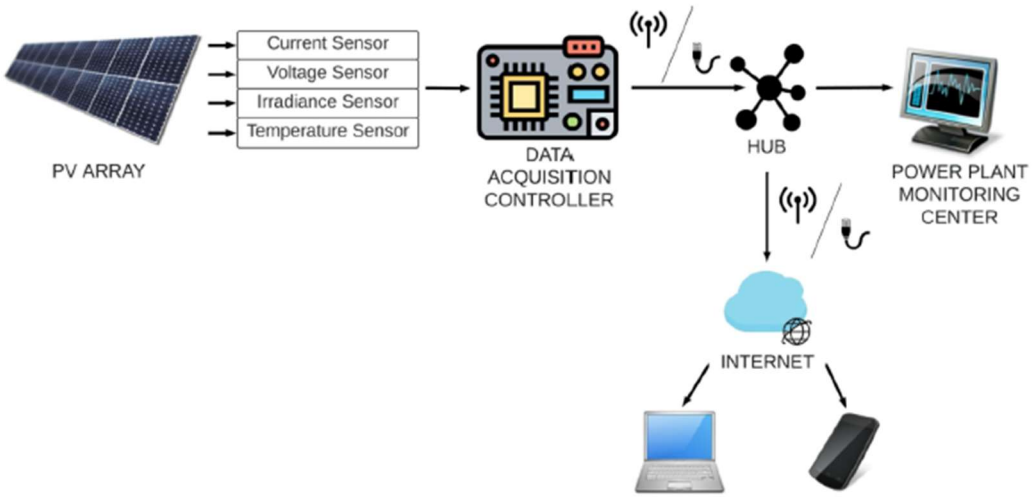

Figure 1-1-17: Array level DAQ and monitoring system layout[22].

1.6.1 Current measurements

Current can be measured at both the AC and DC sides while working with PV plants. Specifically, the following are the primary methods and approaches used in these measurements:

- Fluxgate principle.
- Faraday-Lenz law.

- Faraday rotation effect.
- Hall effect.
- Magnetoresistance effect.
- Ohm’s law.

Numerous independent values, such as grid line current, PV module current, and line current at the inverter output, can be measured using current sensors. Naturally, the current sensor output needs to be amplified in order to provide an accurate measurement; hence, the sensitivity will vary depending on the amplifier's gain. Below is a concise synopsis of the primary techniques for obtaining current values.

Using a shunt resistor is the first step. This instrument is capable of measuring at various current magnitudes and over a broad frequency range. When there is a unidirectional component in the current waveform, such as with direct current (DC), it is better to employ it. The signal needs to be amplified because the shunt resistor has a low voltage drop; but, doing so will make the device less compact and more expensive. Should shunts be necessary for measuring high currents, their design becomes bulky and leads to issues with heating because of voltage loss. Additionally, shunt resistors are linked to the current conductor in a serial fashion; nevertheless, this kind of connection results in the loading resistance effect. These factors make utilising a shunt resistor to measure current less practical.

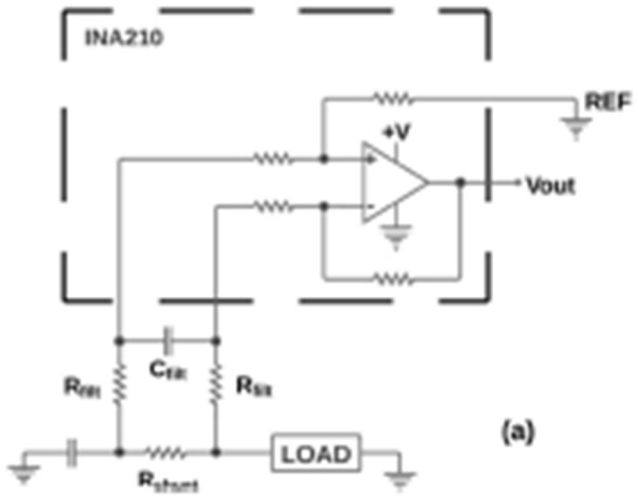

Figure 1-18: A shunt resistor layout with amplifier[22].

A Hall effect current sensor (HECS) can be used as a substitute for the sunt resistor. Its large measurement range, high precision, galvanic isolation between the input and output, numerous sensor configuration options, and outstanding linearity make it the ideal option. Additionally, these devices allow for the performance of AC and DC measurements. These HECSs are actually divided into two groups: closed-loop and open-loop:

- HECS closed-loop: a secondary winding carries the current created by converting the Hall voltage into current via a transistor circuit. This instrument is known for its quick response times and high accuracy; yet, non-linear errors can occasionally occur often. A few scholarly references have demonstrated the measuring of current up to 50 A.
- HECS open-loop: this instrument is recommended for battery-powered applications since it lacks a secondary winding. Their linearity range is more constrained, though. A current measurement up to 30 A with a sensitivity of 0.66 mV/A has been shown in certain investigations.

A common current transducer in power systems, the current transformer (CT) is an additional illustration of a current measurement device. The fundamental idea is that, similar to Faraday's law, the CT produces a fluctuating magnetic field that causes a voltage to be induced in the secondary coil. The current flows via the sensing resistor as a result of this voltage[22].

1.6.2 Voltage measurements

Voltage measurements are made at various voltage levels and locations, including as the output of the PV modules, the inverter's output, cables, and transformers, in order for PV systems to function efficiently and dependably. The divider circuit is a representation of the device used in this kind of application. The literature provides various examples of applications for this sensor. It has been shown to measure temperatures between -25°C and 85°C with an error of ±1% and voltage levels up to 26 V. However, since PV modules have an open circuit voltage higher than 26 V, this sensor is not as useful for many applications[22].

1.6.3 Solar radiation measurements

Solar irradiation is a critical factor in the design of photovoltaic plants and is used to estimate their production, as has been stated extensively in the preceding paragraphs. Pyranometers and pyrheliometers are the two fundamental instruments for this kind of analysis in this instance.

A pyrheliometer has a limited field of view (about 5 degrees) and is positioned directly towards the sun to detect shortwave direct solar radiation, which falls between 300 and 2500 nm. In contrast, pyranometers measure the entire amount of solar radiation in a 180° hemispherical area in the horizontal plane, taking into account a spectral range of 300 to 3000 nm. Below is a list of the most popular kinds of pyranometers used to measure sun radiation:

- Thermopile pyranometers consist of an absorbing detector covered by two glass filter domes. Solar light with wavelengths between 285 and 2800 nm can pass through the glass domes and strike the black heat-absorbing sensor.

- Photometric pyranometers are semiconductor-based sensors that detect light by producing an electric current. Semiconductor-type pyranometers react in approximately 10 μs and are less expensive. Silicon can be utilised as a semiconductor pyranometer sensor because of its high sensitivity to sunlight; however, the wavelength range is quite limited.

Furthermore, according to the PV effect principle, PV reference cells—which are especially employed for photovoltaic systems—have the same structural makeup as a PV module and are utilised to detect solar radiation. PV efficiency is measured under reference conditions by calibrations carried out in accordance with the international standard IEC 60904.

The PV reference cell has an irradiance measurement inaccuracy of roughly ±2.4 percent, whereas the two devices at the top of the list have an uncertainty of about ±5%.

Main performance	Specifications of thermopile pyranometer	Specifications of silicon pyranometer
Spectral range	300–2800 nm	400–1100 nm
Sensitivity	7–14 μV/Wm^{-2}	7–14 μV/Wm^{-2}
Temperature	−40 ~ 50 °C	−40 ~ 65 °C
Response time	<60 s	10 μs

Table 1-2: Technical specifications for solar radiation measurement devices[22].

1.6.4 Temperature measurements

Understanding temperature entails understanding performance, but it's crucial to keep in mind that the PV module's thermal bulk causes a slow temperature response. Installing a sensor on the back surface of the module is the most popular way to detect its average temperature.

In most circumstances, a thermally conductive paste—typically polystyrene, silicon sealant, or extruded polystyrene—can be used to reduce the impact of ambient temperature on module temperature measurement (XPS). Examples of temperature measurement findings can be found in literature: certain devices have an accuracy of ± 0.5 °C and can detect temperatures between -55°C and +150°C. Using digital temperature sensors or K-type thermocouples, which can detect temperatures between -270°C and +1370°C, is an alternative[23].

1.6.5 Data acquisition card

The DAQ card gathers, transforms, and transmits all of the previously described parameters—which are first obtained by their individual sensors as analogue signals—to an interface for a more trustworthy visualisation. There are many DAQ products available on the market that are categorised according to microcontrollers, data transmission, and data storage; however, Arduino boards are the best choice for a variety of autonomous remote measurements and control system applications due to their open access, standard connections, and low cost. Its installation on PV systems for monitoring is made easier by its interoperability with electrical and meteorological sensors. Its installation on PV systems for monitoring is made easier by its interoperability with electrical and meteorological sensors. It should be noted

that all of these characteristics can be incorporated into a SCADA for large PV plants, particularly when a large number of variables and circuits are involved

Data must, of course, be communicated after it is gathered. Either a wired or wireless setup may cause this. As the name implies, the first one allows data transmission over a conductor and an existing power line, but transmission bath impedance within cables can cause distortions and attenuation in the received signals. The most popular route is Ethernet technology. Wireless configuration offers several benefits, including reliability, security, and fast speed. It also has a lot of potential for use with industrial monitoring systems, but the costs can be high and the wiring can be complicated.

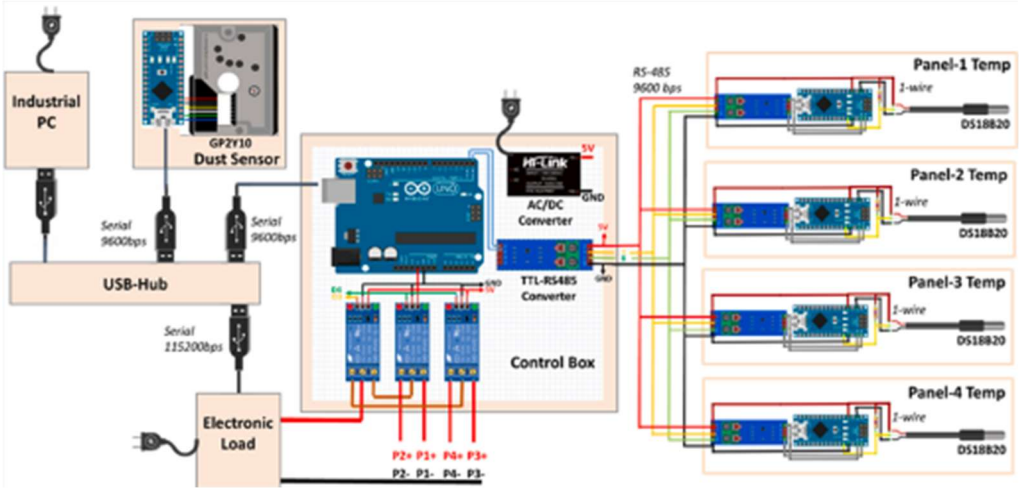

Figure 1-19: Example of a DAQ system block[24].

1.7 PV system energy production assessment

It's critical to assess a PV system's productivity as accurately as feasible throughout design. Given that the amount of energy produced is directly proportional to the amount of solar radiation that enters the photovoltaic generator, the following relationship can be expressed, taking into account the existence of two proportionality factors[25]:

$$E_{AC} = H_g \cdot S_{PV} \cdot \eta_{STC} \cdot PR \tag{1-22}$$

Where:

- E_{AC} - Energy production of the PV plant (kWh).
- H_g - Solar irradiation (kWh/m^2).
- S_{PV} - Total surface of PV generator (m^2).
- η_{STC} - Conversion efficiency (-).
- PR - Performance Ratio (-).

An analogous relationship can be expressed by dividing the daily irradiation (kWh/m^2) by the irradiance of 1 kW/m^2 to find the number of hours per day that a photovoltaic array works at its rated power (h_{eq}). This is due to the fact that a PV generator's rated output is set at a specified reference irradiance, which is determined by tilt and orientation. This virtual duration is defined as "number of equivalent hours" (also known as reference yield or peak solar hours)[8]. Thus, this final idea can be summed up as follows:

$$E_{AC} = P_N \cdot h_{eq} \cdot PR \tag{1-23}$$

With:

- E_{AC} - Energy production of the PV plant (kWh).
- P_N - Sum of power ratings of PV modules at STC, also given by the product between $N_s \cdot N_p \cdot P_{mod}$ (kW).
- h_{eq} - Number of equivalent hours per day, month, year (h/day, h/month, h/year).
- PR - Performance Ratio (-).

In summary, the amount of PV energy produced in a day may be calculated by multiplying the rated power of the PV generator by the number of hours comparable to a day. This is a theoretical value that is part of the performance ratio idea, which is the ratio of energy generated to theoretical energy. This parameter varies depending on the PV system and is also sometimes referred to as the efficiency of "BOS" (Balance Of System). Stand-alone systems with an integrated battery

solution can achieve values between 0.55% and 0.65%, while typical values for PV plants connected to the network are between 0.7% and 0.8%. The following formula can be used to further clarify this idea:

$$PR = \frac{E_{AC}}{P_N \cdot H_g \cdot {}^{1}/_{G_{STC}}} \quad (1\text{-}24)$$

Where:

- PR - Performance Ratio (-).
- E_{AC} - Energy production of the PV plant (kWh).
- P_N - Sum of power ratings of PV modules at STC (kW).
- H_g - Solar irradiation (kWh/m^2).
- G_{STC} = 1 kW/m^2 - STC irradiance.

It is important to note that, in accordance with IEC Standard 61724, the yield is another connection that is helpful to assess the energy productivity:

$$E_{AC} = P_N \cdot Y_R \cdot PR = P_N \cdot Y_F \quad (1\text{-}25)$$

Where:

- P_N - Sum of power ratings of PV modules at STC, also give by the product between $N_s \cdot N_p \cdot P_{mod}$ (kW).
- Y_R - Reference yield or peak solar hours calculated as the ration between H_g and G_{STC} (kWh/m^2/kW/m^2).
- Y_F - Final yield, evaluated as E_{AC}/P_N.
- PR - Performance Ratio (-).

Since one of the objectives of this work is to construct an energy model that would reflect the ideal energy production, it is crucial to evaluate the losses that affect the modules during the conventional process of energy conversion after evaluating the main relations useful to predict the productivity of PV systems[8]. Various losses are concealed within the PR and are as follows[25]:

- Tolerance with respect to STC data and intrinsic mismatch of modules current-voltage characteristics: 3% of losses.
- Frontal glass reflection and dirt: the reflection effect is proportionate to the sun beams that are not normal to the solar glasses (losses of 5–6%), while the impact of dirt is minimal and is determined by the location of the PV plant (losses about 10%).
- A low irradiance level (<400 W/m^2) and a different sun spectrum (with AM=1.5) than the reference one.
- The usage of fuses, breakers, blocking diodes, and wire (which loses roughly 2% of its power).
- A temperature that is higher than or lower than 25 °C. In this instance, losses range from 8% to 12% depending on the plant's location, therefore better cooling is crucial.
- The shading effect, or uneven lighting across all modules, results in minor losses because it only affects the initial few hours close to sunrise and the last few hours close to dusk.
- MPP tracker and DC-AC conversion of the inverter.

Taking these factors into account, the *Performance Ratio* can be represented as the result of several efficiencies that include every contribution listed in the previous list:

$$PR = \eta_{mis} \cdot \eta_{d-r} \cdot \eta_{sp-l} \cdot \eta_{wir} \cdot \eta_{shad} \cdot \eta_{temp} \cdot \eta_{PCU} \quad (1\text{-}26)$$

1.8 Energy models for estimating photovoltaic performance

It is stated that there is a strong correlation between the radiation incident on the module and the nominal power, also known as peak power, that is put on a solar generator. However, there are a number of reasons why the anticipated production of energy may decline.

The preceding paragraphs have already covered the causes and sources of losses. The exact value of each kind of loss for a particular system can be quite challenging to ascertain, though, as doing so typically necessitates the use of intricate mathematical models that don't always yield accurate assessment results. The values for these average losses are frequently obtained from the information already obtained from the analysis of the installed system. They essentially follow statistics, typically falling between 11% and 45% of the total. This is a wide range of fluctuation, and depending on the variables chosen, this can lead to wildly different energy predictions.

Therefore, it is interesting to develop models that can objectively consider most of these losses and reduce the number of values, avoiding a subjective selection (based, for example, on the experience of the person conducting the study), in order to reduce the uncertainty in estimating the energy produced by the PV generator. In the lines that follow, a few examples will be provided.

Osterwald's methodology is one of the most widely used conventional methods for these kinds of computations since it produces excellent results[26]. This method, which is also one of the easiest, may be completely understood in terms of the following relationship:

$$P_m = P_{m,STC} \cdot \frac{G}{G_{STC}} \cdot [1 - \gamma \cdot (T_c - T_{STC})] \quad (1\text{-}27)$$

Where:

- P_m – Maximum power of the cell (W).
- $P_{m,STC}$ – Cell maximum power in Standard Test Conditions (STC) (W).
- G – Measured irradiance (W/m^2).
- G_{STC} – Irradiance in Standard Test Conditions equals to 1000 W/m^2.
- γ – Cell maximum power temperature coefficient (°C^{-1}).
- T_c – Cell temperature (°C).
- T_{STC} – Temperature in Standard Test Conditions equals to 25 °C.

Of course, literature contains a plethora of further examples of relations. Choosing the installation site coordinates and installation parameters, such as the tilt and azimuth of the modules, as well as utilising temperature and irradiance

profiles obtained from weather stations, PVGIS, or other sources, can help ascertain how much power a PV generator can produce in many situations. To produce the most, modules in the northern hemisphere obviously need to be oriented southerly during the design stage, and the tilt needs to be selected according to latitude. The irradiance and temperature profile are used to assess the PV generator's energy production after the optimal configuration has been determined.

The single diode model (SDM) is used in literature more frequently than other models for the calculation of energy generation. The P_{DC} is calculated using the equivalent circuit, but one of the primary problems with using this model is that it requires incorrect definition of the five parameters ($I_{ph}, R_{sh}, R_s, n, I_0$).) that are included in the single diode model. Numerous sets of parameters can be found in the literature, but they are either assumed to be constant values, connected to outdated modules, or simply helpful for study. Because of this, it is incorrect to evaluate the power and energy production of actual PV modules using these data. However, when working with commercial PV modules, it may be feasible to determine their values through an experimental process by utilising particular equations to specify their reliance on temperature and irradiance, as well as estimating their energy production [27].

P_{DC}, or DC power production, is defined as the P-V curve's greatest value. Next, using the following formula, the AC production P_{PV} at T_C (cell temperature) and G is determined:

$$P_{PV}(G, T_c) = P_{DC}(G, T_C) \cdot \eta_{ARRAY} \cdot \eta_{PCU} \quad (1\text{-}28)$$

Where:

- η_{ARRAY} allocation of losses resulting from dirt, glass reflection, I-V curve mismatch, and Joule effect in cables.
- η_{PCU} takes into account conversion losses as well as tracking the maximum power point (MPP).

1.9 Causes of underperformance in PV plants

The idea of losses at the level of photovoltaic cell and photovoltaic module has been extensively discussed in paragraphs 1.1.6 and 1.7. Regretfully, there are a few more elements that can affect a PV plant's performance; these will be briefly mentioned in the lines that follow.

1.9.1 Reliability and availability

A PV plant, in contrast to many power generation arrangements, does not have moving parts; hence, extensive maintenance is not anticipated. Furthermore, this technology's minimal costs of operation, maintenance, and installation help to make it one of the most dependable. Since PV modules are the most crucial component, it is obvious that their dependability directly affects the reliability of the complete PV plant. Production flaws and mechanical cracks may occasionally be regarded as the primary cause of losses.

As was previously mentioned, unfavourable operating circumstances like as inclement weather, low irradiance values, high air temperatures, and the natural deterioration of PV materials can all have a significant effect on PV production and cannot be completely avoided. The plant is not regarded as being as maintenance-free if failures resulting from problems with transportation, design, or operating stages are also taken into consideration.

The ability of a system or component to function as intended for a predetermined amount of time under predetermined environmental and operating circumstances is known as reliability. This definition makes it essential for assessing potential problems in photovoltaic plants and ensures that the generated power is accurately estimated. Numerous examples and findings of reliability analyses on photovoltaic generators can be found in the literature. These analyses may consider the system as a whole, the network as a global variable or at the component level, the deterioration of PV modules and faults associated with harsh climate conditions, or a thorough risk analysis.

Depending on the component's life stage, this analysis can be used to determine a failure rate for the component, which shows a predicted number of times an object will break over a given period of time. Additionally, the mean time to failure

(MTTF), mean time to repair (MTTR), and mean time between failures (MTBF) are characteristics included in this assessment. By knowing these numbers, it is possible to compare the expected dependability of various systems.

Availability, which is defined as the likelihood that the system will function when needed, is typically combined with reliability analysis. It is measured as the ratio of uptime, or the system's effective operation time, to its expected operation time. The availability of a component spans from 0% to 100%. This idea will come up a lot in this thesis while discussing plant inverters [28].

1.9.2 Failures in PV plants

It is impossible to establish a single, unique structure for PV plants that would apply to all PV systems because each system requires a fixed number of equipment and is modular, meaning that devices can be added or removed without causing problems. A simplified diagram of a photovoltaic plant typically illustrates how the parts are connected in a cascade fashion. As a result, the failure of a breaker, diode, or fuse connected to a string can have an impact on the plant's overall power output. It is important to note that a decrease in power output brought on by low irradiance or an electronic mismatch between PV modules is only regarded as a cause of power loss rather than a defect.

Power production and losses are influenced by the type of DC/AC converter configuration used. Components that have the lowest reliability over a given operating time (such as ten years) are string and multistring inverters (with more than one MPPT), centralised inverters, and string inverters with only one MPPT. Fuses fall under the same heading as well. When fitted incorrectly, for instance, they may experience a faster breaking time. For instance, direct sun exposure can cause a significant amount of heat stress, which can quickly damage the fuse enclosures.

The mean time to failure (MTTF) for a selection of PV plant component parts is displayed in the following figure. This is an illustration from the literature that provides a summary of the devices that are more prone to malfunctions.

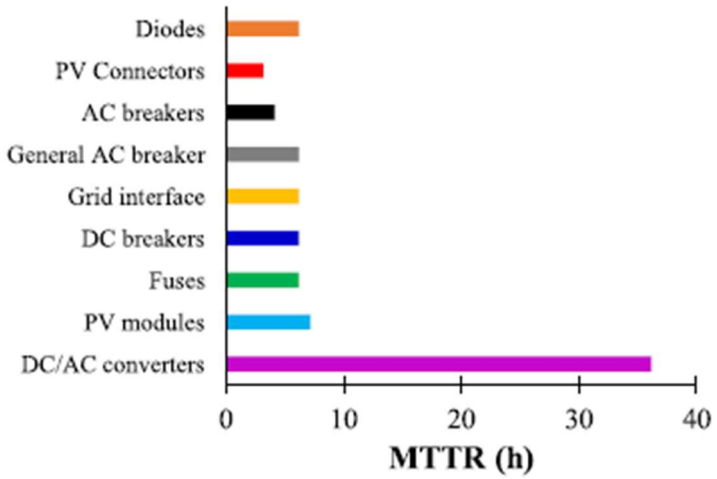

Figure 1-20: Mean time to failure (MTTF) for PV plant components[28].

Of course, maintenance tasks are involved with defects. Because an availability of more than 90% should be ensured, high rated power plants require less maintenance. This results in a shorter time between failure discovery and failure restoration, which reduces power losses. Conversely, low-rated power plants typically lack maintenance contracts. However, some preventive measures can be taken to lower the likelihood of failures, such as installing high-efficiency photovoltaic modules, sizing the DC/AC converter, or reducing the number of parallel PV strings connected in series (thereby avoiding the need for numerous fuses).

Chapter 2

2 Objective of the master thesis and calculation model used

2.1 Introduction

This master thesis, written by the undersigned, has been conducted through the collaboration of three universities: Politecnico di Torino, Universidad de Jaén, and Lublin University of Technology. The main subject of this thesis will be briefly mentioned here, but the various issues of the case study will be subsequently explored in depth. This project focuses on studying a photovoltaic plant located in Poland, near the town of Bordziłówka, approximately 77 km from the city of Lublin. The PV plant in question is a 1.4 MWp facility installed in 2014. The adverse meteorological conditions of the area, with frequent snow falls during certain periods of the year, tend to cover the solar irradiance sensors, leading to incorrect data readings, among other issues.

The aim of this study is to find an alternative method to evaluate whether the energy production of the PV plant aligns with the prediction based on solar irradiance and temperature conditions. For this comparison, data measured from the PV plant (such as solar irradiance, temperature, and instantaneous power) will be analyzed and compared to data from a weather station (which records solar irradiance and ambient temperature) located in a nearby town, named Włodawa, 44.8 km away from the PV plant. Additionally, this study will incorporate other datasets from relevant databases (PVGIS, SOLCAST) to fill any gaps in the data received from the weather station and the PV plant, and to facilitate comparisons.

By using these combined datasets along with specific models, a study capable of comparing the expected DC energy production with the actual DC production is aimed to be created. This comparison can help identify alternative methods to detect issues within the PV plant that cause a decrease in energy production.

This study is organized around two main analysis. The first objective involves a detailed analysis of various models used to transpose solar irradiance measured on a horizontal plane to an inclined plane. The second objective focuses on applying models to predict energy production and on comparing actual energy production data with model-based predictions. The primary goal is to assess whether these models, when applied to the available data, can effectively monitor performance. This process involves using various irradiance and temperature data to estimate the ideal energy production on specific days and comparing these estimates with the actual energy measured from the inverter on the DC side to identify any alignment or discrepancies.

In the subsequent sections, the primary models used to compute solar angles, such as zenith and azimuth angles, and various models for transposing solar irradiance data from horizontal to inclined planes will be explored. Specifically, the ASHRAE model and the Olmo model for these purposes will be explained in the following lines.

2.2 Solar Angles

In this subsection, the fundamental concepts related to solar angles, which are essential for understanding the location of the Sun referred to a specific point on the Earth's surface, will be explored. This includes the definitions of primary solar angles and the mathematical models necessary for their calculation. Latitude, longitude, standard time, solar time, and various solar angles such as the zenith angle, azimuth angle, and others will be defined[29].

2.2.1 Key angles description

Solar angles play a crucial role in determining the Sun's position in the sky at any given time and location. These angles involve some others below explained with the help of Figure 2-1:

- *Solar Declination (δs)*: The angle between the rays of the Sun and the plane of the Earth's equator.
- *Solar Hour Angle (ωs)*: The angle between the local meridian and the meridian passing through the Sun.
- *Solar Altitude Angle (αs)*: The angle between the Sun's rays and the horizontal plane.
- *Zenith Angle (θz)*: The angle between the Sun's rays and the vertical direction (zenith).
- *Solar Azimuth Angle (γs)*: The horizontal angle between the direction of the Sun and the south direction[29].

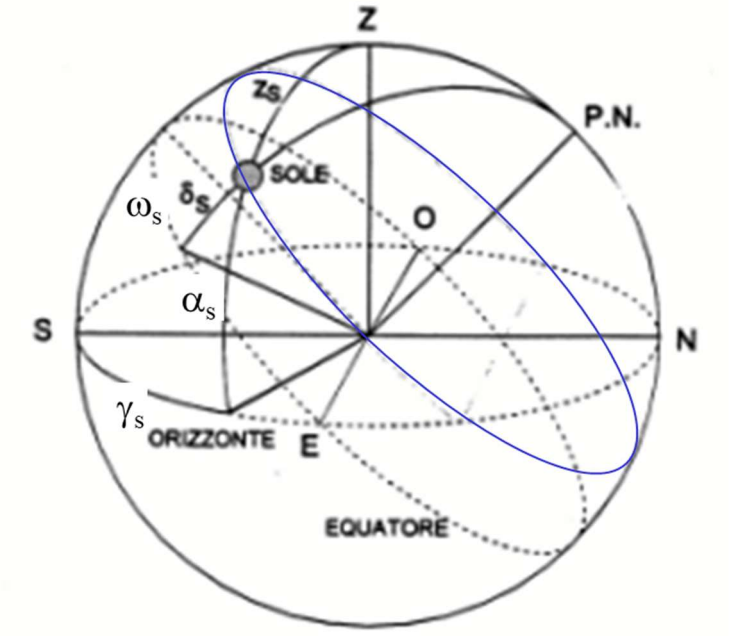

Figure 2-1 - Solar angles[29]

Latitude, Longitude and Time Zone

Latitude (Φ) represents the angle between the equator and a point on the Earth's surface measured along the meridian of that point (positive towards North) (refer to Figure 2-2). *Longitude* (L) indicates the angle between the prime meridian (Greenwich) and the meridian of the point under study (positive towards West). Longitude affects the time zone of a location, determined by the longitudinal position relative to the prime meridian.

Longitude plays a crucial role in defining *time zones*. Generally, time zones are divided by lines of longitude, with each zone representing a one-hour difference from Coordinated Universal Time (UTC, also called Zulu time zone). In Europe, most countries use Central European Time (CET), which is UTC+1. However, the United Kingdom, Ireland, and Portugal use Western European Time (WET), which is the same as UTC. Additionally, several countries in Eastern Europe, such as Greece, Bulgaria, and Romania, use Eastern European Time (EET), which is UTC+2. The different time zone above mentioned can graphically visualise in Figure 2-2. Specifically, Poland, which is the focus of this study, uses Central European Time (CET), aligning with UTC+1. This classification ensures that timekeeping is relatively uniform within each zone, reflecting the longitudinal position relative to the prime meridian[29].

Figure 2-2 – Time zone[29]

Standard Time and Solar Time

Standard time is the local time based on the time zone of a specific location. Solar time, on the other hand, is based on the position of the Sun in the sky dome and can differ from standard time due to the equation of time which is defined by Equation 2-2. The equation of time accounts for the Earth's elliptical orbit and axial tilt, causing variations in the apparent solar time throughout the year. The solar time can be calculated using the following formula:

$$Solar\ time = Standard\ time - \frac{(L_{loc} - L_{std})}{15} + \frac{E}{60} + DST \quad (2\text{-}1)$$

where:

- *Lloc* is the local longitude,
- *Lstd* is the standard longitude, the longitude of the meridian for the local time zone,
- *E* is the equation of time in minutes, which takes into account the perturbations in the Earth's rate of rotation affecting the time when the Sun crosses the observer's meridian. This correction varies according to the day of the year. The formula for the equation of time is:

$$E = 229.2(0.000075 + 0.001868\cos(B) - 0.032077\sin(B) - 0.014615\cos(2B) - 0.04089\sin(2B)) \quad (2\text{-}2)$$

Where *B* is in degrees:

$$B = \frac{360}{365}(n - 1) \quad (2\text{-}3)$$

and n is the day of the year.

- *DST* is the daylight-saving time correction, where *DST*=1 when daylight-saving time is observed, and DST=0 when daylight-saving time is not observed, varying with the time of the year[29].

Hour Angle

Hour angle is the angular displacement of the Sun from the local meridian, at $\frac{360°}{24\,h} = 15$ degrees per hour:

ω = (*Solar Time* - 12) × 15° (2-4)

With these definitions ω will be negative in the morning before noon and positive in the afternoon after noon. Solar time must be in hours and hour angle in degrees.

Declination

Declination, δ, is the angle between the Earth-Sun line and the Earth Equator plane, with positive values indicating direction towards the North. This angle significantly influences the seasons, with its impact being more pronounced at higher latitudes (in terms of absolute value), while seasonal differences tend to diminish closer to the Equator. The declination is a continuously varying function throughout the year, reaching its minimum value of -23.45 degrees at the winter solstice and its maximum value of +23.45 degrees at the summer solstice. The declination angle above mentioned can be graphically visualise in Figure 2-3[29].

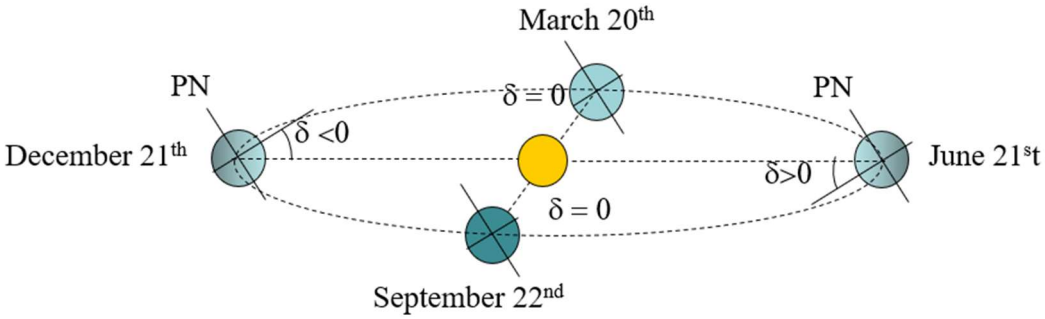

Figure 2-3 - Declination angle[29]

For most engineering calculations, the declination can be determined using the approach given by Cooper formula, which expresses it as a function of the time of year, denoted by "*n*" representing the ordinal day of the year (from 1 to 365):

$$\delta = 23.45 \sin\left(360\frac{284+n}{365}\right) \quad (2\text{-}5)$$

Where δ and the sinusoidal argument are both in degrees[29].

Zenith Angle

The Zenith angle (θ_z) depends on three angles:

- Φ = latitude (depending on geographical location)
- ω = hour angle (depending on the hour of the day)
- δ = declination (depending on the day of the year)

The Equation 2-6 defines the zenith angle:

$$\cos\theta_z = cos\,\Phi\cos\delta + \sin\Phi\sin\delta \quad (2\text{-}6)$$

Gives the angular distance from the Zenith or above the horizon of the Sun. Figure 2-4 is presented to enhance clarity on the concept of the Zenith angle.

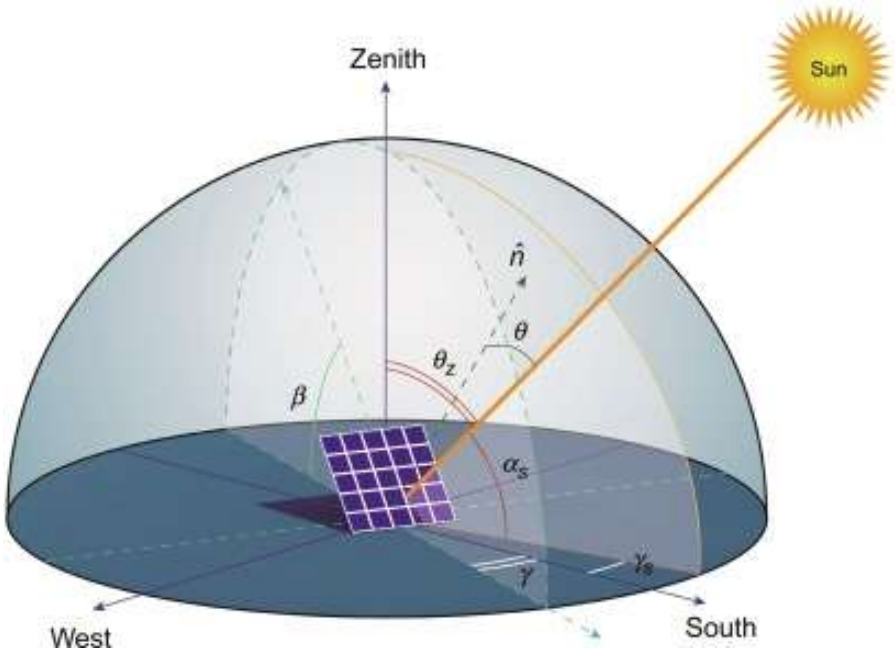

Figure 2-4 – Zenith angle[30]

Solar Azimuth Angle

The solar azimuth angle (γ_s) can have values in the range of 180° to - 180°, and has the same sign convention as the hour angle, ω. The solar azimuth angle is calculated with:

$$\gamma_s = sign(\omega) \left| \frac{\cos(\theta_z) \sin(\Phi) - \sin(\delta)}{\sin(\theta_z) \cos(\Phi)} \right| \quad (2\text{-}7)$$

The graphical representation of the angle described in Figure 2-4 above can be examined[29].

Angle of incidence

The geometric relationship between a plane of any particular orientation (tilt angle above the horizontal (β), and surface azimuth (γ_s)) and the incoming beam solar radiation, that is, the position of the Sun relative to that plane, is described by the *incidence angle* (θ) between Sun beam and normal to surface. The angle discussed earlier can be visualized through Figure 2-4 above.

To compute θ at a certain time during the year, the following equation can be used:

$$\cos\theta = \cos\theta_z \cos\beta + \sin\theta_z \sin\beta \cos(\gamma_s - \gamma) \quad (2\text{-}8)$$

If the angle θ exceeds 90°, it means that the Sun is behind the surface. For tilted surfaces sloped due South (typical for North hemisphere) $\gamma = 0$.

The fundamental concepts of solar angles and related parameters, such as latitude, longitude, solar time, and standard time, have been introduced in this subsection. The necessary formulas for computing the solar altitude angle, zenith angle, and azimuth angle were discussed. These concepts and formulas are essential for understanding the Sun's position and are crucial for analyzing the performance of photovoltaic systems[29].

2.3 Irradiance correction: ASHRAE model

The ASHRAE model provides a simple yet sufficiently accurate method for engineering computations of clear sky radiation. It leverages empirical adaptations of Beer-Bouguer's Law to estimate the beam component of direct normal irradiance and considers diffuse radiation as a combination of isotropic, circumsolar, and horizon brightening components. Additionally, starting from this model, the irradiance data received from the weather station will be adapted to an inclined plane at an angle beta. This angle represents the orientation of the photovoltaic panels in the system under consideration. The adaptation process will utilize inverse formulas. Further details will be explained in Chapter 4, 'Description of the Procedure Followed'[31].

2.3.1 Model description

In the ASHRAE model, the beam component of irradiance (G_{bn}) is determined by an empirical adaptation of Beer-Bouguer's Law:

$$G_{bn} = A\ e^{-B \cdot AM} = A\ e^{-\frac{B}{cos\,(\theta_z)}} \tag{2-9}$$

Where A represents the apparent solar constant (W/m²), B denotes the extinction coefficient (-), and θ_z is the solar zenith angle. Under this assumption, G_{bn} depends solely on the air mass. However, both the apparent solar constant and the extinction coefficient vary throughout the year due to changes in atmospheric turbidity.

Diffuse radiation from the sky is composed of three main parts: an isotropic part, received uniformly from the entire sky; circumsolar diffuse radiation, resulting from forward scattering of solar radiation concentrated around the sun; and horizon brightening, concentrated near the horizon, particularly pronounced in clear skies. The ASHRAE model assumes a completely isotropic sky, where diffuse radiation does not depend on orientation. The diffuse horizontal irradiance (G_{dh}) is calculated as:

$$G_{dh} = C\ \ G_{bn} \tag{2-10}$$

Where *C* is a coefficient dependent on atmospheric conditions and the day of the year. The values of the three parameters *A*, *B* and *C* depend on the day of the year. They are given in the Table 2-1, showed below, for the 21^{st} of each month.

21st of month	***A* (W/m²)**	***B* (-)**	***C* (-)**
January	1229	0,142	0,058
February	1213	1,144	0,06
March	1185	0,156	0,071
April	1134	0,18	0,097
May	1103	0,196	0,121
June	1087	0,205	0,134
July	1084	0,207	0,136
August	1106	0,201	0,122
September	1150	0,177	0,092
October	1191	0,16	0,073
November	1220	0,149	0,063
December	1232	0,142	0,057

Table 2-1 - values of parameters *A*, *B* and *C*[31]

The total horizontal irradiance (G) is obtained by summing the beam and diffuse components:

$$G = G_{bn} + G_{dh} = (\cos(\theta_z) + C)\, G_{bn} \tag{2-11}$$

When calculating irradiance over a tilted surface, an additional isotropic component arises from irradiance reflected from the ground onto the tilted surface. The total irradiance on a tilted surface (G_t) is expressed as:

$$G_t = G_{bn}\cos(\theta) + G_d\, F_{c-s} + \rho\, G\, F_{c-g} \tag{2-12}$$

Where F_{c-s} and F_{c-g} represent collector-sky and collector-ground view factors respectively:

$$F_{c-s} = \frac{1+\cos(\beta)}{2} \tag{2-13}$$

$$F_{c-g} = 1 - F_{c-s} = \frac{1-\cos(\beta)}{2} \quad (2\text{-}14)$$

ρ is the *albedo* of the underlying surface, representing the fraction of solar radiation reflected by the ground.

In summary, the ASHRAE model offers a practical framework to estimate solar irradiance under clear sky conditions, incorporating both beam and diffuse components to facilitate engineering applications in solar energy systems and building energy performance assessments[31].

2.4 Irradiance correction: Olmo model

The Olmo model is a method developed to estimate solar radiation on inclined surfaces using data collected on horizontal surfaces. This model is advantageous because it does not require separate measurements of direct and diffuse solar radiation components. Instead, it relies on the total solar irradiation on a horizontal surface, along with incidence and solar zenith angles, as input parameters[32].

2.4.1 Model description

In the Olmo model, the global irradiance (G_β) on an inclined surface is estimated from the corresponding solar radiation (G) on a horizontal surface using the following equation:

$$G_\beta = G\ \psi_0 \quad (2\text{-}15)$$

Here, β is the surface inclination angle, and ψ_0 is a function that converts horizontal solar radiation to that incident on a tilted surface. This function is given by:

$$\psi_0 = e^{K_t\,(\theta^2 - \theta_z^2)} \quad (2\text{-}16)$$

where θ and θ_z (in radians) are the incidence and solar zenith angles, respectively.

The *clearness index* (K_t) is a crucial parameter in this model. It is defined as the ratio of the global solar radiation received at the Earth's surface to the extraterrestrial solar radiation received at the top of the atmosphere:

$$K_t = \frac{G}{G_0} \tag{2-17}$$

The extraterrestrial solar radiation (G_0) can be calculated using the formula:

$$G_0 = E_0\, SC \tag{2-18}$$

where *SC* is the solar constant, representing the intensity of solar energy across the electromagnetic spectrum that crosses a unit area perpendicular to the direction of the solar beam outside the Earth's atmosphere. This value is referred to as the Total Solar Irradiance (*TSI*), which fluctuates, so *SC* is currently defined as the long-term average. Nowadays, the value of *SC* is estimated to be 1367 W/m²[33]. E_0 is the correction factor (-) of the Earth's orbit and is given by:

$$E_0 = 1 + 0.033 \cos\left(2\pi\, \frac{n_{day}}{365}\right) \tag{2-19}$$

where n_{day} is the day of the year.

To account for anisotropic reflections, Olmo model proposed a multiplying factor (F_C), which is given by:

$$F_C = 1 + \rho\, sin^2\left(\frac{\theta}{2}\right) \tag{2-20}$$

where ρ is the *albedo* of the underlying surface, representing the fraction of solar radiation reflected by the ground.

Combining these elements, the Olmo model to determine the global solar radiation on an inclined surface (G_β) from the horizontal surface radiation (G) is expressed as:

$$G_\beta = G\, \psi_0\, F_C \tag{2-21}$$

However, since K_t, which is calculated as G/G_0, is utilized by the Olmo model, it has been acknowledged that this evaluation may not fully accommodate the variability in cloud cover throughout the day. When applied instantaneously, during the early and late hours of the day, K_t values are very low because G is very low

while G_0 remains relatively constant. This is because, during these times, the sun is rising or setting, resulting in lower solar radiation measurements on the horizontal plane. Therefore, during these times of the day, K_t might indicate a falsely low value, suggesting that the day is cloudy.

The Olmo model was modified to address this issue. The model remains essentially the same, but K_t is replaced by the *clear-sky index* (K_c) (Equation 2-24). K_c is calculated by keeping the same numerator as K_t, which is the measured G on the horizontal plane but changing the denominator. Instead of using G_0, $G_{clear-sky}$ is used. This value represents the solar radiation that would be received at that specific time of the day if it were a completely sunny day. $G_{clear-sky}$ can be calculated using the ASHRAE model previously shown or can be directly obtained from databases such as PVGIS or SOLCAST.

Combining these elements, the modified Olmo model for determining the global solar radiation on an inclined surface (G_β) from the horizontal surface radiation (G) is expressed as:

$$G_\beta = G\ \psi_0\ F_C \tag{2-22}$$

where ψ_0 is now defined using K_c:

$$\psi_0 = e^{K_c\,(\theta^2-\theta_z^2)} \tag{2-23}$$

The clear sky index K_c is defined as:

$$K_c = \frac{G}{G_{clear-sky}} \tag{2-24}$$

These two models will be utilized and analyzed for the specific case study under consideration[32].

Chapter 3

3 Description of the installations and data under study

3.1 Introduction

Chapter 3 delves into the detailed description and analysis of the installations and datasets under study. It provides a comprehensive overview of the photovoltaic plant, detailing its geographical location, installed capacity, and the technical specifications of its main and experimental sections. Furthermore, it outlines the methodology employed for monitoring and data collection, shedding light on the tools and techniques utilized to gather information on energy production and environmental parameters.

As previously mentioned in Chapter 2, the adverse meteorological conditions of the area, with frequent snowfalls during certain periods of the year, tend to cover the solar irradiance sensor, leading to incorrect data readings, among other issues. For this reason, this study incorporates additional datasets from relevant databases (nearby weather station, PVGIS and SOLCAST) to fill any gaps in the data recorded from the PV plant, and to facilitate further analysis.

In summary, Chapter 3 sets the stage for a detailed examination of the installations and data, which provides essential background information necessary for understanding the subsequent chapters's findings and conclusions.

3.2 Photovoltaic plant description

The aim of this section is to offer a comprehensive overview of the PV system, including its key components, employed technologies, and main features. This will enable a full understanding of the structure and characteristics of the photovoltaic system. Furthermore, the data collected from the system will be presented, which includes energy production information and other relevant parameters. These data will be described providing a clear understanding of the system's characteristics and its components.

In short, this subsection represents an important starting point for understanding the photovoltaic system under study, which offers a detailed description of its technical characteristics that will be further analyzed in subsequent subsections.

3.2.1 PV Plant

The photovoltaic (PV, hereafter) system under study is installed in Bordziłówka, specifically at a latitude of 51° 50' 47" N and a longitude of 23° 9' 45" E and at an altitude of 145 meters above sea level. This system is designed to exploit the local solar irradiance and comprises a total installed capacity of 1.4 MWp, which includes both the main installation and an experimental section featuring various PV technologies. The primary installation consists of polycrystalline silicon (pc-Si) modules, while the experimental section includes CIGS, CdTe, and a-Si thin-film modules. A section of the PV plant under study can be visualise in Figure 3-1[34][35].

Figure 3-1 - Experimental setup consisting of the pc-Si PV modules under study[34].

Main Installation

The main part of the PV plant consists of 5560 Renesola JC250M-24/Bb polycrystalline silicon modules, each with a nominal power of 250 Wp, resulting in a total capacity of approximately 1.39 MWp for this section. The modules are mounted at an optimal tilt angle of 34° facing south, with rows spaced 6.3 meters, to minimize shading and optimize energy capture[35].

The electrical parameters for the pc-Si modules are as follow in the Table 3-1:

Parameter	Value
Maximum power (P_{max})	250 Wp
Maximum power (P_{max})	37.4 V
Nominal voltage (V_{mpp})	30.1 V
Short-circuit current (I_{sc})	8.83 A
Nominal current (I_{mpp})	8.31 A
Efficiency	15.4%
Temperature coefficients	β = -0.30 %/°C, α = +0.04 %/°C, γ = -0.40 %/°C

Table 3-1 - Electrical parameters for the poly-Si modules[35]

The main system is grid-connected via approximately 70 Delta Solivia 20TL inverters, each with a nominal DC power of 20.4 kW and AC power of 20kW. These inverters, which connect to the pc-Si strings, feature two maximum power point trackers (MPPTs) and an efficiency of up to 98%[34].

Experimental Section

The experimental section of the PV plant includes three different types of thin-film modules and a subset of pc-Si modules. Specifically, it comprises:

- 24 CIGS modules (155 Wp each, total 3.72 kWp)
- 44 CdTe modules (75 Wp each, total 3.3 kWp)
- 36 a-Si modules (95 Wp each, total 3.42 kWp)

- Additionally, 85 pc-Si modules, each with a power output of 250 Wp, are included in the experimental section.

Each type of thin-film module is connected to the same brand inverter, Delta Solivia 3.3TR (3 inverter in total), which has a nominal AC power of 3.3 kW and a maximum efficiency of 96.2%. These inverters support a DC operating voltage range from 200 V to 1000 V and are equipped with a single MPPT.

The polycrystalline (pc-Si) modules are connected to the grid using an inverter with nominal apparent AC power 20 kW, characterized by the maximum efficiency of 98%, Euroeta efficiency of 97.8%, operating temperature range −20° to 60°C and maximum input voltage of 1000 V. The inverter is equipped with two maximum power point trackers (MPPT), 51 modules are connected to the one tracker (3 strings) and 34 modules to the second tracker (2 strings). A schematic diagram of this connection is shown in Figure 3-2.

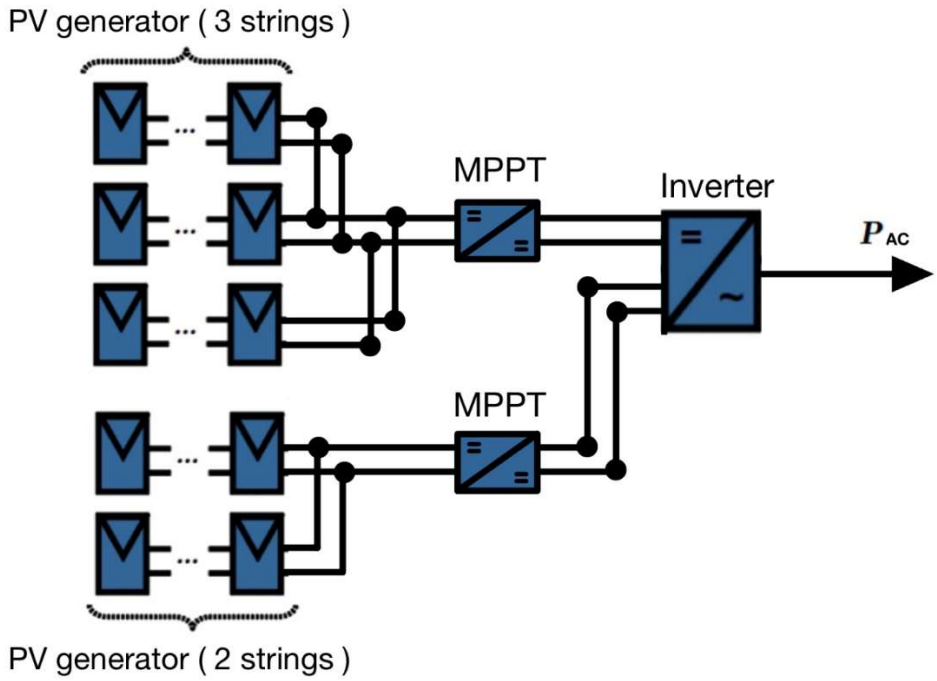

Figure 3-2 - System connection scheme

The technical specifications for the thin-film modules are as follows in the Table 3-2:

Module Type	Efficiency (%)	V_{oc}(V)	I_{sc} (A)	V_{mpp}(V)	I_{mpp}(A)	Power Temperature Coefficient (%/°C)
CIGS	12.6	109	2.2	82.5	1.88	-0.31
CdTe	10.6	59.6	2.15	42	1.82	-0.25
a-Si	6.0	100	1.62	73	1.3	-0.20

Table 3-2 - Technical specifications for the thin-film modules[35]

It is important to note that the experimental section was specifically designed for carrying out research and analyses on these technologies. However, in this thesis's case study, the analysis will focus solely on the data from the polycrystalline silicon modules, specifically for June 2022. As previously mentioned in Chapter 2, the local adverse meteorological conditions, such as frequent snowfalls, often lead to sensor coverage and incorrect data readings. This issue prompted the need for conducting this study. Analyzing data from June, a month typically devoid of snow, may seem unusual in this context. However, when addressing complex issues, it is prudent to begin with scenarios where conditions are favourable before progressing to more challenging situations in subsequent research phases. Future studies aim to extend the analysis to encompass longer time periods and larger sections of the PV plant, which will be addressed in subsequent research endeavours[35].

Monitoring and Data Collection

The system's performance is closely monitored using a combination of reference cells and meteorological data. Solar irradiance is measured by a monocrystalline silicon reference cell, calibrated to an accuracy of ±5% and covering a range of 0–1200 W/m². The temperature of the PV modules is measured on-site using Pt1000 temperature sensor[34].

3.2.2 Data recorded in the PV plant

Regarding the PV plant dataset, the data is available only for the experimental section with a total output of 21.25 kW. This string comprises two sub-strings (DC1 and DC2), each connected to a maximum power point tracker (MPPT) and they are both linked to the same inverter, as illustrated in Figure 3-2 previously. The recorded parameters include DC input powers (DC1 and DC2) and three-phase AC output power (AC1, AC2, and AC3), all measured in watts (W). It is important to note that the data are provided with non-reagular time steps, sometimes recorded every 4 minutes, other times every 5 or 6 minutes, throughout June 2022. This issue arises due to timing errors in the measurement system. Additionally, module's temperature (T_{ref}), in Celsius degrees and irradiance taken from a reference cell are also measured.

Solar irradiance was measured using a monocrystalline silicon cell (5 × 3.3 cm), which was tilted at the same angle as the modules. This system works by converting sunlight into an electrical current, which is proportional to the intensity of the solar irradiance. The output current is then used to determine the irradiance level. The irradiance range of the sensor is 0–1400 W/m², with a resolution of 1 W/m². The accuracy of the sensor is ±5%. The temperature of the module was measured using a Pt1000 resistance temperature detector, which has a measurement range from -40°C to 70°C.

3.3 Weather station description

This section explores essential data collected from a nearby weather station, crucial for the analysis conducted in this thesis. As mentioned earlier in Chapter 2, the data from this facility are analyzed because the weather station is located at a relatively close distance to the photovoltaic plant, approximately 44 km away. Therefore, these data can be used for comparative analysis purposes. The station's equipment and the received data, including measurements of solar irradiance and air temperatures, will be examined to provide an empirical basis for the evaluations.

3.3.1 Włodawa Weather station

The weather station considered in this study is located in the town of Włodawa, Poland, at the geographical coordinates 51° 32' 41" N latitude and 23° 32' 52" E longitude.

The station is equipped with a pyranometer Kipp and Zonen CMP3 designed to measure solar irradiance on the horizontal plane, which is a critical parameter for assessing solar energy potential. Additionally, there is a system on-site to measure air temperature; however, detailed information regarding its features (brand and model) are currently unavailable.

The irradiance data collected from the weather station by the pyranometer on the horizontal plane and the air temperature measurements are managed and maintained by The Institute of Meteorology and Water Management - National Research Institute (IMGW-PIB) in Poland. IMGW-PIB is responsible for collecting and broadcasting meteorological and hydrological data across the country. These data, obtained from IMGW-PIB, are utilized for the analysis of solar energy applications in the region, among other purposes.

3.3.2 Data available from Włodawa weather station

For the Włodawa weather station, data measured by a pyranometer installed at the station is accessible, providing irradiance (W/m²) readings solely for the horizontal plane. These readings are recorded at one-minute intervals for June 2022. Additionally, the weather station provides daily averages (T_{ave}), maximums (T_{max}), and minimums (T_{min}) of temperature. This study focuses exclusively on the data from the month of June. As mentioned before, there are plans to extend the temporal scope of the analysis in the future, but this is not addressed in the current study.

3.4 SOLCAST

SOLCAST is a leading provider of solar energy forecasting and solar radiation data services. It uses advanced satellite imagery, weather models, and machine learning techniques. Then, SOLCAST delivers highly accurate and real-time solar irradiance forecasts. These forecasts are crucial to optimize solar power PV plant performance, to manage energy grids, and to advance research and development in renewable energy.

SOLCAST offers a range of services through their API (application programming interface), which can be accessed in both free and paid tiers. While the free tier provides limited access suitable for small-scale projects or research purposes, it is important to note that accessing the full range of data and features requires a paid subscription. This limitation may pose a challenge for comprehensive analysis. The paid tiers offer unlimited data access and additional features designed for commercial and industrial applications. However, it is essential to consider the associated costs when evaluating the suitability of SOLCAST's services for a particular project or research endeavor, as unlimited data access requires a paid subscription. In case study under consideration, which focuses solely on data from June 2022, there are no issues as the amount of data to be downloaded is limited, and a premium account is not necessary. However, it is important to note that if this study is to be extended to longer time periods, the cost associated with using this database must be taken into consideration.

As previously discussed, data from SOLCAST's API will be utilized in the analysis. These data will be valuable for conducting comparisons and filling gaps in the PV plant monitoring system dataset that are required but, not readily available for reason that will be explain later.

3.4.1 Data analysed from SOLCAST

Data specific to June 2022, recorded at a 5-minute interval, was accessed leveraging SOLCAST. This dataset includes irradiance (W/m^2) measurements on both horizontal and inclined planes, based on the PV plant's coordinates. Moreover, clear-sky irradiance data for the horizontal plane was extracted utilizing the Włodawa weather station's coordinates.

3.5 PVGIS

PVGIS, which stands for Photovoltaic Geographical Information System, is an important online tool developed by the European Commission for predicting the energy performance of photovoltaic systems based on their geographical location. This service offers a range of free tools that allow users to estimate the performance of their solar installations, providing information on solar irradiance, photovoltaic energy production, and other relevant parameters. However, it is important to note that PVGIS provides data only up to the year 2020, and there is no availability of more recent data beyond that date.

As discussed earlier, PVGIS data will be utilized for the analysis. These data will be valuable for conducting comparisons and filling gaps in the dataset that are required but not readily available.

3.5.1 Data analysed from PVGIS

Using PVGIS, the coordinates of the PV plant's location were provided to extract data pertaining to that specific site. Specifically, data related to the air temperature (T_{amb}, in °C) and solar irradiance (G, in W/m²) for a typical meteorological June day at the given coordinates was requested. The data retrieved from PVGIS is provided with an hourly frequency, meaning there is one data point per hour. Additionally, solar irradiance data for a clear-sky day in June was selectively extracted using the coordinates of the Włodawa weather station. The hourly data frequency allows the variations in air temperature and solar irradiance throughout the day to be analyzed, providing detailed insights into the conditions that affect the performance of the PV plant.

Chapter 4

4 Description of the procedure followed

4.1 Introduction

In this chapter, the main steps used to conduct the procedures of this master thesis will be described. To perform the numerical calculations necessary, the MATLAB programming language was used throughout the study. Various data from different sources were used as inputs, but since the data received from the photovoltaic plant comes only to June 2022, the entire study will be based exclusively on data from this period. However, in this thesis, only this timeframe will be addressed. In the future, after consolidating the foundations of the analysis, the temporal scope could be expanded to cover a longer period.

Below, a block diagram is illustrated in Figure 4-1, which outlines various procedures executed. In each subsequent subchapter will describe in detail what was done within each of these blocks. Each of these steps is crucial for ensuring a comprehensive analysis of the photovoltaic plant's performance. As mentioned in Chapter 2, this study is organized around two main analysis. The first one entails a comprehensive examination of various models useful for converting solar irradiance measured on a horizontal plane to an inclined plane. The second analysis focuses on using these models to predict energy production and on comparing the actual energy production data with the predictions. The primary aim is to assess whether these models, when applied to the available data, can effectively monitor the performance of the PV plant. This involves using different irradiance and temperature data to estimate the ideal energy production for specific days and comparing it with the actual energy measured from the inverter on the DC side to

evaluate any misalignment or discrepancies. The following subchapters will provide detailed explanations and insights into the methods and procedures used in each block of the diagram.

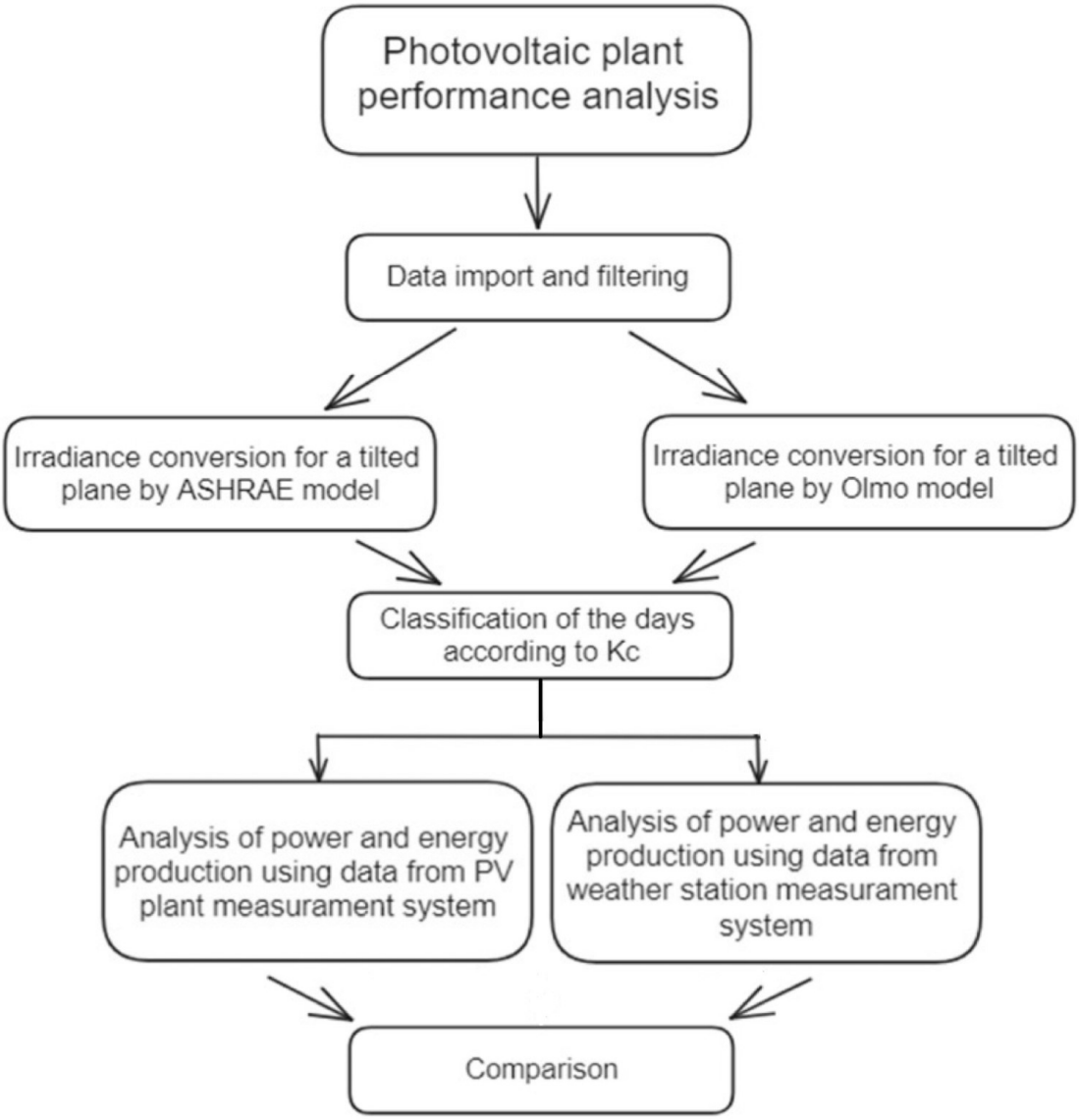

Figure 4-1 - Block diagram

4.2 Data import and filtering

The initial step in this study involves importing data from various available sources for analysis. Datasets from both the photovoltaic (PV) plant and the Włodawa weather station are accessed. These datasets were provided in CSV format and imported into MATLAB for subsequent processing. As these data sources have already been described in detail in Chapter 3, their specifics will not be reiterated here.

Experimental data essential for this research is primarily obtained from these two sources. However, in subsequent steps of the study, to facilitate comparisons and ensure precision, data from the PVGIS and SOLCAST databases are also incorporated. Similar to the primary datasets, the data from PVGIS and SOLCAST are also downloaded in CSV format and imported into MATLAB.

During this step, it is crucial to ensure that the data import process is conducted correctly, verifying the accurate transition from CSV to MATLAB format. By integrating data from these diverse sources and selectively extracting relevant parameters, a comprehensive approach to data collection is ensured, enabling detailed analyses and accurate comparisons for the study.

The second step, data filtering is a crucial step to ensuring the accuracy and reliability of the analysis. It involves identifying and correcting errors or inconsistencies in the dataset. In this study, filtering and correction mechanisms were applied to the data received from both the PV plant and the Włodawa weather station. The data obtained from PVGIS and SOLCAST were already clean and error-free, so no additional filtering was necessary for these sources.

- **Filtering of PV Plant Data**

The initial step in filtering the PV plant data was to reorder the information chronologically. The data provided by the PV plant were in reverse order, starting from the most recent to the oldest. The order was not convenient for the analysis, so the order was reversed to ensure a sequential arrangement from the beginning to the end of June.

In addition, the day 21th of June, 2022 was decided to be excluded from the analysis. This decision was made due to missing data for the entire time period between 8 am and 3 pm, likely caused by measurement or data recording errors.

Throughout the entire analysis, this day will not be considered to prevent it from potentially inaccurately influencing the results obtained.

Upon examining the irradiance data from the PV plant, anomalies were noticed in the first six days of June. The data showed irregular spikes in irradiance, reaching up to 65535 W/m², which is physically impossible since the maximum global irradiance measured by PVGIS for June for the location under consideration (PV plant) is 880 W/m². These spikes were randomly distributed and disrupted the normal bell-shaped irradiance pattern expected over the course of a day. To correct this, a MATLAB script was implemented to filter out these erroneous values. The filter was designed to remove all irradiance values exceeding 1200 W/m². After applying this filter, the irradiance data for the first six days of June aligned more realistically with expected values. This issue was isolated to the first six days, possibly due to a measurement system error, and no further filtering was required for the remaining days, as the data were consistent.

The correction above mentioned can be graphically visualise in Figure 4-2. It is possible to visualize the results of this type of filtering before and after applying the data filter for a day that exhibited this issue, June 3rd, 2022. In red, the measured irradiance data without filtering can be seen, while in blue, the data with the filter applied is shown.

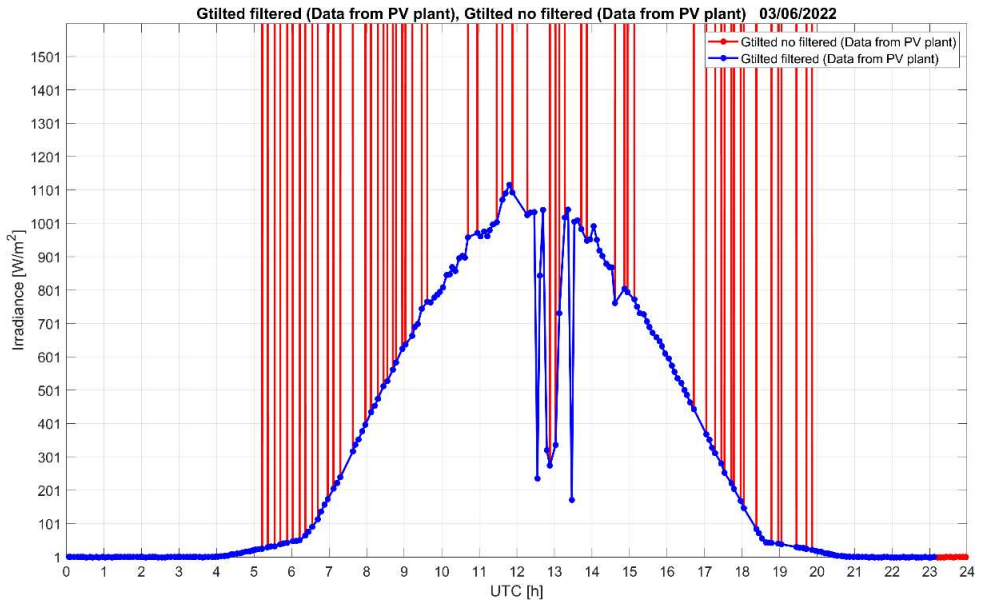

Figure 4-2 - G_{tilted} filtered (data from PV plant in blue), G_{tilted} no filtered (data from PV plant in red) 03/06/2022

- **Filtering of Włodawa Weather Station Data**

The data received from the Włodawa weather station covered June and July 2022. Since the PV plant data only spanned June, the analysis focused exclusively on that month. Therefore, the first step in filtering the Włodawa weather station data was to remove all records postdating June 30th. Additionally, incorrect irradiance values were observed during nighttime hours when the sun had set. These erroneous values were negative, which is impossible for solar irradiance. To rectify this, a second filter was applied that converted all negative irradiance values to zero. This correction ensured that the data accurately reflected the absence of solar irradiance during nighttime.

In summary, the data filtering process involved reordering and correcting the PV plant data for initial anomalies and adjusting the weather station data to remove negative nighttime irradiance values. This thorough filtering ensured that the datasets were clean and reliable for subsequent analysis.

4.3 Irradiance conversion for a tilted plane

The data from the weather station in Włodawa want to be used to fill the gaps of the measurement system in the PV plant under study. To achieve this goal, the horizontal Irradiance data from weather station must be extrapolated to a tilted surface equal to the one in the PV plant. Such interpolation will be done using the ASHRAE method and the Olmo method, which have been extensively described in Chapter 2.

The application of the ASHRAE model in various scenarios will be shown, followed by the implementation of the Olmo model. Initially, the ASHRAE method was applied to transpose irradiance data from the horizontal plane. This data was measured by the pyranometer at the Włodawa weather station and then transposed to the tilted plane at the beta angle, equivalent to the inclination of the solar panels in the photovoltaic system.

Subsequently, to verify the accuracy of the ASHRAE method, a check was conducted. Specifically, a control test was implemented to ensure that the computations performed as expected: the known daily horizontal irradiance provided by SOLCAST was used to interpolate values onto a tilted surface using

the ASHRAE method. Then, the results were compared with the daily tilted irradiance provided by SOLCAST. Subsequently, the irradiance values on the tilted plane were compared to verify the functionality of the ASHRAE method.

Finally, the procedure used to analyze radiation and subsequently calculate the daily energy (J/m^2) based on the daily irradiance patterns obtained from the application of the aforementioned models will be illustrated. It is important to note that this chapter will explain all procedures, methods, and reasons for applying these models. However, the actual results obtained from them will be presented later in Chapter 5.

4.3.1 ASHRAE model application

The ASHRAE model, the first model presented in Chapter 2, is a clear sky model, making it highly useful for calculating the irradiance pattern on either a tilted or horizontal plane for a specific geographical location. However, the objective here was to apply a model that, given a geographical location and measured solar irradiance data on a horizontal plane, would output the solar irradiance on a tilted plane. It is convenient to remember that the tilted plane is a particular angle denotated by beta (β). So, the ASHRAE model was used as a starting point, and some modifications to the formulas were made to reach the desired goal.

Given a specific geographical location, in this case, the weather station in Włodawa, and the solar irradiance measured by the pyranometer at the weather station, it allows for the transposition of this solar irradiance onto a tilted plane. This tilted plane must be inclined at the same angle as panels in the photovoltaic system under study are inclined. The aim is to convert the horizontal irradiance data measured by the weather station to tilted data at angle beta, so that these can be compared to the data measured on the same plane as the photovoltaic system.

The first application involved applying this model to the irradiance data measured on the horizontal plane by the weather station. Then, the same application was carried out using horizontal plane irradiance data downloaded from SOLCAST, with the coordinates of the PV plant provided. As known, SOLCAST already provides irradiance data for a tilted plane, so the purpose of applying this model to the horizontal plane data was to compare the results of these transformations with

the data SOLCAST already provided for a tilted plane at the same angle. This comparison allows to know the closeness of agreement between the two methods.

Finally, the ASHRAE model was also used without any modifications to the formulas, as introduced in Chapter 2, to calculate the solar irradiance pattern for various days under clear sky conditions. In this case, no measured data on a horizontal plane was used; instead, only the location of the PV plant and the inclination of the panels were provided. This was done to obtain the clear sky day patterns, which will be useful for future analyses.

In subsequent steps, the application of the models will assume that the various solar angles were calculated by applying exactly the formulas shown in Chapter 2.2, section named Solar Angles. Therefore, the calculation process for these angles will not be repeated each time.

The models will be compared graphically by overlaying the different patterns obtained on graphs showing irradiance throughout the day.

Next, three subsections will be introduced to explain each of these applications in detail.

❖ ASHRAE model on Włodawa weather station data

The formulas that will be presented below represent the inversion of the basic ASHRAE model formulas, applied to calculate solar irradiance on tilted surfaces using horizontal irradiance data obtained from the Włodawa weather station. The original ASHRAE model is typically used without any modifications to calculate the irradiance on a surface with a given tilt at a specific location. However, in this case, it was necessary to invert some of the ASHRAE model formulas to adapt them for a different purpose. The goal is to convert the irradiance measured on a horizontal plane to that on a tilted plane, as explained previously. These calculations assume that solar angles θ and θ_z have been previously computed using formulas detailed in Chapter 2.2, Solar Angles, with values obtained via MATLAB.

The ASHRAE model was applied starting from horizontal irradiance data measured by the weather station in Włodawa. The horizontal irradiance data is provided minute by minute, and thus the output tilted irradiance data is also minute by minute.

1. Calculation of Beam Normal Irradiance (G_{bn})

The beam normal irradiance (G_{bn}) is calculated using the formula:

$$G_{bn} = \frac{G}{\cos(\theta_z)+C} \quad (4\text{-}1)$$

where:

- θ_z is the zenith angle,
- G is the solar irradiance measured on a horizontal plane by the Włodawa weather station,
- C is a dimensionless coefficient interpolated based on the day of the year. These coefficients were obtained through interpolation of the data from Table 2-1 presented in Chapter 2.3.1, using a MATLAB program.

If $\theta_z \geq 90°$, indicating that the sun is below the horizon, G_{bn} is set to zero under these conditions to ensure no direct irradiance when the sun is below the horizon. This correction will be made each time the ASHRAE model is applied.

2. Calculation of Diffuse Horizontal Irradiance (G_{dh})

The ASHRAE model assumes an isotropic sky to calculate diffuse horizontal irradiance:

$$G_{dh} = C\ G_{bn} \quad (4\text{-}2)$$

where C is the coefficient interpolated as mentioned earlier.

3. Calculation of View Factors (F_{cs}, F_{cg})

The view factors for the sky (F_{cs}) and ground (F_{cg}) are calculated using the tilt angle (β), exactly as illustrated in Chapter 2.3.1, Equations 2-13 and 2-14:

$$F_{cs} = \frac{1+\cos(\beta)}{2} \quad (2\text{-}13)$$

$$F_{cg} = \frac{1-\cos(\beta)}{2} \quad (2\text{-}14)$$

These view factors determine the distribution of diffuse and ground-reflected radiation on the tilted surface.

4. Albedo (ρ)

The albedo, ρ, of the underlying surface is set to 0.15, representing the fraction of incident light reflected from the surface (in this case, it was supposed grass as a surface in the surroundings of the irradiance sensor).

5. Calculation of Total Irradiance on a Tilted Surface (G_t)

The total irradiance on a tilted surface includes contributions from direct, diffuse, and ground-reflected radiation, and is calculated using the Equation 2-12 illustrated in Chapter 2.3.1:

$$G_t = G_{bn}\cos(\theta) + G_d F_{c-s} + \rho G F_{c-g} \quad (2\text{-}12)$$

where:

- G_t is the total irradiance on the tilted surface,
- $G_{bn}\cos(\theta)$ represents the direct component,
- $G_{dh} F_{cs}$ represents the diffuse component,
- $\rho G F_{cg}$ represents the ground-reflected component.

These calculations are crucial for understanding how solar irradiance varies on a tilted surface compared to a horizontal one, directly impacting the energy production from photovoltaic systems.

All results obtained through the application of this model, including graphs and considerations, will be presented in Chapter 5.

❖ **ASHRAE model on SOLCAST data**

The formulas presented in this section provide a detailed guide on applying the ASHRAE method to transpose irradiance from a horizontal plane to an inclined plane, using horizontal irradiance data provided by SOLCAST. SOLCAST allows for direct download of irradiance data for inclined planes, making it potentially unnecessary to first download horizontal irradiance data. However, in this instance, horizontal irradiance data from SOLCAST for June 2022 was utilized. The ASHRAE method was applied to transpose this data to an inclined plane with the same angle beta as the photovoltaic panels in the system under study. This approach facilitates comparison of the irradiance data transposed using the ASHRAE method with the directly provided SOLCAST data for the same location, time period, and inclination angle beta, enabling assessment of the ASHRAE model's effectiveness for this purpose. It is important to note that, similar to the ASHRAE model applied on Włodawa weather station data, some formula inversions are also required in this context. Additionally, the parameter C is no longer applicable in this scenario because, as shown in the previous subsection regarding the application of the ASHRAE model to weather station data, the coefficient C was used to calculate diffuse horizontal irradiance. However, Solcast provides this value directly, eliminating the need for its calculation.

Solar irradiance data, including values for global horizontal irradiance (G_{ghi}), diffuse horizontal irradiance (G_{dhi}), and tilted irradiance (G_{gti}), were extracted from a CSV file provided by SOLCAST. These data cover 5-minute intervals over a one-year period, enabling precise temporal analysis of solar exposure on non-horizontal surfaces such as tilted solar panels.

1. Calculation of Horizontal Direct Irradiance (G_{bh}):

The horizontal direct irradiance (G_{bh}) is calculated as the difference between the global horizontal irradiance (G_{ghi}) and the diffuse horizontal irradiance (G_{dhi}).

$$G_{bh} = G_{ghi} - G_{dhi} \tag{4-3}$$

2. Conversion of Normal Direct Irradiance (G_{bn}):

Using the ASHRAE model, normal direct irradiance (G_{bn}) is computed as:

$$G_{bn} = \frac{G_{bh}}{\cos(\theta_z)} \tag{4-4}$$

where θ_z represents the solar zenith angle.

3. Collector View Factors (F_{cs}, F_{cg}):

Sky (F_{cs}) and ground (F_{cg}) view factors are calculated based on the surface tilt angle (β), following Equations 2-13 and 2-14 from Chapter 2.3.1.

$$F_{c-s} = \frac{1+\cos(\beta)}{2} \tag{2-13}$$

$$F_{c-g} = 1 - F_{c-s} = \frac{1-\cos(\beta)}{2} \tag{2-14}$$

ρ is the *albedo* of the underlying surface, representing the fraction of solar radiation reflected by the ground.

4. Calculation of Total Irradiance on an Inclined Surface:

Total irradiance on an inclined surface (G_t) is determined by combining the following components, as described by Equation 2-12 in Chapter 2.3.1, it is possible to revise the formula written differently in Equation 4-5:

$$G_t = G_{t,direct} + G_{t,diffuse} + G_{t,reflected} \tag{4-5}$$

where:

- $G_{t,direct}$ represents the direct component of irradiance, calculated as:

$$G_{t,direct} = G_{bn}\cos(\theta) \tag{4-6}$$

G_{bn} is the normal direct irradiance, and θ is the angle of incidence of the sun on the inclined surface.

- $G_{t,diffuse}$ represents the diffuse component of irradiance, calculated as:

$$G_{t,diffuse} = G_{dhi}\, F_{cs} \tag{4-7}$$

G_{dhi} is the diffuse horizontal irradiance, and F_{cs} is the sky view factor.

- $G_{t,reflected}$ represents the reflected component of irradiance, calculated as:

$$G_{t,reflected} = \rho\, G_{ghi}\, F_{cg} \tag{4-8}$$

ρ (0.15) is the surface albedo, G_{ghi} is the global horizontal irradiance, and F_{cg} is the ground view factor.

❖ **ASHRAE model for clear-sky condition on Włodawa weather station**

In this subchapter, the ASHRAE model is applied in its original form, without modifications to the formulas introduced in Chapter 2. This approach utilizes the model for its intended purpose, which is to calculate the solar irradiance pattern for days characterized by clear sky conditions. This method does not rely on measured data from a horizontal plane; instead, only the location of the Włodawa weather station and the inclination of the surface are provided. The beta angle in the scenario under examination is equal to zero, which is crucial to keep in mind because it is needed to compute the irradiance on the horizontal plane. This approach aims to obtain clear sky day patterns, which will be useful for future analyses. More specifically, its application will be beneficial for calculating the K_c, or "clear-sky index." The usage and the various steps involved in calculating this coefficient will be explained in detail in Chapter 4.3.2. The coordinates used for calculating the various solar angles correspond to the Wladowa weather station's location.

1. Interpolation of Parameters for ASHRAE Model:

The ASHRAE model requires specific parameters that vary monthly: the apparent solar constant (*A*), the extinction coefficient (*B*), and the coefficient (*C*). These data were extracted from an Excel file (where the values from Table 2-1 contained in Chapter 2.3.1 were recorded) and interpolated for each day of the year.

- *A(i)* = Interpolated value from A
- *B(i)* = Interpolated value from B
- *C(i)* = Interpolated value from C

This interpolation ensures that the values smoothly transition between the months.

2. Conversion from Horizontal to Tilted Angle (G_{bn}):

For the calculation of normal direct irradiance (G_{bn}), the ASHRAE model was applied. The model uses the zenith angle (θ_z), and for angles where the sun is below the horizon ($\theta_z \geq 90°$), G_{bn} is set to zero.

$$G_{bn} = \begin{cases} A\, e^{\left(-\frac{B}{\cos(\theta_z)}\right)} & if\ \ \theta_z < 90° \\ 0 & if\ \ \theta_z \geq 90° \end{cases} \quad (4\text{-}9)$$

3. Calculation of Diffuse Horizontal Irradiance (G_{dh}):

The diffuse horizontal irradiance (G_{dh}) is considered isotropic in the ASHRAE model and is calculated using the coefficient C in the Equation 2-10:

$$G_{dh} = C\ G_{bn} \quad (2\text{-}10)$$

4. View Factors for Sky and Ground (F_{cs}), (F_{cg}):

The view factors for the sky (F_{cs}) and ground (F_{cg}) are calculated using the tilt angle (β). As in the previous chapters, the view factors are always calculated in the same manner; therefore, to avoid repetition, the formula will not be shown again here.

5. Calculation of Total Irradiance on a Tilted Surface (G_t):

The total irradiance on a tilted surface (G_t) is calculated by combining direct, diffuse, and ground-reflected components. As in previous chapters, the same formula is used; therefore, to avoid repetition, it will not be shown again here. The equation referenced is 2-12 from Chapter 2.

In Figure 4-3, a summary diagram is shown with the main steps to follow for the application of the ASHRAE method.

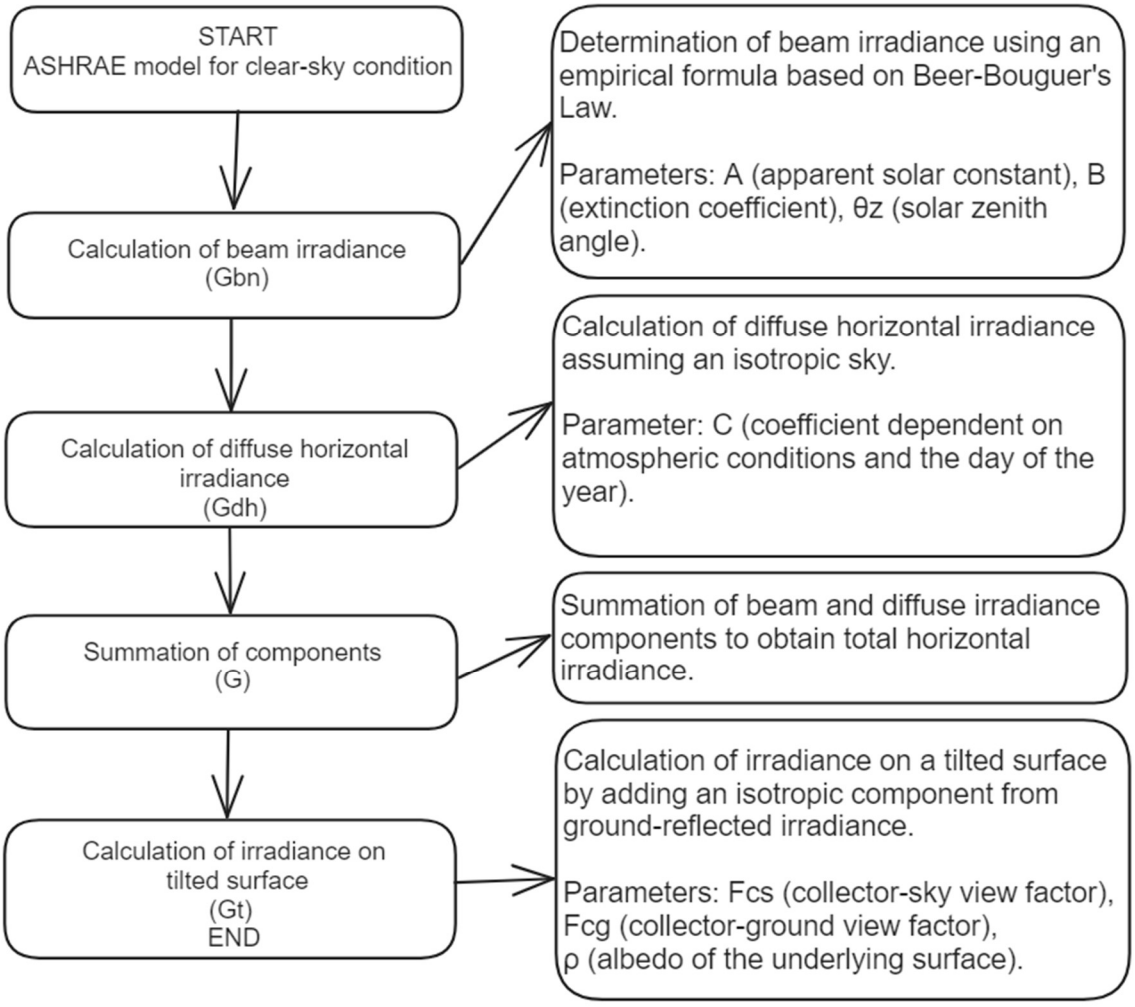

Figure 4-3 - ASHRAE model for clear-sky conditions summary diagram

4.3.2 Olmo model application

In the previous chapter, Chapter 2, the Olmo model was meticulously described step by step. This subchapter will describe the actual application of the Olmo model in the case study. As previously noted, the Olmo model, like the ASHRAE model, serves the purpose of transposing irradiance measured on a horizontal plane to a desired inclined plane. Despite having already applied the ASHRAE model for this task, the decision was made to also assess the Olmo model's performance. Specifically, since the ASHRAE model is primarily designed as a clear-sky model suitable for sunny days, its efficacy on cloudy days was uncertain.

The Olmo models, incorporating the K_t (clearness index) and K_c (clear sky index) coefficients to account for cloudiness, were considered potentially more suitable for transposing irradiance on such days. This evaluation aimed to determine the relative effectiveness of both models in the study.

Both models (with K_t and K_c) were applied to the data measured from the pyranometer located on Wlodawa weather station. The application of the model will be shown below. First, the case utilizing the K_t will be presented, followed by the case using the K_c. All the obtained results will be shown in Chapter 5.

❖ **Olmo model with K_t "clearness index"**

In this section, the step-by-step application of the Olmo model using the clearness index (K_t) will be detailed. In the case study, the model converts horizontal solar irradiation measured from the pyranometer at the Włodawa weather station to the irradiation incident on a tilted surface, which has the same beta angle as the PV plant.

1. Calculation of Correction Factor of the Earth's Orbit (E_0)

The first step involves calculating the E_0 correction factor of the Earth's orbit, which accounts for the variation in the Earth-Sun distance throughout the year. This factor is given by the same formula as shown previously in Equation 2-19[32]:

$$E_0 = 1 + 0.033 \cos\left(2\pi \frac{n_{day}}{365}\right) \quad (2\text{-}19)$$

2. Defining the Solar Constant (*SC*)

Next, the solar constant, denoted as *SC*, is defined. It represents the average solar radiation received per unit area at the top of the Earth's atmosphere, perpendicular to the Sun's rays: *SC* =1367 W/m².

3. Calculation of Normal Extraterrestrial Irradiance (G_0)

The normal extraterrestrial irradiance, G_0, is calculated by multiplying the solar constant with the E0 correction factor. This calculation follows the same formula as shown previously in Equation 2-18:

$$G_0 = E_0\, SC \quad (2\text{-}18)$$

This represents the solar irradiance on a plane normal to the solar beam outside the Earth's atmosphere.

4. Calculation of Hourly Clearness Index (K_t)

The hourly clearness index, K_t, is a dimensionless parameter indicating the clarity of the atmosphere. It is calculated as the ratio of the measured irradiance, G, to the normal extraterrestrial irradiance, G_0, following the formula shown previously in Equation 2-17:

$$K_t = \frac{G}{G_0} \quad (2\text{-}17)$$

To assess which calculation method works best, three different approaches were used to determine the clearness index:

- Instantaneous K_t: this method calculates K_t for each minute, corresponding to the frequency of data collection by the Włodawa weather station.

- Hourly K_t: in this method, K_t is calculated by averaging the irradiance data over each hour. The numerator of the K_t ratio is the hourly average irradiance.

- Daily K_t: here, the K_t value is calculated using the daily average irradiance data, with the numerator of the K_t ratio being the average irradiance over the entire day.

All three methods were used to calculate K_t, and for each method, the irradiance on the tilted surface was graphed over the 30 days of July, Excluding the 21st, which, as previously mentioned, was removed from the analysis due to a lack of data measured by the monitoring system in the PV plant.

5. Conversion from Horizontal to Tilted Surface Irradiance

The core of the Olmo model involves converting horizontal radiation to the radiation incident on a tilted surface. This conversion is achieved through the function ψ_0, which is defined as shown previously in Equation 2-16:

$$\psi_0 = e^{K_t\,(\theta^2 - \theta_z^2)} \tag{2-16}$$

Here, θ is the tilt angle of the surface, and θ_z is the zenith angle of the sun.

6. Define Albedo and calculation of Anisotropic Reflections

The albedo of the underlying surface, ρ, represents the fraction of incident light that is reflected in all directions. For this application, an albedo value of 0.15 was used.

The multiplying factor for anisotropic reflections, F_c, is calculated as previously shown in Equation 2-20:

$$F_C = 1 + \rho\, sin^2\left(\frac{\theta}{2}\right) \tag{2-20}$$

7. Calculation of Tilted Surface Irradiance (G_β)

Finally, the irradiance on the tilted surface, G_β, is computed by combining all the above factors, following the equation shown previously in 2-21:

$$G_\beta = G\ \psi_0\ F_C \tag{2-21}$$

This step completes the application of the Olmo model using the clearness index (K_t), providing the necessary irradiance values on the tilted surface for further analysis. By comparing the results from the three different K_t calculation methods, the most effective approach for modeling the irradiance on a tilted surface can be determined.

All results obtained through the application of this model, including graphs and considerations, will be presented in Chapter 5.

❖ Olmo model with K_c "clear-sky index"

In this section, the application of the Olmo model using the clear sky index (K_c) will be detailed. The development of the model remains identical to that applied with K_t, with the only difference being the substitution of K_t with K_c, as explained in Chapter 2.4.1. Therefore, the formulas will not be presented again here.

Chronologically, this model was applied after evaluating the results obtained from the initial application with K_t. Based on these evaluations, it was decided to apply this model using only a daily calculated K_c. As detailed in the Chapter 2.4.1, K_c was calculated in three different ways. The procedure used will be briefly explained below, but the detailed analysis for calculating K_c will be provided in Chapter 4.4, Classification of Days According to K_c", as it requires a more in-depth analysis.

1. Calculation of Clear Sky Index (K_c)

K_c is calculated by keeping the same numerator as K_t, which is the measured irradiance G on the horizontal plane but changing the denominator. As previously

shown in Equation 2-24 instead of using G_0 (the normal extraterrestrial irradiance), $G_{clear-sky}$ is used.

$$K_c = \frac{G}{G_{clear-sky}} \tag{2-24}$$

This value represents the solar radiation that would be received at that specific time of day if it were a completely sunny day. $G_{clear-sky}$ can be calculated using the ASHRAE model for clear-sky conditions, as explained earlier in Chapter 4.3.1, or it can be directly obtained from databases such as PVGIS or SOLCAST.

2. Application of the Olmo Model with K_c

After calculating the K_c using the three different methods mentioned above, for the application of the Olmo model with K_c, the values obtained used the clear-sky irradiance data provided by the PVGIS database as the denominator for calculating K_c. This decision was made because the results obtained were more consistent and PVGIS is one of the most widely used programs in the sector, providing reliable data. The irradiance on the tilted surface was then graphed over the 30 days of July using the daily K_c values.

The results of this application will be compared with the real measured irradiance at the installation and the results from the ASHRAE model. This comparative study will be discussed in Chapter 5, highlighting the accuracy and effectiveness of the Olmo model using K_c in modeling solar irradiance on a tilted plane.

In Figure 4-4, there is a summary diagram illustrating the key steps for applying the Olmo model with both K_t and K_c as described above.

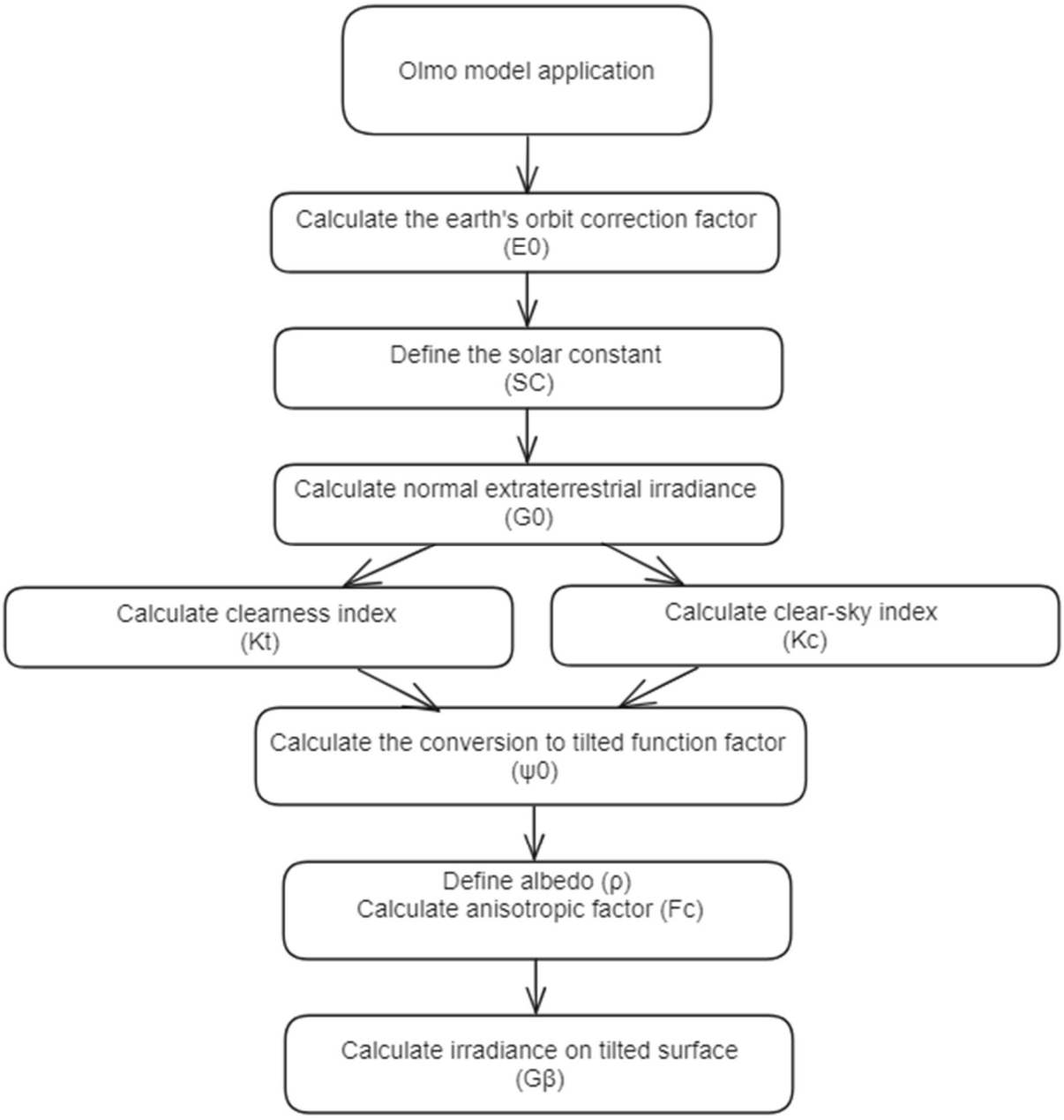

Figure 4-4 - Olmo model summary diagram.

4.3.3 Radiation analysis

In the previous chapters, two models used for transposing horizontal irradiance data, measured at the Włodawa weather station, to irradiance on an inclined plane with an angle beta (the same inclination angle as the photovoltaic panels in the system) were examined. The two models discussed for this purpose were the ASHRAE model and the Olmo model. All results obtained and considerations will be presented in Chapter 5. Following evaluations of the efficiency of these models in performing the described task, and after assessments (detailed in Chapter 5), it was decided to proceed with the subsequent steps using the irradiance data transposed with the ASHRAE model applied to the horizontal irradiance data measured by the pyranometer at the Włodawa weather station, as well as the horizontal irradiance data directly provided by SOLCAST for the same location (weather station). Additionally, for the analysis conducted in this chapter, the irradiance data provided by SOLCAST for the Włodawa weather station location on an inclined plane with an angle beta, equivalent to the inclination angle of the solar panels, will also be analyzed. All the proposed methods tend to show peaks in the irradiance daily shape. So, instead of comparing point by point the results from all the sources of irradiance, it is wiser to compare the irradiation which is the area under the irradiance curve. Moreover, irradiation in tightly connected with the final goal of this study which is the E_{DC} produced by the PV generator. Thus, irradiation is the index to by used to compare the results in the final step. In this chapter, the steps taken to calculate the daily solar radiation, starting from the irradiance data on the inclined plane derived from the three sources just described, will be shown. The objective is to compare the daily calculated radiation (J/m^2) from the three different models with the actual measurements of solar irradiance on the inclined plane at the photovoltaic plant. This comparison aims to evaluate which of these three models performs best for this application by comparing them with the actual measured data on PV plant.

To achieve this, an integral calculation was necessary to determine the energy, effectively representing the area under the irradiance curve. As previously mentioned, the SOLCAST database provides data with a time-step of five minutes, thus representing a five-minute average. Conversely, the data from the photovoltaic system varies, with time steps sometimes being four, five, or six minutes. However, on average, this time step also approximates five minutes. Therefore, to ensure an accurate analysis, the data from the Włodawa weather station, which was provided

every minute, was averaged over five-minute intervals to align with the other datasets.

Additionally, the comparison included data directly measured by SOLCAST on an inclined plane, as described earlier in Section 3.4.1.

❖ **Data Processing and Integration**

The MATLAB code provided facilitated the processing and integration of data from different sources. The following steps were executed:

1. Data Importation:

As already said, data were imported from different sources, including the radiation measured by the measurement system in the PV plant.

2. Integral Calculation:

To calculate the daily radiation, the "trapz" function in MATLAB was employed. This function uses the trapezoidal rule to approximate the integral of a set of discrete data points. The trapezoidal rule works by dividing the area under a curve into trapezoids rather than rectangles. The area of each trapezoid is calculated, and then these areas are summed to obtain the total integral. The formula for the trapezoidal rule is:

$$\int_a^b f(x)\,dx \approx \sum_{i=1}^{n-1} \frac{(x_{i+1}-x_i)}{2} [f(x_i) + f(x_{i+1})] \quad (4\text{-}10)$$

This method is more accurate than simple rectangular integration, especially for data that changes linearly between points.

In this formula:

- $\int_a^b f(x)\,dx$: Represents the integral of the function $f(x)$ from a to b, which is the area under the curve of $f(x)$ between these two points.

- $\sum_{i=1}^{n-1}$: Denotes the summation of the areas of all the trapezoids formed between the data points, from the first interval to the *n-th* interval.
- $x_{i+1} - x_i$: Represent consecutive data points on the *x*-axis.
- $f(x_i)\ and\ f(x_{i+1})$: Are the values of the function $f(x)$ at the points x_i and x_{i+1} respectively.
- $\frac{(x_{i+1}-x_i)}{2}$: Is the width of each trapezoid divided by 2, as the trapezoidal rule calculates the area by averaging the heights of the two parallel sides of the trapezoid.

By summing the areas of all the trapezoids, the total integral (area under the curve) is obtained. This method provides a good approximation for the integral, especially when the function changes linearly between the data points.

3. Statistical functions used for comparison:

The performance of each model was evaluated using two primary metrics: Mean Absolute Error (MAE) and Mean Absolute Percentage Error (MAPE), which are defined respectively by Equation 4-11 and Equation 4-12. The performance evaluation metrics were calculated for three models. To assess the performance of each model, we will compare it with the actual radiation value at the photovoltaic plant, calculated through the integration of irradiance measured by the reference cell day by day:

- **Model 1**: Radiation from SOLCAST, G_t calculated using the ASHRAE model.
- **Model 2**: Radiation directly measured from SOLCAST on the tilted plane.
- **Model 3**: Radiation from the Włodawa weather station using the ASHRAE model.

For each model, the *MAE* and *MAPE* were computed as follows:

- ***MAE* (Mean Absolute Error)**: This metric measures the average magnitude of errors in a set of predictions, without considering their direction. It is calculated as the mean of the absolute differences between predicted and actual values.

$$MAE = \frac{1}{n}\sum_{i=1}^{n}|Prediction_i - Actual_i| \quad (4\text{-}11)$$

In this formula, $Actual_i$ represents the actual measured values at the PV plant, and $Prediction_i$ represents the predicted values from each model.

- ***MAPE* (Mean Absolute Percentage Error)**: This metric expresses the average magnitude of errors as a percentage of the actual values, providing a perspective on the error relative to the size of the actual values.

$$MAPE = \frac{100}{n}\sum_{i=1}^{n}\left|\frac{Prediction_i - Actual_i}{Actual_i}\right| \quad (4\text{-}12)$$

In this formula, $Actual_i$ represents the actual measured values at the PV plant, and $Prediction_i$ represents the predicted values from each model.

The results obtained from these calculations will be presented in Chapter 5: Results. This forthcoming chapter will provide a detailed comparison of the performance of each model, highlighting the accuracy of the radiation predictions and offering insights into the effectiveness of the ASHRAE model when applied to both Włodawa weather station and SOLCAST data.

4.4 Classification of days according to K_c

To advance the study and analyze power outputs effectively, it is crucial to classify days into sunny, partly cloudy, and cloudy categories based on the K_c coefficient, defined by Equation 2-24:

$$K_c = \frac{G}{G_{clear-sky}} \tag{2-24}$$

where G represents the measured global irradiance, from the pyranometer located in Włodawa weather station, on the horizontal plane, and $G_{clear-sky}$ denotes the clear-sky irradiance, indicating the solar radiation under completely clear skies.

The analysis focuses on the days of June 2022, which exhibit varying irradiance depending on the weather conditions. This classification is crucial for future analyses of the energy production of the PV plant. Different evaluations for the final energy calculation might be applied based on the type of day.

To estimate the latter, three different sources were used:

- ASHRAE Method. The first source uses the ASHRAE model (explained in Section 4.3.1). The clear-sky irradiance ($G_{clear-sky}$ in Equation 2-24) is calculated by applying the ASHRAE method, using the Włodawa weather station coordinates and a tilt angle of zero degrees. Both numerator and denominator compare measurements on a horizontal plane.

- SOLCAST. The second source is SOLCAST, which provides clear-sky irradiance data ($G_{clear-sky}$ in Equation 2-24) for specified coordinates (Włodawa weather station) and a horizontal plane.

- PVGIS. The third source is PVGIS, which also provides clear-sky irradiance data ($G_{clear-sky}$ in Equation 2-24) using the same input parameters as SOLCAST.

The motivation for calculating values with three different K_c indices lies in redundancy. Having multiple results calculated with different models allows for comparisons to identify the most suitable model for this type of analysis. The classification is done using the K_c index. This index compares the radiation

calculated through the integration of irradiance measured by the pyranometer at the Włodawa weather station. It is then compared to the radiation under clear-sky conditions at the same location. Here is a detailed breakdown of the process involved in calculating K_c using PVGIS clear-sky irradiance data, but the same procedure was applied to the other two data sources, SOLCAST and the ASHRAE method previously mentioned:

1. **Averaging Włodawa Weather Station Data to Match PVGIS Intervals:**

The horizontal irradiance data measured by the pyranometer from the weather station is averaged over each hour to align with the hourly intervals of the PVGIS data. This ensures that both datasets are on a consistent temporal scale for accurate comparison. To align the data from the Włodawa weather station with SOLCAST data, the weather station data is averaged over 5-minute intervals, while for the third data used (calculated with ASHRAE clear-sky method), which is already at minute-level resolution, data from weather station requires no further averaging.

2. **Radiation Calculation:**

The total daily radiation is computed by integrating the 1-hours averaged Włodawa weather station horizontal irradiation data and the corresponding clear-sky irradiation on horizontal surface given by PVGIS data for each day in the study period. In this case as well, to perform this integral, the same "trapz" function in MATLAB was used, as previously explained in Chapter 4.3.3.

3. **K_c Calculation and Classification:**

K_c values are determined by dividing the averaged weather station irradiance by the PVGIS clear-sky irradiance obtained in step 1. Based on predefined thresholds:

- Days with $K_c \leq 0.45$ are classified as cloudy.
- Days with $0.45 < K_c \leq 0.75$ are classified as partly cloudy.

- Days with K_c > 0.75 are classified as sunny.

4. Histogram Generation:

For each type of K_c calculation (ASHRAE, SOLCAST, PVGIS), histograms are generated to illustrate the distribution of days across the calculated K_c values. These results will be presented in Chapter 5, Results.

4.5 Analysis of power and energy production

In this chapter, the focus shifts from transposing irradiance from the horizontal to the tilted plane and classifying days to a detailed analysis of energy production. As stated in the introduction, this section delves into the final part of the thesis. The ultimate goal is to compare the actual energy generated by the photovoltaic plant with the energy estimated based on the irradiance measured by the weather station.

Here, the primary steps involved are outlined without delving into excessive detail, as this area is still exploratory. Osterwald's method, described in Chapter 1.8, is central to the approach. Then, Equation 1-27 is utilized:

$$P_m = P_{m,STC} \cdot \frac{G}{G_{STC}} \cdot [1 - \gamma \cdot (T_c - T_{STC})] \quad (1\text{-}27)$$

where:

- P_m represents the maximum power output of the PV generator under study.
- $P_{m,STC}$ is the maximum power output under Standard Test Conditions (STC), specifically 21,25 kW for the experimental subsection.
- G denotes the measured irradiance (W/m²). Instead of this value, G obtained through transposing horizontal irradiance data measured by the Włodawa weather station using the ASHRAE method could be substituted. Furthermore, an additional analysis could replace this value with irradiance data directly provided by SOLCAST on the tilted plane,

and finally evaluate which of the two methods performs better for this purpose. Additionally, G can be replaced with irradiance on the tilted plane directly measured by the reference cell in the photovoltaic system. This allows for comparing the calculated Pm value with the one actually provided by the inverter to verify the accuracy of the measured data.

- G_{STC} signifies the irradiance under Standard Test Conditions, fixed at 1000 W/m².

- γ represents the temperature coefficient of the cell's maximum power, specifically -0,4 %/°C for the experimental subsection.

- T_c stands for the cell temperature (°C). If analyzing power production based on irradiance data measured directly in the PV plant by the reference cell, then the cell temperature to be used is directly the one measured in the PV plant. However, if calculating power based on irradiance data provided by SOLCAST or measured at the Włodawa weather station, this temperature value is not available but can be calculated by Equation 4-13 using the air temperature T_A and the module's NOCT (Nominal Operating Cell Temperature) coefficient of 45°C. The formula to estimate T_c from T_A is:

$$T_c = T_A + \frac{NOCT - 20°C}{800\,\frac{W}{m^2}}\,G \tag{4-13}$$

This formula adjusts T_A based on solar irradiance conditions.

The air temperature (T_A) is recorded by the Włodawa weather station and reflects external thermal conditions over the course of the day. However, the station provides only the maximum (T_{max}), minimum (T_{min}), and average (T_{avg}) daily temperatures, which are insufficient for applications requiring a detailed temporal profile of temperature variations. To address this limitation, a method was developed to reconstruct the daily temperature trend based on sinusoidal behavior.

Analysis of air temperature patterns revealed that temperature variations during a typical day resemble a sinusoidal curve. Temperature generally reaches a minimum in the early morning hours, gradually increases to a maximum in the early afternoon, and then decreases again through the evening and night. By leveraging this periodic behavior, it is possible to generate a continuous temperature profile

using only the daily extremes (T_{max} and T_{min}) and the respective times at which they occur (t_{max} and t_{min}). The times of the daily temperature extremes (t_{max} and t_{min}) were determined by analyzing PVGIS data for the month of June. These values typically reflect the general times of sunrise and early afternoon for t_{min} and t_{max}, respectively. The amplitude of the temperature variation was calculated as:

$$A = \frac{T_{max} - T_{min}}{2} \tag{4-14}$$

The mean temperature, which represents the baseline about which the sinusoidal oscillates, was defined as:

$$T_{mean} = \frac{T_{max} + T_{min}}{2} \tag{4-15}$$

A sinusoidal function was used to model the temperature trend throughout the day:

$$T(t) = T_{mean} + A\,cos\,(\frac{\pi\,(t - t_{min})}{12} - \Phi) \tag{4-16}$$

where t is the time in hours. The phase shift (Φ) was introduced to ensure that the maximum and minimum temperatures align with t_{max} and t_{min}, respectively:

$$\Phi = \frac{\pi\,(t_{max} - t_{min})}{12} \tag{4-17}$$

Using the sinusoidal equation, a temperature value was calculated for each minute of the day, resulting in a continuous profile of T_A over 24 hours. This process was repeated for each day of the month, using the corresponding $T_{max}, T_{min}, t_{max}$ and t_{min} values as inputs.

To evaluate the accuracy of the sinusoidal method, PVGIS data were utilized as a benchmark. PVGIS provides hourly temperature trends for various locations, computed as an average over the selected time period. Specifically, the temperature profile for a single representative day in June 2022 was downloaded from PVGIS, which included T_{max}, T_{min}, and their respective times ($t_{max}\ and\ t_{min}$). Using these four inputs, the sinusoidal method was applied to generate a temperature profile, which was then compared with the actual PVGIS profile. As shown in Figure 4-5, the reconstructed sinusoidal trend closely aligns with the real temperature curve, with only minimal discrepancies.

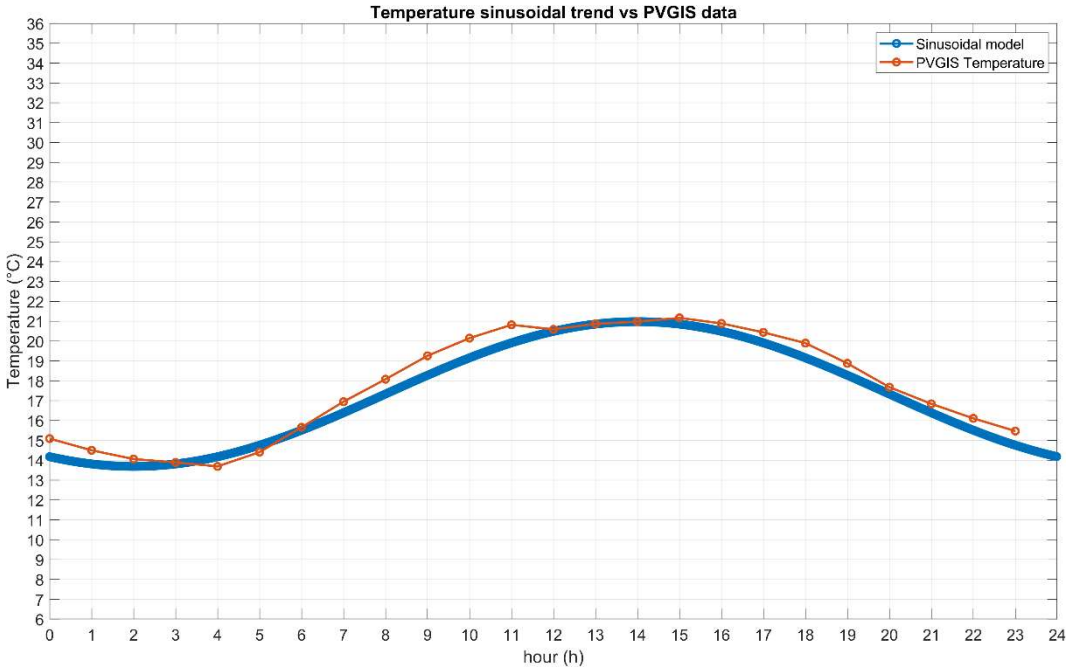

Figure 4-5 – Temperature sinusoidal trend vs PVGIS data

Given the successful validation of the sinusoidal model, this approach was applied to estimate the air temperature profiles for all days in June 2022. The resulting profiles provided a detailed temporal representation of air temperature, which could be further utilized in subsequent analyses, such as evaluating PV plant performance under varying thermal conditions.

NOCT (Nominal Operating Cell Temperature) specifies the temperature at which the module operates nominally under standard conditions, with a value of 45°C for the experiment.

The solar irradiance G measured on the tilted plane of the module directly influences the heating of the solar cell and, consequently, its temperature.

The integration of the energy given by Osterwald provides the DC energy (E_{DC}) which will be compared to the E_{DC} given by the inverter.

The main focus of the analysis is to apply Equation 1-27 to calculate P_m using irradiance data derived from the weather station and transposed onto the inclined

plane through one of the previously described models. The primary objective of the thesis is to use Włodawa weather station data to analyze energy productivity.

This comprehensive approach ensures a thorough examination of energy production dynamics, combining theoretical models with empirical data to evaluate solar energy system performance under real-world conditions.

Chapter 5

5 Results

5.1 Introduction

Following the discussions in the previous chapters concerning the description of the available data, the setup of the PV plant and the nearby meteorological station, the applied models, and their real-world applications, this chapter will present the various results obtained from the analyses performed. Initially, in the first subsection, the results from the application of the ASHRAE model for transposing solar irradiance from a horizontal plane to an inclined one will be shown. These results pertain to both the meteorological station data and the data received from SOLCAST. Subsequently, the results from the application of the Olmo model in its two previously described forms (with K_t and K_c) for the transposition of irradiance on the inclined plane will be presented. In addition the results obtained from ASHRAE model application for calculating clear-sky irradiance on a horizontal plane for different days at the location of the photovoltaic plant will be shown.

In subsection 5.3, the results from the analysis for the classification of days into sunny, partially cloudy, or cloudy, applying the three different methods described in Chapter 4.4 for calculating the clear-sky index K_c, will be shown. Subsection 5.4 provides all the results related to energy production, including the comparison between predicted and actual energy production.

5.2 Irradiance conversion for a tilted plane results

As previously mentioned, this subsection will present the results obtained using the models for transposing irradiance from a horizontal plane to an inclined plane and for calculating clear-sky irradiance. The results from the application of both the ASHRAE model and the Olmo model will be shown.

It is important to highlight that for each study conducted, graphs were generated for all the days of the month considered, which is June (Except for day 21, which as previously mentioned, was excluded from the analysis due to the lack of irradiance data measured by the reference cell at the PV plant). However, in the course of this discussion, not all daily results will be presented. Instead, only the graphs of the most representative days or those relevant to the specific aspects being described will be shown.

5.2.1 ASHRAE model results

In this section, the results obtained from the application of the ASHRAE model will be analyzed, as previously discussed. The analysis will encompass three distinct sets of data: the tilted irradiance trend results derived from the application of the ASHRAE model when applied to the data from the Włodawa weather station, the results obtained using data from SOLCAST, and the unmodified ASHRAE model results used to determine clear-sky day data for the coordinates of the PV plant. The findings from these analyses will be presented and compared to highlight any discrepancies and to draw conclusions regarding the model's reliability and applicability.

- **ASHRAE model applied on horizontal irradiance weather station measurements**

After applying the modified ASHRAE method with the inversion of formulas, as explained in section 4.3.1, the irradiance data measured on the horizontal plane from the Włodawa weather station were input into this model to obtain the irradiance transposed onto a plane inclined at 34°. In Figure 5-1 below, the difference between the irradiance measured on the horizontal plane and the

irradiance transposed to the inclined plane can be observed. The presented example illustrates a typical sunny day, specifically 11th of June, 2022, but it is important to note that this calculation was performed for all days in June 2022.

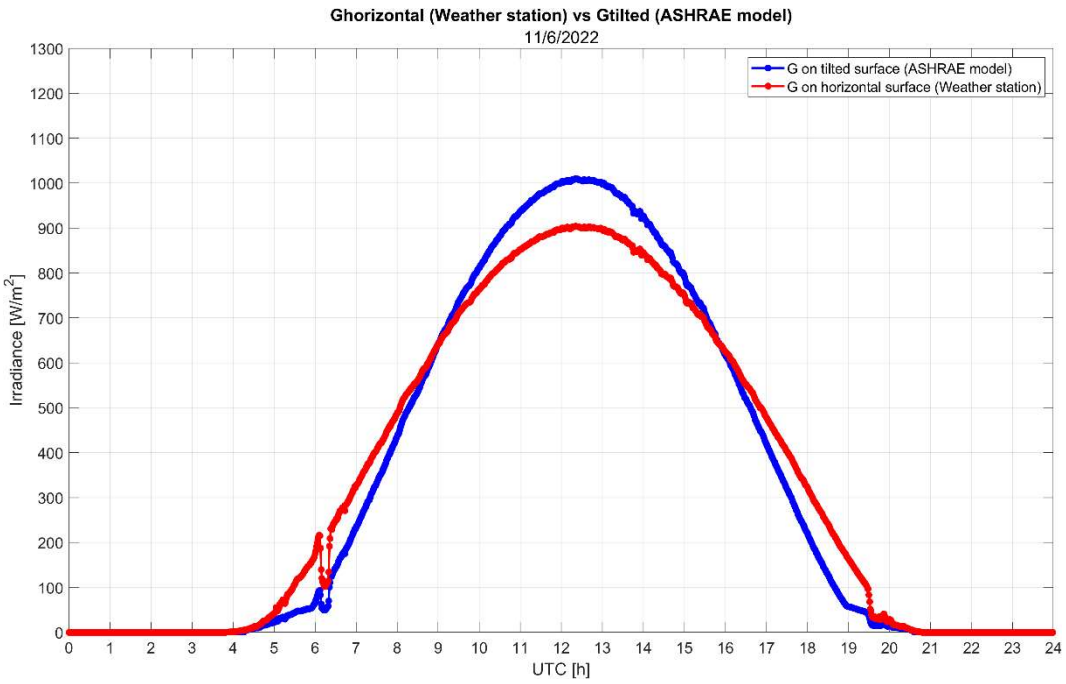

Figure 5-1 - $G_{horizontal}$ (from Włodawa weather station measurement system - red) vs G_{tilted} (ASHRAE model applied for a tilt surface of 34° using as source of data experimental horizontal solar irradiance from Włodawa weather station - blue) 11/6/2022

As seen in Figure 5-1, the peak irradiance measured on the horizontal plane (red line) is approximately 900 W/m². After transposing this irradiance onto the inclined plane, the peak irradiance increases significantly, reaching about 1000 W/m². This increase occurs because the inclination of the panels optimizes the angle of incidence, thereby capturing more solar radiation.

Upon further analysis of the data measured by the weather station, anomalies in the irradiance values can be identified, as shown in Figure 5-2 in the next page.

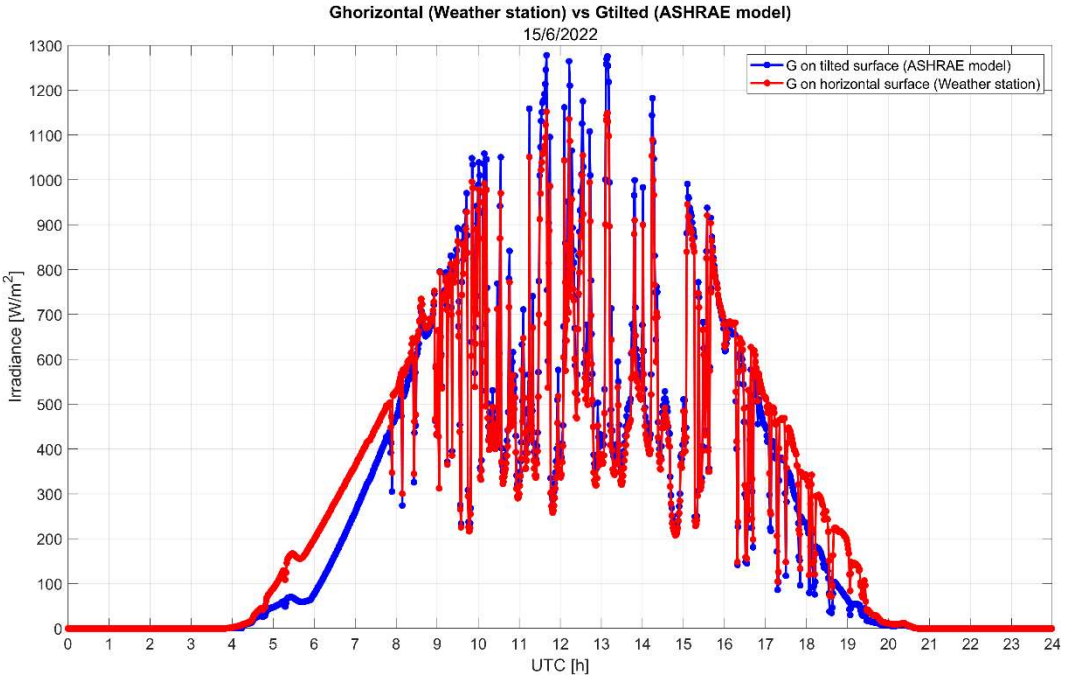

Figure 5-2 - $G_{horizontal}$ (from Włodawa weather station measurement system - red) vs G_{tilted} (ASHRAE model applied for a tilt surface of 34° using as source of data experimental horizontal solar irradiance from Włodawa weather station - blue) 15/6/2022

This issue primarily arises on days that are not perfectly sunny (with a perfect bell-shaped irradiance curve), particularly on days with cloud cover. In these cases, the measured values exhibit irregular peaks of irradiance, which can exceed the maximum irradiance expected at solar noon. Figure 5-2 illustrates 15th of June, 2022, a day with cloud cover, but this problem is present in all data from the weather station on cloudy days. This anomaly could lead to incorrect evaluations of energy production in subsequent analyses. Therefore, it will be necessary to implement a data filtering system to correct this issue in future analyses. To confirm this observation, it is noted that this problem only occurs on cloudy days. As shown in the data from 11th of June, 2022, in Figure 5-1, this issue is absent.

When analyzing the irradiance data measured on the inclined plane by the photovoltaic system, it is evident that, as shown in Figure 5-3 in the next page, the data measurement is accurate on perfectly sunny days.

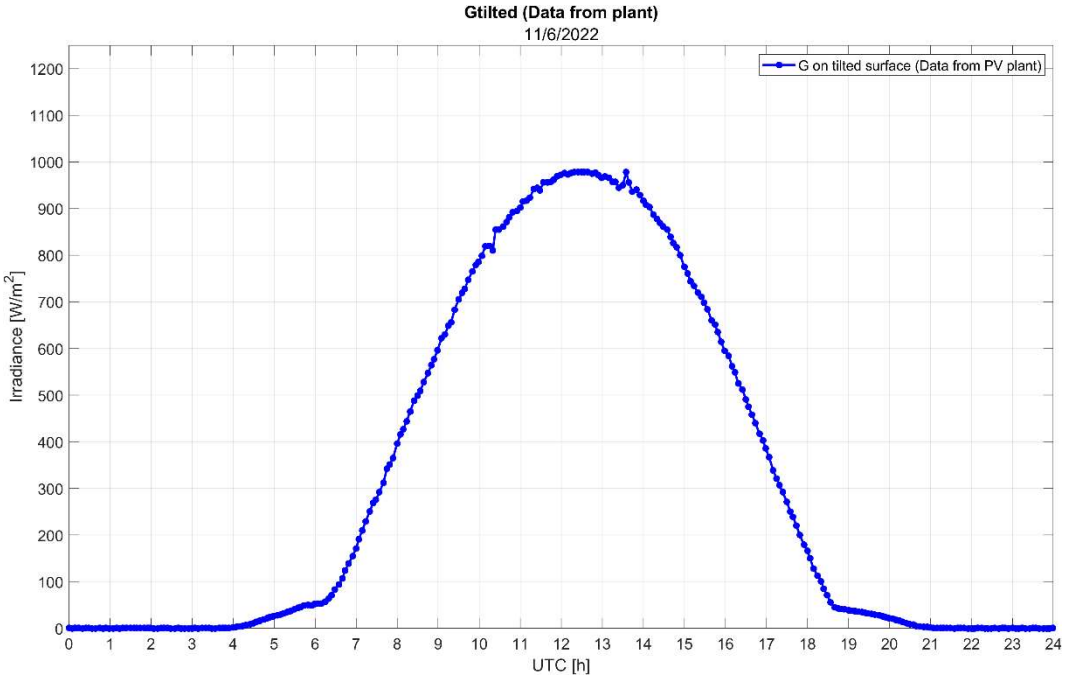

Figure 5-3 - G_{tilted} (data from the measurement system in the PV plant - blue) 11/06/2022

In the graph above, depicting the same sunny day shown in Figure 5-1 (11th of June, 2022), a nearly perfect bell-shaped curve can be observed.

However, even in this case, anomalies can be noted when days are not perfectly sunny but have cloud cover. In Figure 5-4 in the next page, representing 15th of June, 2022, a randomly chosen cloudy day to illustrate the issue, it can be seen that during hours with cloud cover (recognizable in the graph by the broken line with various local peaks), there are anomalous peak values. Again, a filtering system will likely be required in future energy production analyses to mitigate this problem.

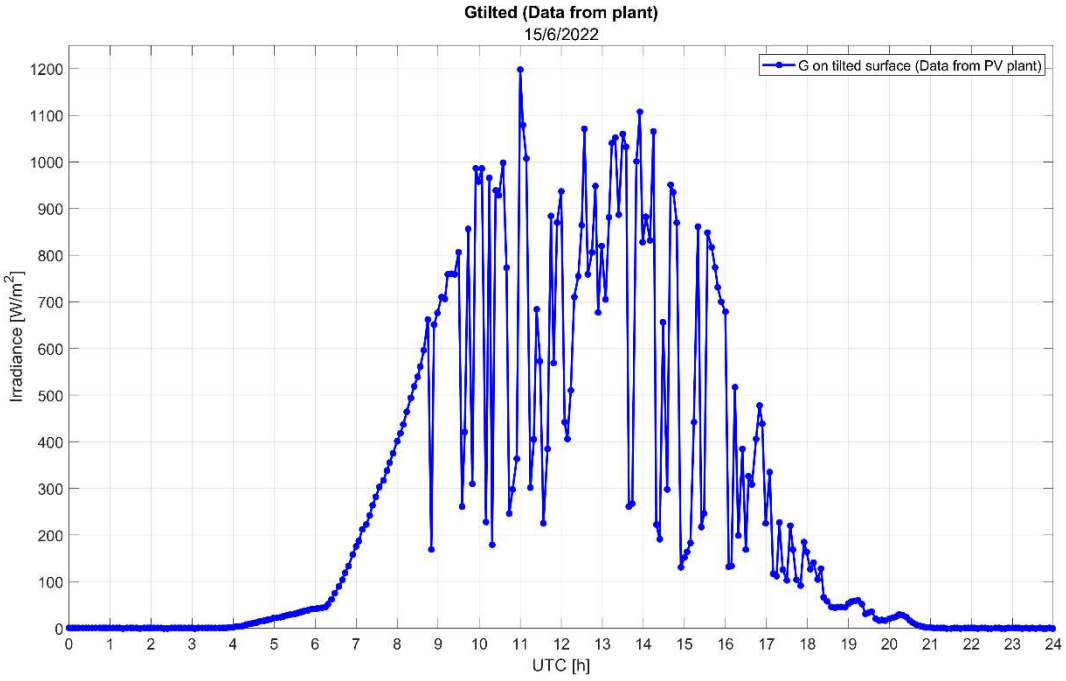

Figure 5-4 - G_{tilted} (data from the measurement system in the PV plant - blue) 15/06/2022

Once the individual analyses of the photovoltaic system data, the Włodawa weather station data on the horizontal plane, and the transposed data on the inclined plane are conducted, it is useful to compare the transposed data from the weather station with the actual data measured by the system to evaluate the effectiveness of the transposition model.

In Figure 5-5 in the next page, a comparison graph of these two trends for 11th of June, 2022, a completely sunny day, is presented. The blue line represents the irradiance on the inclined plane measured by the reference cell located at the PV plant, while the red line shows the irradiance obtained by transposing the horizontal plane data measured from the pyranometer installed at the Włodawa weather station using the ASHRAE method.

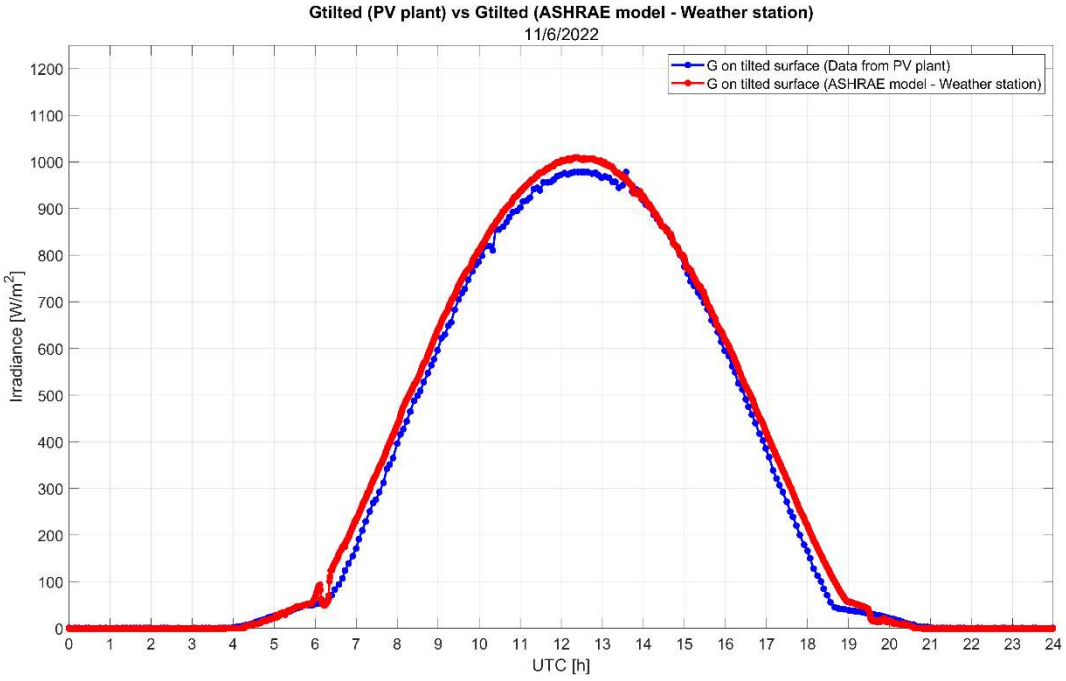

Figure 5-5 - G_{tilted} (data from the measurement system in the PV plant - blue) vs G_{tilted} (ASHRAE model applied for a tilt surface of 34° using as source of data experimental horizontal solar irradiance from Włodawa weather station - red) 11/06/2022

It is apparent that these two trends are very similar, within the limits of natural differences, indicating that the ASHRAE model performs well in transposing irradiance on sunny days. However, on cloudy or partially cloudy days, as shown in Figure 5-6 in the next page, the results can vary significantly between the two trends.

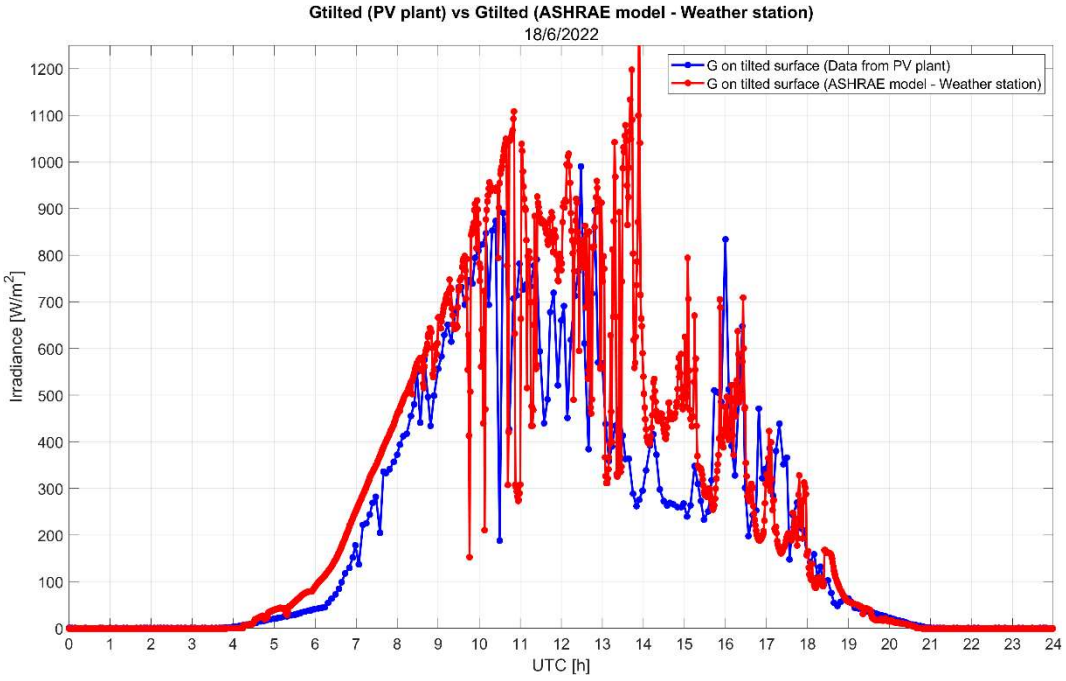

Figure 5-6 - G_{tilted} (data from the measurement system in the PV plant - blue) vs G_{tilted} (ASHRAE model applied for a tilt surface of 34° using as source of data experimental horizontal solar irradiance from Włodawa weather station - red) 18/06/2022

In this graph, representing the two trends for 18th of June, 2022, a partially cloudy day, several points can be seen where the two lines diverge considerably.

This significant discrepancy can be attributed to the fact that the ASHRAE model is a clear sky model, designed to analyze exclusively sunny days. It is suspected that the model performs well on sunny days, but its performance is less reliable on overcast days. However, this hypothesis will be verified in the subsequent subsection (ASHRAE model on SOLCAST data results) by applying this method to the data provided by SOLCAST for a cloudy day.

Additionally, an important factor that cannot be overlooked is the considerable distance between the weather station and the photovoltaic system, approximately 45 km. This distance can lead to discrepancies in the measured data due to different meteorological conditions at the two locations. For example, a cloud may pass over one location but not the other, or there may be a significant time delay in cloud passage from one location to the next.

❖ **ASHRAE model applied on horizontal irradiance obtained from SOLCAST database**

As previously discussed, in chapter 4.3.1, in this part of the study, the decision was made to analyze the SOLCAST data. The modified ASHRAE method, with the inversion of certain formulas, was applied—the same method used in the preceding subsection—to verify its accuracy.

It is important to note that SOLCAST is a database that provides a multitude of satellite data useful for analyses in the field of photovoltaics. For the purpose under consideration, it has been used to download irradiance data measured on the horizontal plane and directly on an 34° inclined plane for the location of the Włodawa weather station.

The method was applied to the horizontal irradiance data obtained from SOLCAST for the weather station's location, and the irradiance transposed to an inclined plane of 34° was obtained. This transposed irradiance was then compared to the irradiance on an 34° inclined plane already provided by SOLCAST.

In the graph in the next page, Figure 5-7, the sunny day previously considered, 11th of June, 2022, is depicted, comparing the horizontal irradiance obtained by SOLCAST (red line), the inclined plane irradiance provided by SOLCAST (light orange line), and the inclined plane irradiance obtained by applying the ASHRAE transposition method to the horizontal irradiance data obtained from SOLCAST (blue line).

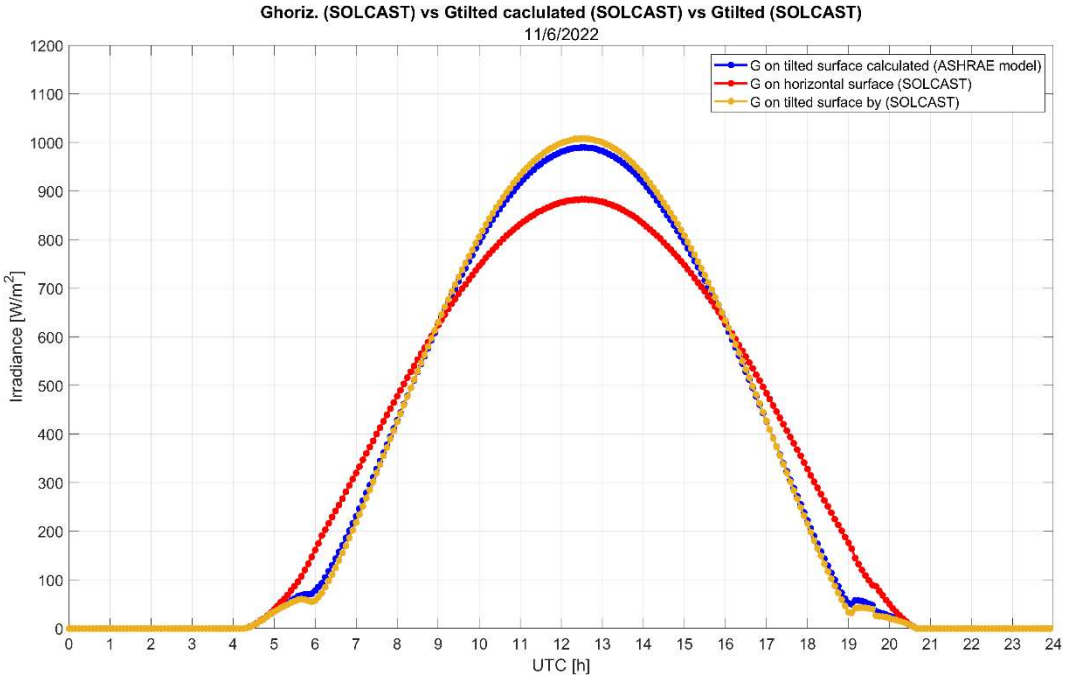

Figure 5-7 - $G_{horizontal}$ (SOLCAST horizontal irradiance source for the PV plant location - red) vs G_{tilted} (ASHRAE model applied for a tilt surface of 34° using as source of data horizontal irradiance provided by SOLCAST for the PV plant location - blue) vs G_{tilted} (SOLCAST tilted irradiance source for the PV plant location – light orange) 11/06/2022

As can be seen from Figure 5-7, the transposition from the horizontal plane to the inclined plane is consistent, showing an increase in peak irradiance at solar noon for the same reasons explained previously. A very important observation is that the light orange curve (the tilted irradiance provided by SOLCAST) fits very well with the blue curve (the tilted irradiance calculated using the ASHRAE method). This confirms that this method works very well when applied to a sunny day.

In Figure 5-8 below, the same type of graph is shown, but this time for a partially cloudy day 17th of June 2022.

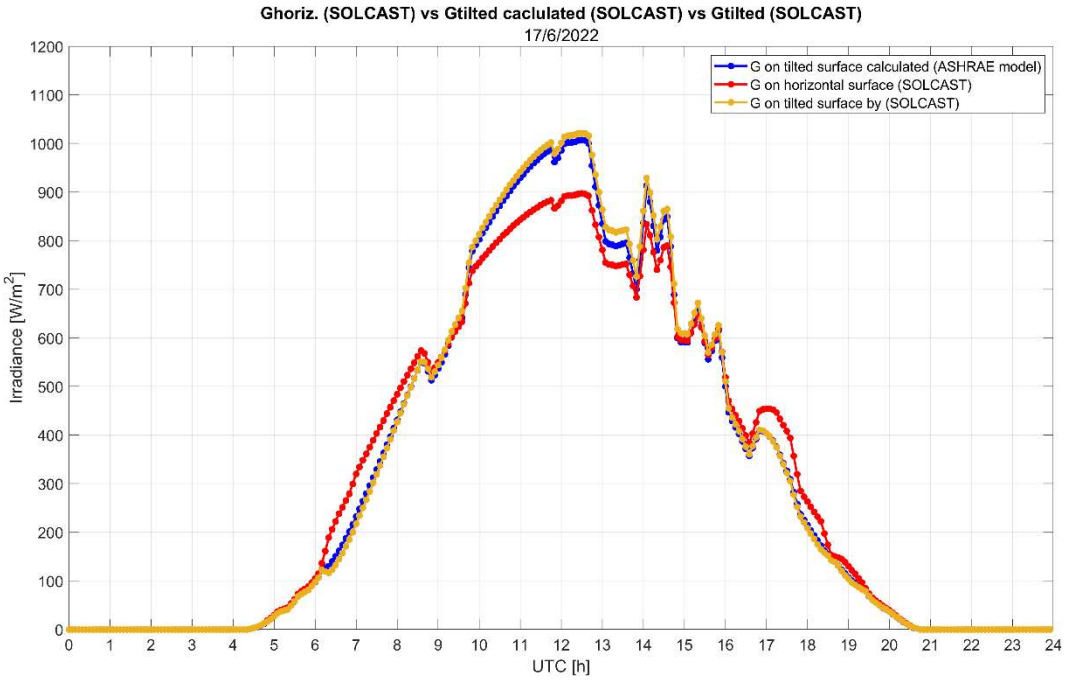

Figure 5-8 - $G_{horizonta}$ (SOLCAST horizontal irradiance source for the PV plant location - red) vs G_{tilted} (ASHRAE model applied for a tilt surface of 34° using as source of data horizontal irradiance provided by SOLCAST for the PV plant location - blue) vs G_{tilted} (SOLCAST tilted irradiance source for the PV plant location – light orange) 17/06/2022

As observed, the irradiance trend does not form a perfect bell curve due to the cloudy conditions. However, it is crucial to note how well the blue and light orange curves fit in this case. This would suggest that the ASHRAE method works well even for cloudy or partially cloudy days, indicating that the discrepancy observed previously, when the ASHRAE method was applied to the Włodawa weather station data for a cloudy day (see Figure 5-6), is likely not due to the malfunction of the ASHRAE method on non-sunny days. Instead, it is probably due to other factors mentioned earlier, such as the significant distance between the PV plant and the weather station and measurement errors in the irradiance data from the PV plant and the weather station.

In Figure 5-9 below, the comparison between the experimental irradiance measured on the inclined plane by the measurement system in the photovoltaic plant (blue line), the tilted irradiance provided by SOLCAST (light orange line), and the tilted irradiance obtained by applying the ASHRAE method using as a source of horizontal irradiance that one provided by SOLCAST (red line) is shown for a sunny day, 11th of June, 2022.

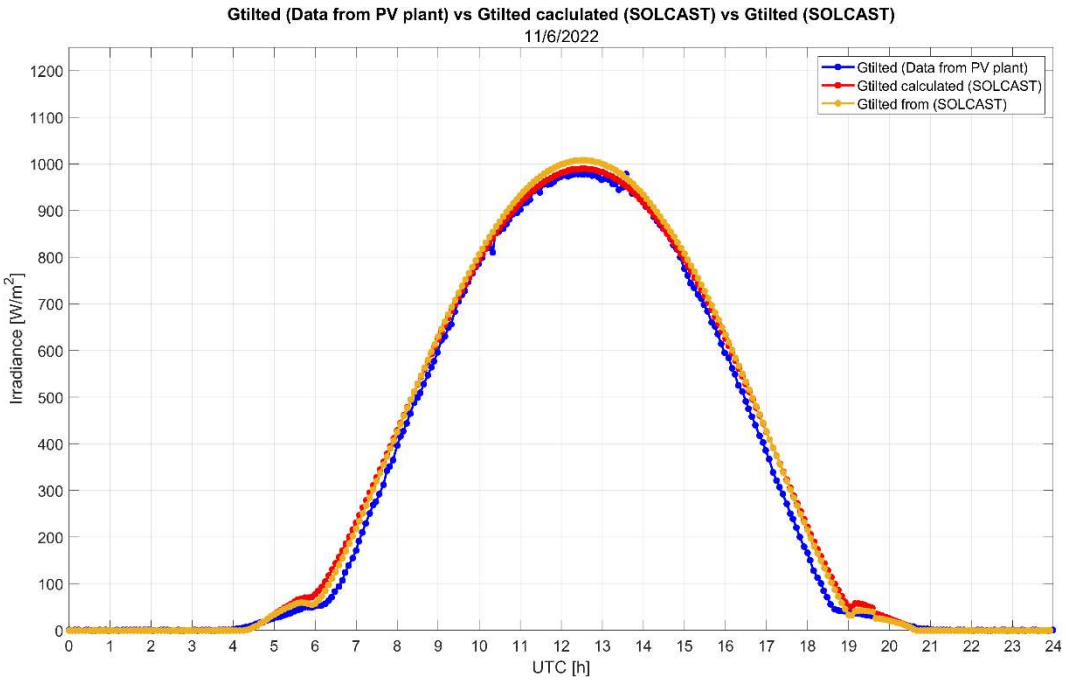

Figure 5-9 - G_{tilted} (data from the measurement system in the PV plant - blue) vs G_{tilted} (ASHRAE model applied for a tilt surface of 34° using as source of data horizontal irradiance provided by SOLCAST for the PV plant location - red) vs G_{tilted} (SOLCAST tilted irradiance source for the PV plant location – light orange) 11/06/2022

Again, the two trends related to SOLCAST fit almost perfectly with the measured irradiance daily evolution at the PV plant. This confirms once more that the measurements from the measurement system in the PV plant on sunny days do not present measurement problems, and the SOLCAST data for sunny days are consistent.

In Figure 5-10 below, the same type of graph is presented for a non-sunny day, 18th of June, 2022.

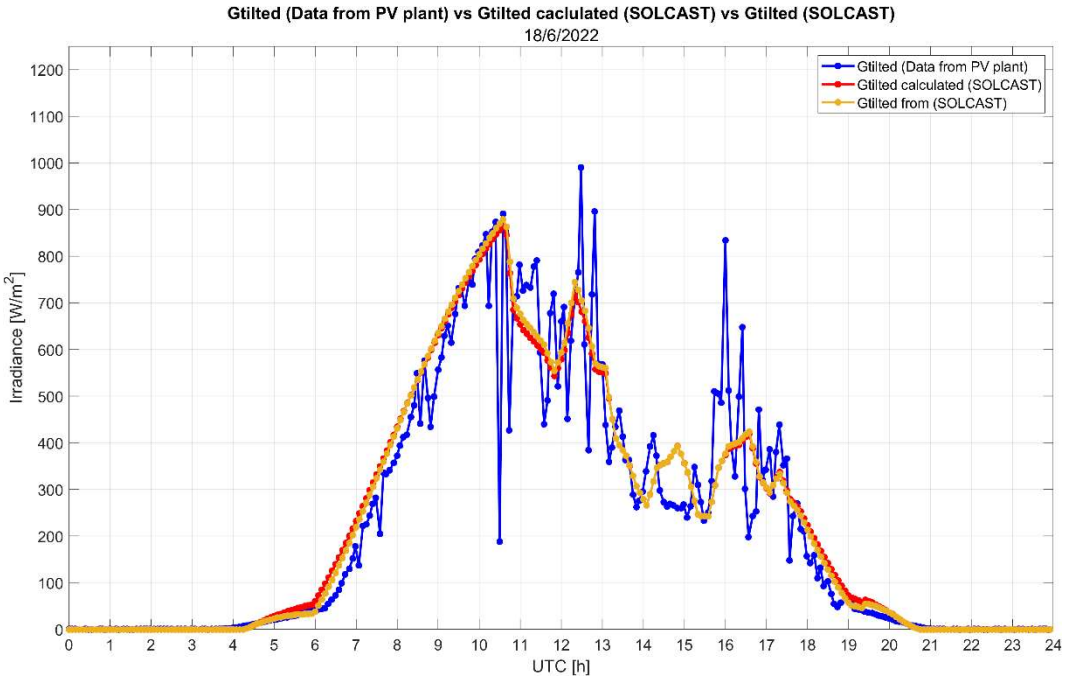

Figure 5-10 - G_{tilted} (data from the measurement system in the PV plant - blue) vs G_{tilted} (ASHRAE model applied for a tilt surface of 34° using as source of data horizontal irradiance provided by SOLCAST for the PV plant location - red) vs G_{tilted} (SOLCAST tilted irradiance source for the PV plant location – light orange) 18/06/2022

In this case, it is evident that the two trends from SOLCAST (red and light orange lines) do not fit perfectly with the measured data from the photovoltaic plant. The general trend of SOLCAST follows the actual measured trend at the PV plant, but there are significant differences concerning the various peaks present at the PV plant and not in the SOLCAST data.

It is essential to remember that SOLCAST data have a 5-minute timestep, with values averaged every 5 minutes, whereas the measurement system in the PV plant data have variable timesteps ranging from 4 to 6 minutes. However, the PV plant data are not averaged over the interval but are instantaneous measurements. This discrepancy could be one reason why SOLCAST data exhibit fewer peaks and a

smoother trend. Additionally, this might further confirm that the peaks present in the measurement system in the PV plant data may be anomalies related to issues of the on-site measurement system, as previously hypothesized.

Another critical aspect to highlight is that, unlike the previous case where the Włodawa weather station data came from a location more than 40 km away from the PV plant, leading to potentially inaccurate comparisons, in this case, the SOLCAST data is provided for the same location as the photovoltaic plant, eliminating this problem. It is also important to remember that SOLCAST data are not field measurements taken by a pyranometer but estimation from satellite data. Therefore, it should be noted that from SOLCAST dataset it cannot identify the instantaneous passage of a cloud over the PV plant (as the reference cell at the PV plant would). For this reason, SOLCAST data might be more suitable for evaluating radiation throughout the day rather than for observing the irradiance trend. This energy analysis in function of irradiation has been conducted, and the results will be presented and compared in the following chapters.

❖ **ASHRAE model for clear-sky conditions on PV plant results**

In this section, the results obtained from applying the ASHRAE model without any inversion of the formulas, as described in Chapter 4.3.1, are presented. These results illustrate the clear-sky conditions for various days in June 2022 calculated on an horizontal plane. This data is essential for the subsequent calculation of the clearness index (K_c) for the location corresponding to the weather station's geographical coordinates. The study focuses on these coordinates because, as discussed in Chapter 4.4 "Classification of Days According to K_c", the K_c will be calculated using the Włodawa weather station as the geographical reference. It must be reminded that the value of K_c will be paramount to identify sunny, partly cloudy and cloudy days in following sections, for a sunny day K_c is maximum while for cloudy day in minimum. How K_c is ranged will define the three categories of days previously mentioned.

In the next page, in Figure 5-11, the clear-sky condition for 1st of June, 2022, obtained through the application of this model, is shown.

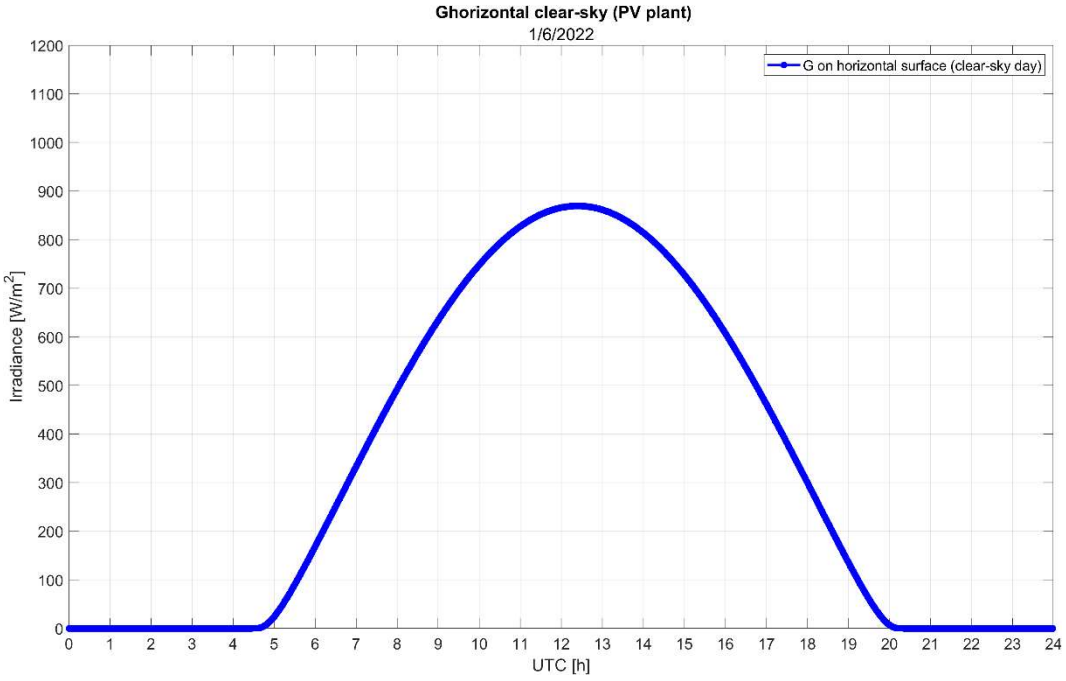

Figure 5-11 - $G_{horizontal}$ clear-sky day (ASHRAE model applied for a horizontal surface on the PV plant location - blue) 01/06/2022

As expected, a perfect bell-shaped curve is observed for the clear-sky day. Only one day is illustrated as an example because all other days analyzed in June exhibit nearly identical patterns. This similarity arises because the model's results depend solely on the location (which remains constant) and the period under consideration (the same month).

5.2.2 Olmo model results

In this section, the results obtained from the application of the Olmo model will be analyzed. As stated in earlier chapters, this additional model was applied to transpose irradiance from the horizontal plane to the tilted plane. This was done to verify if it performed better or worse compared to the ASHRAE model. Specifically, the ASHRAE model is designed for calculating irradiance on clear-sky days, and its performance on cloudy or partially cloudy days is uncertain. Therefore, the Olmo model was used because its formulas incorporate the K_t and

K_c indices, allowing it to account for cloudiness. Detailed information on this model and its application using the two different indices can be found in Chapter 2.4 "Irradiance Correction: Olmo Model".

The analysis will cover two distinct datasets: one involving the application of the model using the clearness index K_t, and the other using the clear-sky index K_c. Both models mentioned above were thoroughly described in Chapter 4.3.2 "Olmo Model Application".

- **Olmo model with K_t "clearness index" results**

In this subsection, the results obtained from the application of the Olmo model using the K_t "clearness index" are presented. The methodology for obtaining these results was detailed in Chapter 4.3.2, specifically within the subsection "Olmo Model with K_t "Clearness Index"". As previously explained, the Olmo model was applied using three different K_t values: instantaneous K_t calculated every minute, hourly averaged K_t, and daily averaged K_t. This approach facilitates a comparative analysis to determine the model's performance across different K_t values.

Starting with instantaneous K_t, Figure 5-12 in the next page illustrates the irradiance transposition achieved for 11th of June, 2022. The graph displays the measured irradiance on the horizontal plane by the pyranometer at the weather station in red, contrasted with the transposed data using the Olmo model with instantaneous K_t in blue.

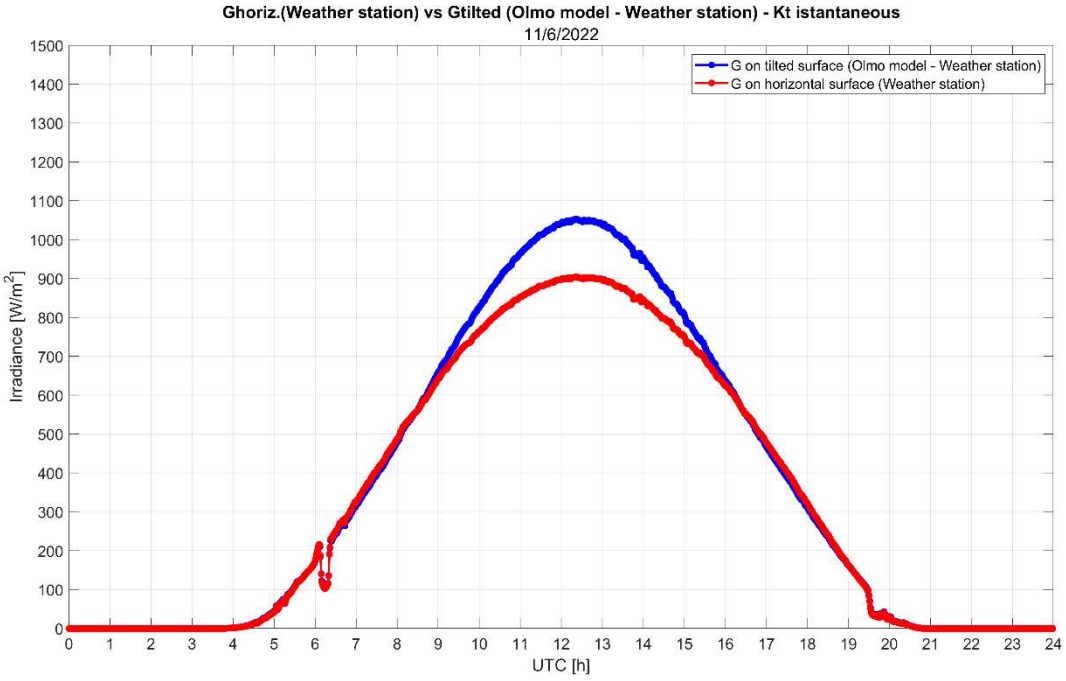

Figure 5-12 - $G_{horizontal}$ (from Włodawa weather station measurement system - red) vs G_{tilted} (Olmo model with K_t instantaneous applied for a tilt surface of 34° using as source of data experimental horizontal solar irradiance from Włodawa weather station - blue) 11/06/2022

The graph indicates a bell-shaped curve typical of sunny days. Initially, the transposition from the horizontal to tilted planes appears accurate, with a peak around 1150 W/m^2 during peak hours, which is higher than that measured on the horizontal plane. However, discrepancies observed in the early and late hours of the day suggest potential issues with the transposition method, which will be further analyzed in Figure 5-16.

Next, examining a cloudy day, Figure 5-13 depicts similar characteristics but for 15th of June, 2022.

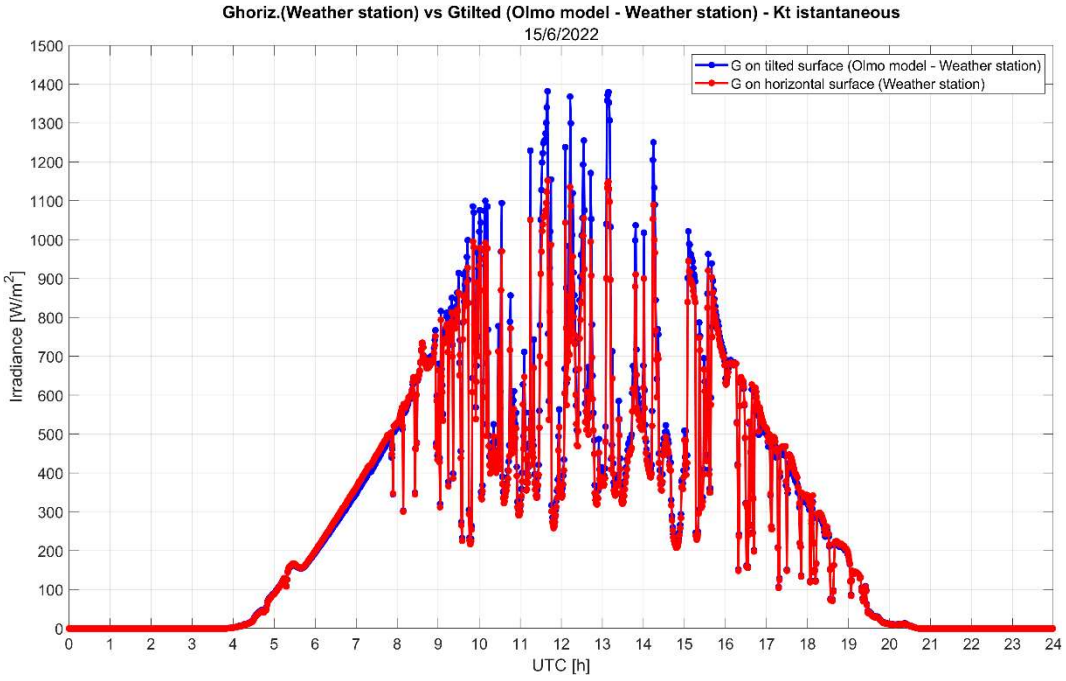

Figure 5-13 - $G_{horizontal}$ (from Włodawa weather station measurement system - red) vs G_{tilted} (Olmo model with K_t instantaneous applied for a tilt surface of 34° using as source of data experimental horizontal solar irradiance from Włodawa weather station - blue) 15/06/2022

As previously discussed, challenges arise in accurately measuring solar irradiance on the horizontal plane at the Włodawa weather station during cloudy days, resulting in peaks exceeding 1150 W/m^2, values that are unrealistic. Despite this, peak irradiance values after transposition using the Olmo model with instantaneous K_t generally exceed those measured on the horizontal plane, consistent with expected outcomes. However, similar issues persist at the beginning and end of the day as noted earlier.

Turning to the Olmo model applied with hourly K_t , Figure 5-14 presents results for the same sunny day of 11th of June, 2022.

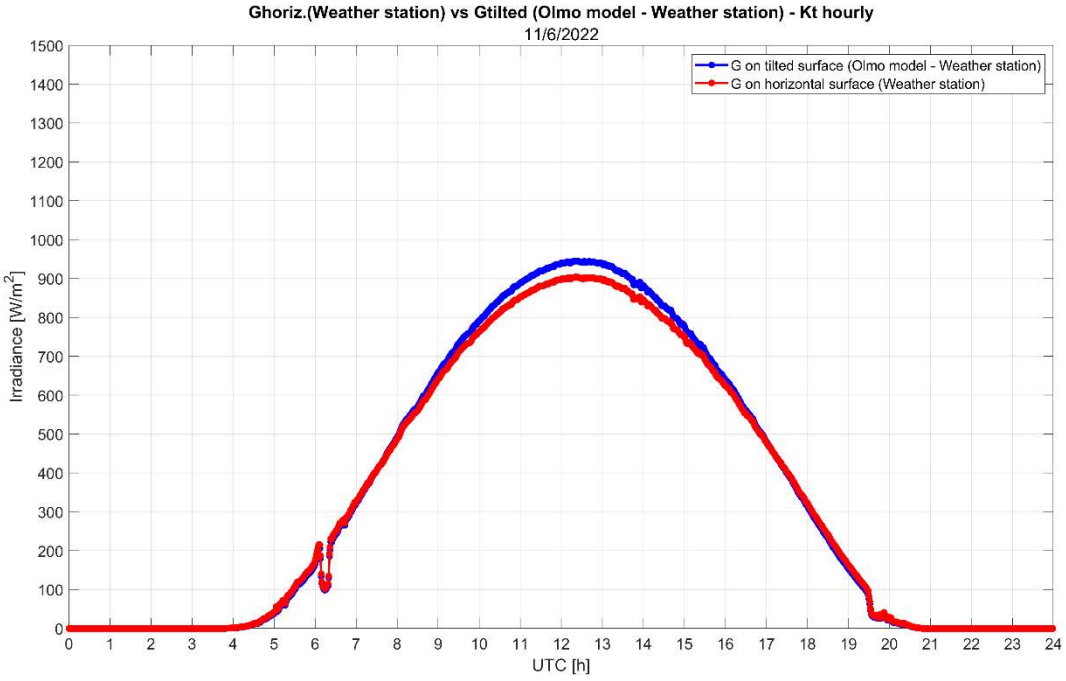

Figure 5-14 - $G_{horizontal}$ (from Włodawa weather station measurement system - red) vs G_{tilted} (Olmo model with K_t hourly applied for a tilt surface of 34° using as source of data experimental horizontal solar irradiance from Włodawa weather station - blue) 11/06/2022

Similar observations apply as with instantaneous K_t, although with a lower peak irradiance value around 950 W/m^2 compared to the approximately 1150 W/m^2 observed with instantaneous K_t.

Figure 5-15 below illustrates a cloudy day, 15th of June, 2022, using the Olmo model applied with hourly K_t.

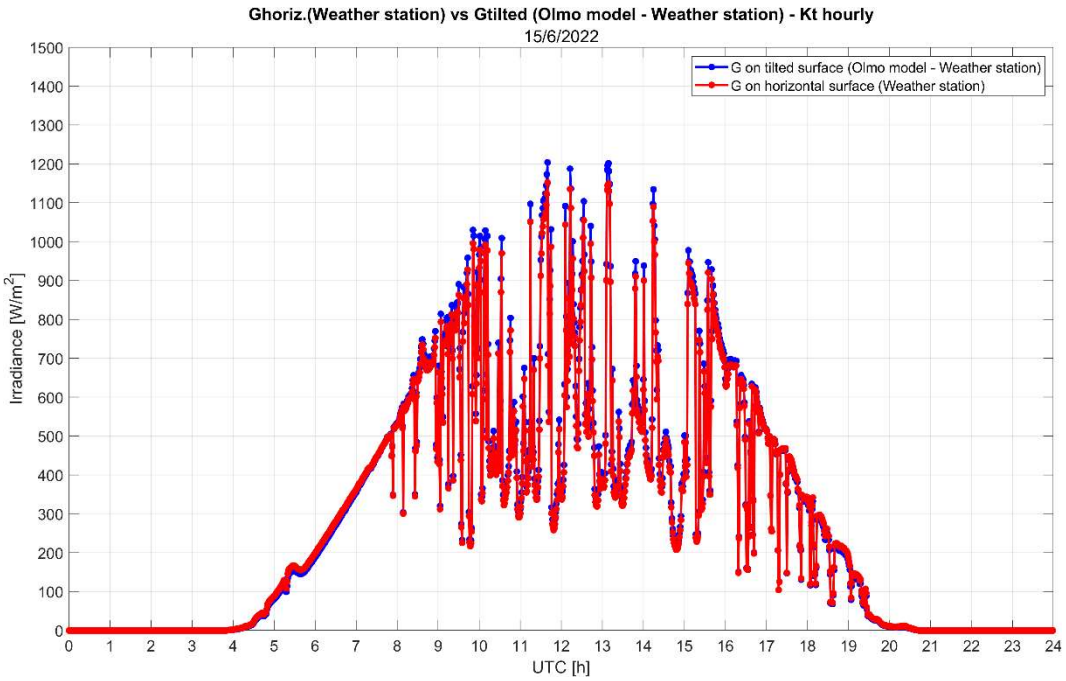

Figure 5-15 - $G_{horizonta}$ (from Włodawa weather station measurement system - red) vs G_{tilted} (Olmo model with K_t hourly applied for a tilt surface of 34° using as source of data experimental horizontal solar irradiance from Włodawa weather station - blue) 15/06/2022

The graph reflects comparable considerations as seen with instantaneous K_t for the same day, although with slightly higher peaks post-transposition, marginally exceeding values measured on the horizontal plane.

Finally, graphs obtained with daily K_t, though not displayed here due to negligible differences compared to hourly K_t results, will be included in the final comparison of various Olmo model results in subsequent paragraphs.

After presenting results for different K_t values, the most effective approach to evaluate these models' efficacy in transposing irradiance from horizontal to tilted planes is to compare them with results obtained using the ASHRAE model applied

to Włodawa weather station data and actual irradiance measurements from the photovoltaic system. Figure 5-16 displays these comparisons for the sunny day of 11th of June, 2022: Olmo model results with instantaneous K_t (red), hourly K_t (orange), and daily K_t (pink); ASHRAE model results (green); and actual measured irradiance on the inclined plane at the photovoltaic system (blue).

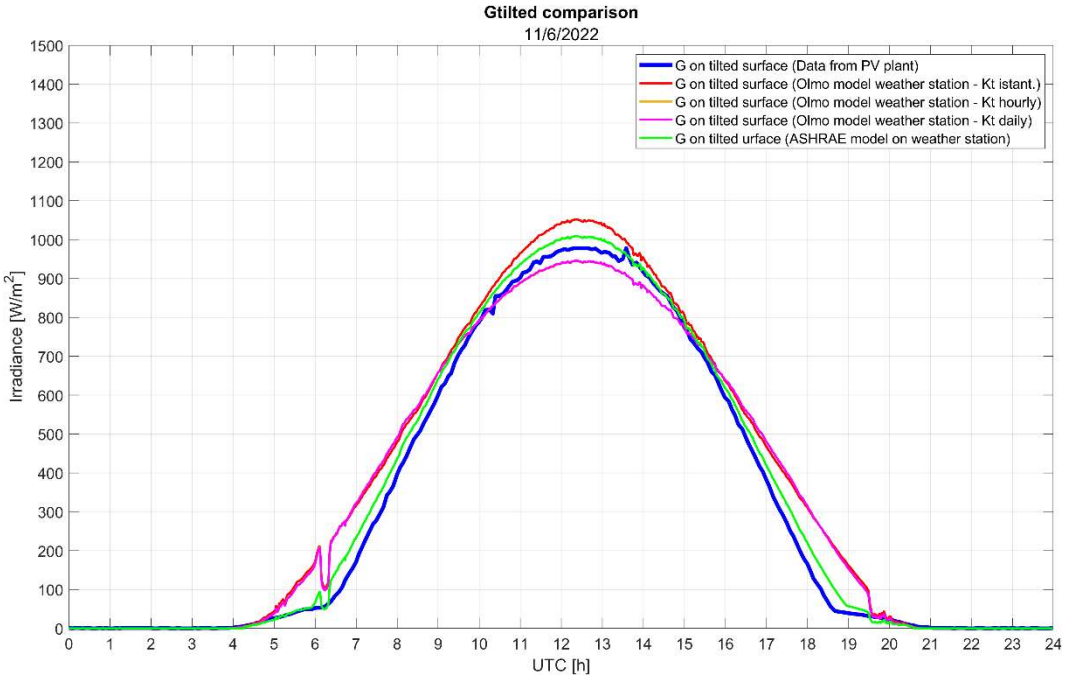

Figure 5-16 - G_{tilted} (data from the measurement system in the PV plant - blue) vs G_{tilted} (Olmo model with K_t istantaneous applied for a tilt surface of 34° using as source of data experimental horizontal solar irradiance from Włodawa weather station - red) vs G_{tilted} (Olmo model with K_t hourly applied for a tilt surface of 34° using as source of data experimental horizontal solar irradiance from Włodawa weather station – light orange) vs G_{tilted} (Olmo model with K_t daily applied for a tilt surface of 34° using as source of data experimental horizontal solar irradiance from Włodawa weather station - pink) vs G_{tilted} (ASHRAE model applied for a tilt surface of 34° using as source of data experimental horizontal solar irradiance from Włodawa weather station - green) 11/06/2022

The graph indicates that for the sunny day analyzed, the Olmo model with instantaneous K_t (red line) exhibits a peak daily irradiance of approximately 1050 W/m^2, notably higher than the actual measured irradiance (blue line) of about 980

W/m^2. Peak irradiance values obtained with hourly and daily K_t models are slightly lower, maintaining a closer proximity to actual measurements than those achieved with instantaneous K_t. However, all Olmo models exhibit poor performance at the beginning and end of the day in replicating actual trends, contrasting with the reliable performance of the ASHRAE model in this scenario.

In Figure 5-17 below, the same type of graph previously shown is presented, but this time for the day 25th of June, 2022, a partly cloudy day.

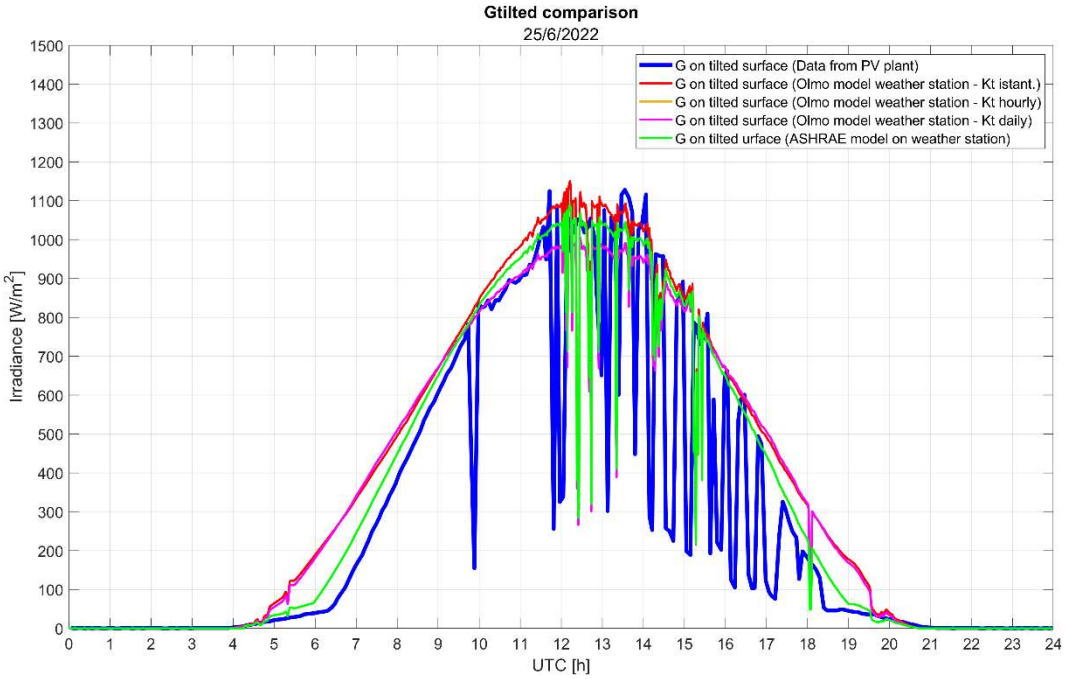

Figure 5-17 - G_{tilted} (data from the measurement system in the PV plant - blue) vs G_{tilted} (Olmo model with K_t istantaneous applied for a tilt surface of 34° using as source of data experimental horizontal solar irradiance from Włodawa weather station - red) vs G_{tilted} (Olmo model with K_t hourly applied for a tilt surface of 34° using as source of data experimental horizontal solar irradiance from Włodawa weather station – light orange) vs G_{tilted} (Olmo model with K_t daily applied for a tilt surface of 34° using as source of data experimental horizontal solar irradiance from Włodawa weather station - pink) vs G_{tilted} (ASHRAE model applied for a tilt surface of 34° using as source of data experimental horizontal solar irradiance from Włodawa weather station - green) 25/06/2022

As can be seen, in the case of a cloudy day, the height of the peaks during the central hours of the day exhibits the same proportions observed in the trends of Figure 5-16. Additionally, during the early and late hours of the day, the Olmo models with K_t demonstrate poor performance, as they fail to accurately fit the data measured at the PV plant. Therefore, it can be concluded that even on cloudy days, the Olmo models with K_t applied for the transposition of solar irradiance from the horizontal plane to the inclined plane from Włodawa weather station are not effective, as the obtained trends significantly deviate from the trends actually measured by the measurement system in the PV plant.

In conclusion, based on the analysis of transposing irradiance from horizontal to tilted planes, the ASHRAE model demonstrates superior performance compared to the Olmo model with K_t. Therefore, the use of the Olmo model with K_t will be discontinued for further analysis in subsequent studies.

In the next section, however, the Olmo model will be analyzed again, this time applied not with K_t (clearness index) but with K_c (clear-sky index). This analysis aims to verify whether the latter performs better in transposing irradiance from a horizontal plane to an inclined plane.

❖ Olmo model with K_c "clear-sky index" results

In this section, the results obtained through the application of the Olmo model, this time applied with the K_c "clearness index," are presented. The entire procedure to obtain these results is detailed in Chapter 4.3.2, specifically in the section "Olmo model with K_c 'clear-sky index'". It is useful to remember that the main difference between this Olmo model and the one explained in the previous section lies in the replacement of the K_t index with the K_c index. This index directly influences ψ_0 (Equation 2-16), the function used to transpose irradiance from a horizontal plane to an inclined plane.

In both cases, these indices are included to account for the presence or absence of clouds during the day. The difference is that K_t accounts for this by comparing the actual measured irradiance on a horizontal plane to the extraterrestrial irradiance (Equation 2-17). Meanwhile, K_c does so by comparing the actual measured irradiance on a horizontal plane to the clear-sky irradiance for the same geographical location (Equation 2-24). After deciding not to proceed with the use

of the Olmo model applied with K_t due to its low performance in transposing irradiance from a horizontal plane to an inclined plane, the model was evaluated with K_c. This was done to see if it performs better in this context.

Unlike the previous application of the Olmo model with different K_t values (instantaneous, hourly, daily), this model was applied with a single K_c value, specifically the daily K_c. The primary reasons for this choice are that K_c values were calculated on a daily basis to classify the days, and it was observed in previous analyses related to K_t that the daily value performed best in transposing solar irradiance from the horizontal plane to an inclined plane.

As explained in the aforementioned chapter, to apply this variant of the Olmo model, it is necessary to first calculate the K_c values for each day. These values were calculated prior to applying this model, as detailed in Chapter 4.4 "Classification of days according to K_c". The various K_c values were calculated daily and based on their numerical value, allowed for the classification of the day as sunny, cloudy, or partly cloudy.

In Figure 5-18 in the next page, the solar irradiance trend for the considered location (Włodawa weather station) can be visualized. Specifically, two trends are shown: one in red, representing the irradiance measured on the horizontal plane by a pyranometer at the weather station, and one in blue, showing the trend on an inclined plane obtained using the Olmo model with daily K_c applied to the data measured on the horizontal plane. This graph shows the day 11th of June, 2022.

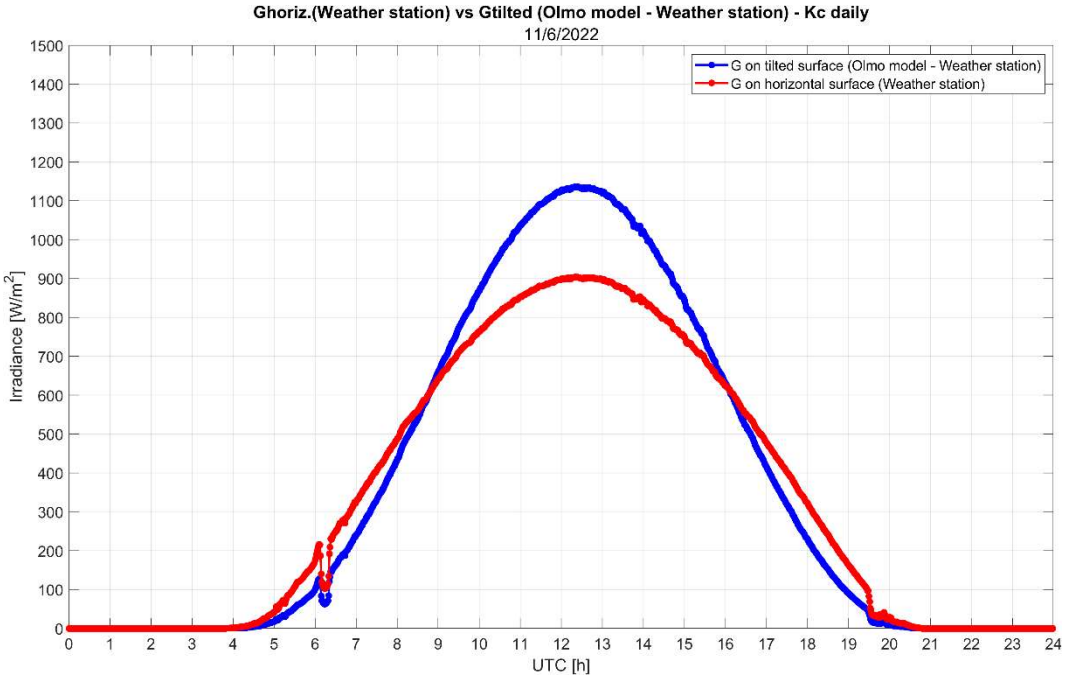

Figure 5-18 - $G_{horizontal}$ (from Włodawa weather station measurement system - red) vs G_{tilted} (Olmo model with K_c daily applied for a tilt surface of 34° using as source of data experimental horizontal solar irradiance from Włodawa weather station - blue) 11/06/2022

As can be observed, the day considered is a sunny day, which is evident from the bell-shaped curve of the solar irradiance measured during the day. The results obtained from the transposition are consistent with the expectations for this type of operation. The peak transposed irradiance surpasses that measured on the horizontal plane at the Włodawa weather station. In this case, the peak value reaches 1140 W/m², which at first glance seems slightly high compared to expected standards, but this will be analyzed further in the following sections. For the early and late parts of the day, the Olmo model with K_c performs better than the previously analyzed model with K_c, as the solar irradiance values are slightly lower compared to those measured on the horizontal plane during these hours, as they should be.

When analyzing a partly cloudy day, as shown in Figure 5-19 below, which illustrates the day 15th of June, 2022, the following results can be noted.

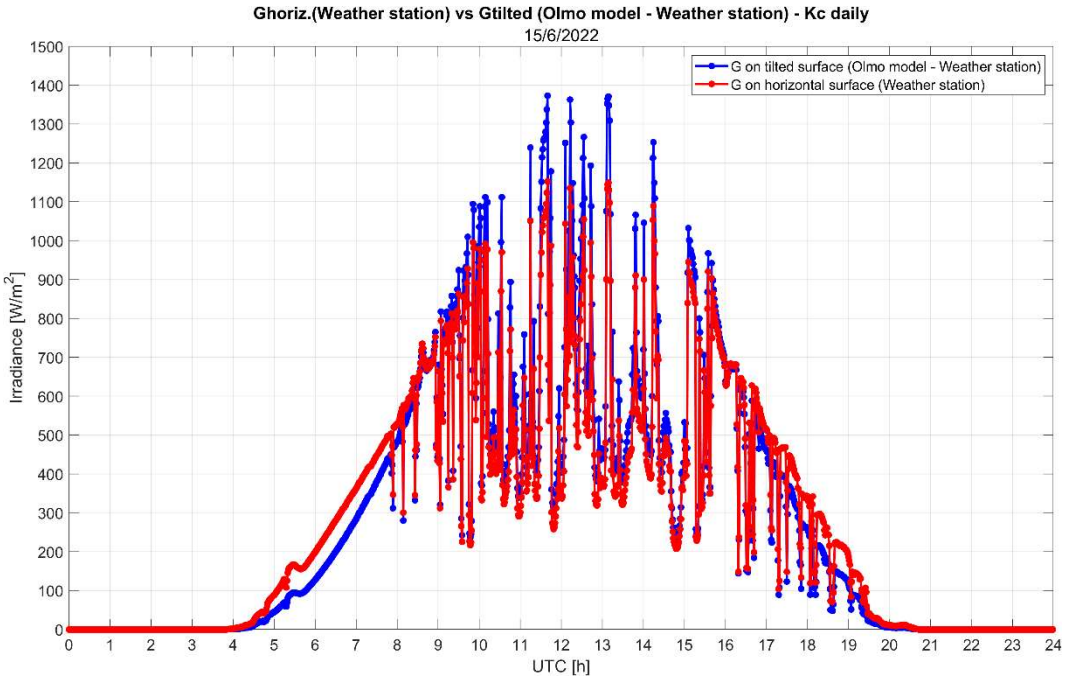

Figure 5-19 - $G_{horizontal}$ (from Włodawa weather station measurement system - red) vs G_{tilted} (Olmo model with K_c daily applied for a tilt surface of 34° using as source of data experimental horizontal solar irradiance from Włodawa weather station - blue) 15/06/2022

As previously mentioned, cloudy days pose challenges in accurately measuring solar irradiance at the Włodawa weather station on the horizontal plane, leading to exaggerated peak estimates exceeding 1150 W/m². Consequently, further filtering will be required in later research to address this issue. Despite this, peak irradiance values upon transposition obtained using the Olmo model with K_c typically surpass those measured on the horizontal plane, consistent with expected results.

To better evaluate the effectiveness of this method, it is useful to compare the newly obtained results with those previously obtained using the ASHRAE model, applied to transpose the horizontal irradiance data provided by the weather station to an inclined plane of the same inclination as the panels, and also with the actual

inclined irradiance data measured at the PV plant. In Figure 5-20 below, a graph is shown comparing these three trends for the day 11th of June, 2022. The trend of the data derived from measurements at the photovoltaic plant is shown in blue, the one obtained with the application of the Olmo model with K_c in pink, and the one obtained with the ASHRAE model in green.

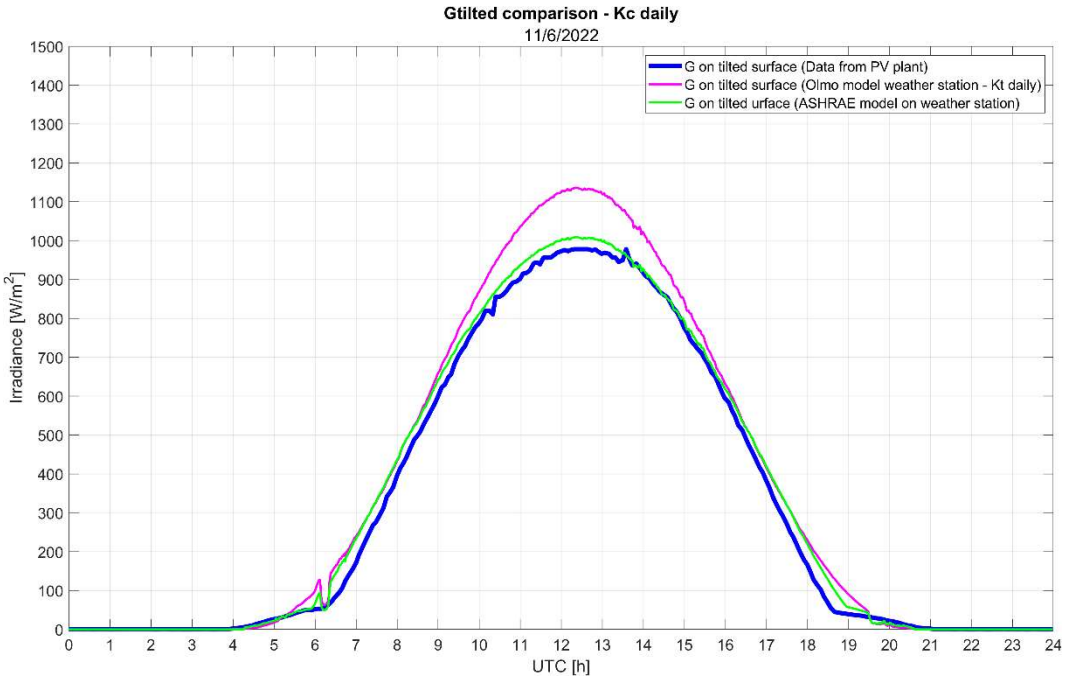

Figure 5-20 - G_{tilted} (data from the measurement system in the PV plant - blue) vs G_{tilted} (Olmo model with K_c daily applied for a tilt surface of 34° using as source of data experimental horizontal solar irradiance from Włodawa weather station - pink) vs G_{tilted} (ASHRAE model applied for a tilt surface of 34° using as source of data experimental horizontal solar irradiance from Włodawa weather station - green) 11/06/2022

As can be seen from the Figure 5-20, the peak obtained with the application of the Olmo model (pink line) is significantly higher than the one actually measured at the PV plant by the on-site measurement system (blue line), with values of approximately 1140 W/m² and 980 W/m², respectively. Regarding the trend of inclined irradiance obtained with the Olmo model with K_c during the early and late hours of the day, it performs better than that obtained with the various Olmo models with K_t, fitting better with the trend actually measured at the PV plant. However,

it can be confirmed once again that the ASHRAE model works better for transposing irradiance from the horizontal plane to the inclined plane. This is evidenced by the smaller difference between the peak obtained with the ASHRAE model and the data actually measured at the PV plant.

Finally, in the graph shown in Figure 5-21 below, the same type of graph previously shown is presented, but this time for a partly cloudy day, specifically 25th of June, 2022.

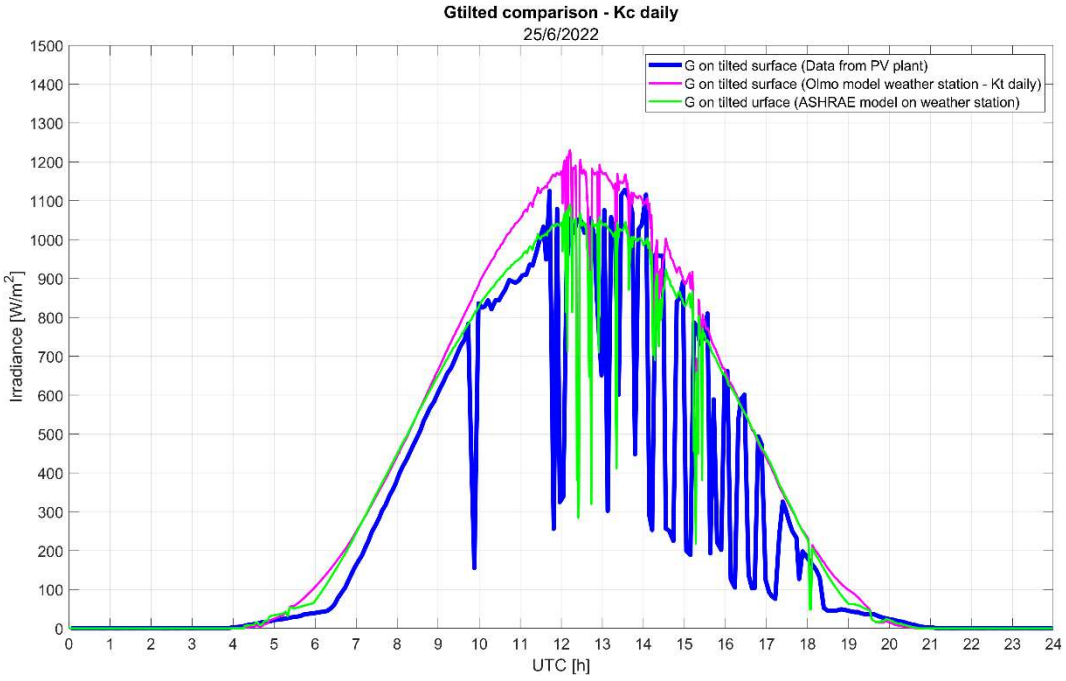

Figure 5-21 - G_{tilted} (data from the measurement system in the PV plant - blue) vs G_{tilted} (Olmo model with K_c daily applied for a tilt surface of 34° using as source of data experimental horizontal solar irradiance from Włodawa weather station - pink) vs G_{tilted} (ASHRAE model applied for a tilt surface of 34° using as source of data experimental horizontal solar irradiance from Włodawa weather station - green) 25/06/2022

In this case, for a partly cloudy day, the same conclusions as in the previous paragraph can be drawn. Therefore, it can be confirmed that the ASHRAE model performs better even for cloudy days compared to the Olmo model applied with

K_c. For this reason, in future analyses, the Olmo model with K_c will be excluded from studies, and only the ASHRAE model will be used.

5.2.3 Radiation analysis results

In the preceding sections, various methods and corresponding results for transposing irradiance from the horizontal plane to an inclined plane were examined, with particular emphasis on the ASHRAE and Olmo models. Following the assessments of these models, the decision was made to proceed exclusively with the ASHRAE model applied to data from the Włodawa weather station and SOLCAST for this analysis. This chapter focuses on the day-by-day calculation of radiation, which represents the total energy received per square meter per day (Wh/m²) in a certain area. The short-term goal of this calculation is to compare the radiation determined using the irradiance transposition models with the actual radiation measured by the photovoltaic system on an inclined plane. The final goal of the irradiation computation is to analyse if the misalignments among irradiance recorded in the PV plant and the predicted one have a significant impact on the solar energy collected by the PV modules, which obviously, will define their energy production.

To achieve this, an integral calculation was necessary to determine the energy, effectively representing the area under the irradiance curve. As previously mentioned, the SOLCAST database provides data with a time-step of five minutes, representing a five-minute average. Conversely, the data from the photovoltaic system varies, with time steps sometimes being four, five, or six minutes. However, on average, this time step also approximates five minutes. Therefore, to ensure accurate analysis, the data from the Włodawa weather station, which was provided every minute, was averaged over five-minute intervals to align with the other datasets. Additionally, the comparison includes data directly measured by SOLCAST on an inclined plane, as described earlier in Section 3.4.1.

The performance of each model was evaluated using two primary metrics: Mean Absolute Error (MAE) and Mean Absolute Percentage Error (MAPE). These metrics were crucial in assessing the accuracy of the models used for irradiance transposition. MAE measures the average magnitude of errors in a set of predictions, without considering their direction, and is calculated as the mean of the absolute differences between predicted and actual values. MAPE expresses the

average magnitude of errors as a percentage of the actual values, providing a perspective on the error relative to the size of the actual values. The performance evaluation metrics were calculated for three models:

- Model 1 = G_{tilted} calculated with ASHRAE model using horizontal irradiance directly given by SOLCAST data for the Włodawa weather station location,

- Model 2 = G_{tilted} directly given by SOLCAST data for the Włodawa weather station location,

- Model 3 = G_{tilted} calculated with ASHRAE model using horizontal irradiance experimentally measured in Włodawa weather station,

In Figure 5-22, the calculated radiation values for the different models are shown day by day for the entire month of June 2022, excluding 21st of June, 2022. As previously described in Section 4.2, this day was excluded from the entire analysis due to the lack of irradiance data measured by the photovoltaic system. The four different trends visible in the graph are:

- Blue line: the daily calculated radiation using G_{tilted} data calculated with the ASHRAE model to convert irradiance data from SOLCAST on a horizontal plane to an inclined plane for the Włodawa weather station location;

- Red line: the irradiance data on the inclined plane with the same inclination as the panels, provided directly by SOLCAST without applying any transposition models for the Włodawa weather station location;

- Green line: the daily calculated radiation using G_{tilted} data calculated with the ASHRAE model to convert irradiance data measured by the pyranometer at the Włodawa weather station on a horizontal plane to an inclined plane;

- Black line: the radiation calculated with the irradiance data actually measured on the inclined plane of the photovoltaic system.

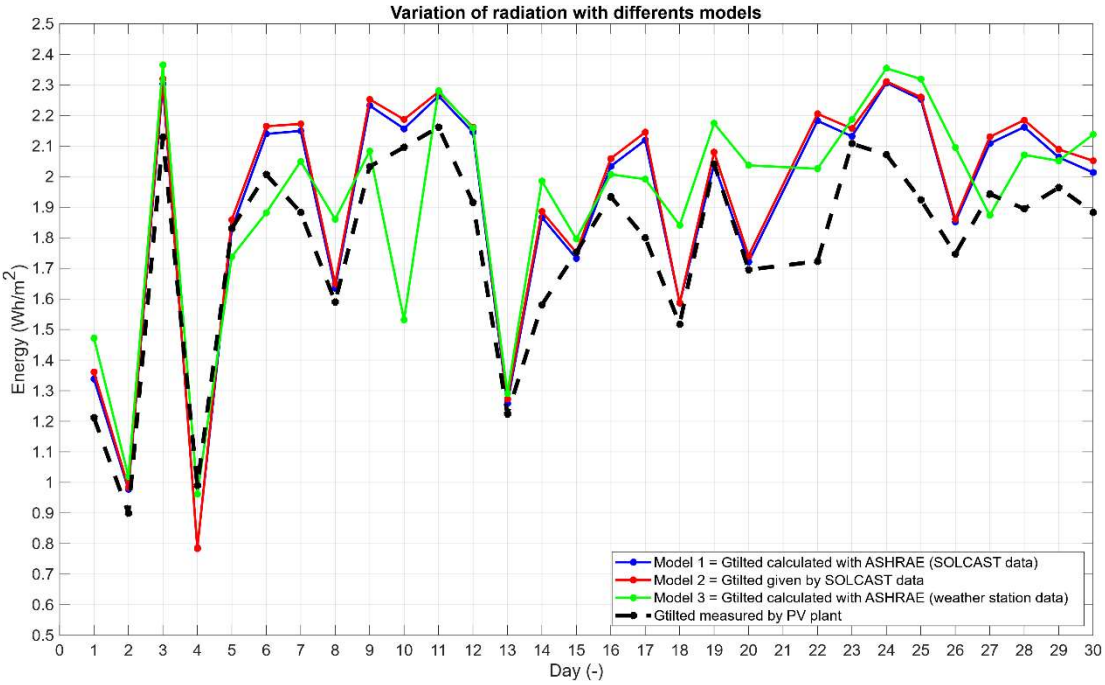

Figure 5-22 - Variation of radiation with different models

To better understand and analyze the results shown in the graph, Table 5-1 below presents the calculated misalignment for the three different models and the true value of irradiation which has been considered the irradiation measured in the PV plant.

	MAE $\left(\frac{Wh}{m^2}\right)$	MAPE (%)
MODEL 1	0.148	8.59
MODEL 2	0.166	9.57
MODEL 3	0.202	11.58

Table 5-1 - MAE & MAPE for different models when the experimental irradiation from PV plant measurement system in considered as true value.

From the analysis of the graph and the table, it can be stated that the model closest to the actual measured radiation values in the system is Model 1, the model that use G_{tilted} calculated with ASHRAE model using horizontal irradiance directly given by SOLCAST data for the Włodawa weather station location, with a MAE of 0.148 Wh/m² and a MAPE of 8.59%. Following this, Model 2 is the next closest, with a MAE of 0.166 Wh/m² and a MAPE of 9.57%. The least accurate model is Model 3, with a MAE of 0.202 Wh/m² and a MAPE of 11.58%.

It is important to note that the worst-performing model, Model 3, uses irradiance data measured by the pyranometer at the nearby weather station. This is significant as the primary aim of this study was to determine if predictions could be made using weather station data to forecast power production and provide feedback on the system's performance. The errors account for all days, including sunny, partially cloudy, and cloudy days. As known, on cloudy days, irradiance data from the Włodawa weather station presents non-negligible measurement misalignments, possibly causing the high MAE. Future improvements could involve applying a filter to reduce these peaks, as discussed in Section 5.2.1 and visible in Figure 5-2.

In a subsequent analysis, for the Model 3, the MAPE was calculated exclusively for the days categorized as "sunny days," based on the clear-sky index K_c (the method for classifying days as cloudy, partially cloudy, or sunny is explained in Chapter 5.3). This calculation aimed to verify whether the MAPE decreases significantly for these days. A substantial reduction would have suggested that the large discrepancies observed in Model 3 were primarily attributable to cloudy and partially cloudy days. The MAPE calculated for sunny days resulted in a value of 11.33%, compared to 11.58% obtained when considering all types of days (cloudy, partially cloudy, and sunny). The minimal difference between these values indicates that the significant discrepancies in Model 3 are not solely due to cloudy and partially cloudy days but also persist for sunny days. Consequently, the analysis of energy production presented in this thesis was conducted without distinguishing between day categories, as it has been demonstrated that the model exhibits consistent limitations across all types of days.

5.3 Classification of days according to K_c results

In this section, the results for classifying days into sunny, partially cloudy, or cloudy are presented. The detailed explanation of the methodology used can be found in Chapter 4.4. The analysis focuses on the days of June 2022, which exhibit varying irradiance depending on the weather conditions. This classification was carried out to evaluate whether the different models applied exhibited varying performance depending on the type of day. In such a case, different procedures could be implemented for the final energy production analysis.

The motivation for calculating values with three different K_c indices lies in redundancy. Having multiple results calculated with different models allows for comparisons to identify the most suitable model for this type of analysis. The classification is done using the K_c index, which compares the radiation calculated through the integration of irradiance measured by the pyranometer at the Włodawa weather station to the radiation under clear-sky conditions at the same location.

To estimate the latter, three different sources were used:

- ASHRAE Method: The first source uses the ASHRAE model (explained in Section 4.3.1). The clear-sky irradiance is calculated by applying the ASHRAE method, using the nearby weather station coordinates and a tilt angle of zero degrees. Both numerator and denominator compare measurements on a horizontal plane.

- SOLCAST: The second source is SOLCAST, which provides clear-sky irradiance data for specified coordinates (Włodawa weather station) and a horizontal plane.

- PVGIS: The third source is PVGIS, which also provides clear-sky irradiance data using the same input parameters as SOLCAST.

To classify the days, threshold values of K_c were set:

- $K_c < 0.45$ for cloudy days,

- $0.45 < K_c < 0.75$ for partially cloudy days,

- $K_c > 0.75$ for sunny days.

Once the irradiance data for the different days is available, an integral calculation is performed to obtain the corresponding radiation day by day. The results obtained with the three different models are presented in the following sections.

5.3.1 K_c according to ASHRAE clear-sky day data results

For this case, the ASHRAE model was applied, as illustrated in Section 4.3.1, to calculate the solar horizontal irradiance trends during clear-sky days for the days of June 2022. Both sets of irradiance data compared here have a one-minute timestep, eliminating the need for any time correction.

It may be useful to remember that the clear-sky index, K_c , is a dimensionless parameter indicating the clarity of the atmosphere. It is calculated as the ratio of the measured irradiance, G, to the clear-sky irradiance, $G_{clear-sky}$, following the formula shown previously in Equation 2-24:

$$K_c = \frac{G}{G_{clear-sky}} \tag{2-24}$$

In all subsequent graphs, these two values will be compared: the numerator G will be depicted in red, while the denominator $G_{clear-sky}$ will be represented in blue.

In Figure 5-23, the irradiance trends used to calculate K_c for 19th of June, 2022, a sunny day, are shown. The blue line represents the clear-sky irradiance calculated using the ASHRAE model for the Włodawa weather station location, specifically the model applied without the inversion of formulas, which is used for calculating the clear-sky irradiance on a horizontal plane for a given geographical location. The red line represents the measured horizontal irradiance from the pyranometer at the Włodawa weather station.

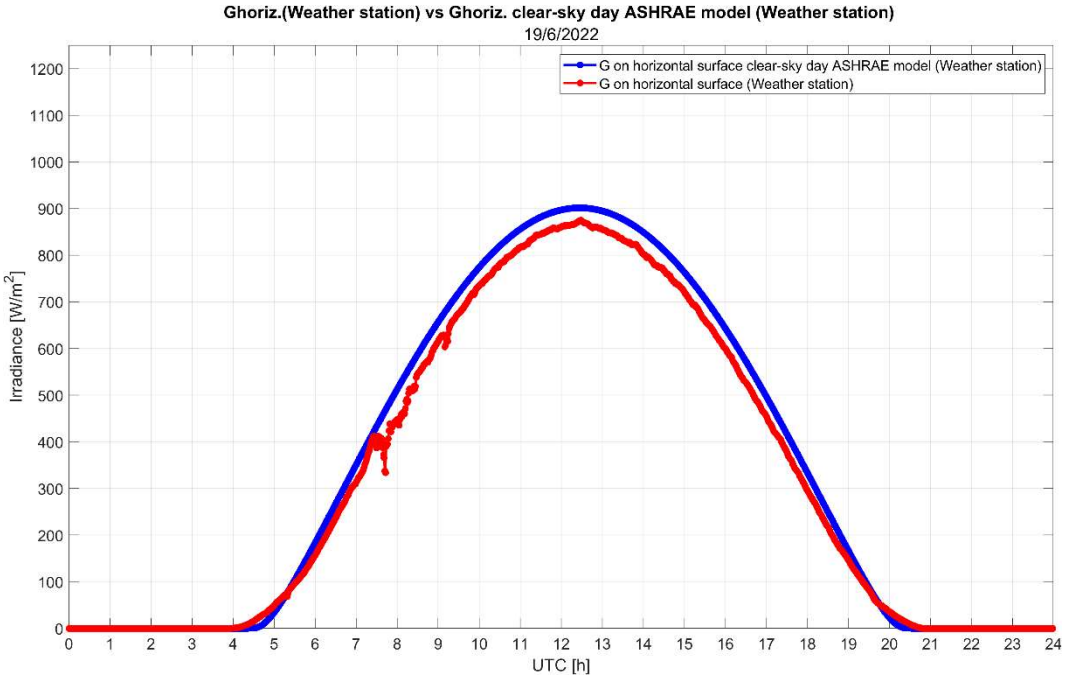

Figure 5-23 - $G_{horizontal}$ (from Włodawa weather station measurement system - red) vs $G_{horizontal}$ clear-sky day (ASHRAE model applied for a horizontal surface on the Włodawa weather station location - blue) 19/06/2022

As expected for a sunny day, both trends show a bell-shaped curve. By calculating the areas under the two curves through integral calculus and taking the ratio of the red to the blue area, the K_c value is obtained (0.89), as shown in Figure 5-25.

In Figure 5-24, a similar graph is shown for a different day, 4th of June, 2022, a cloudy day.

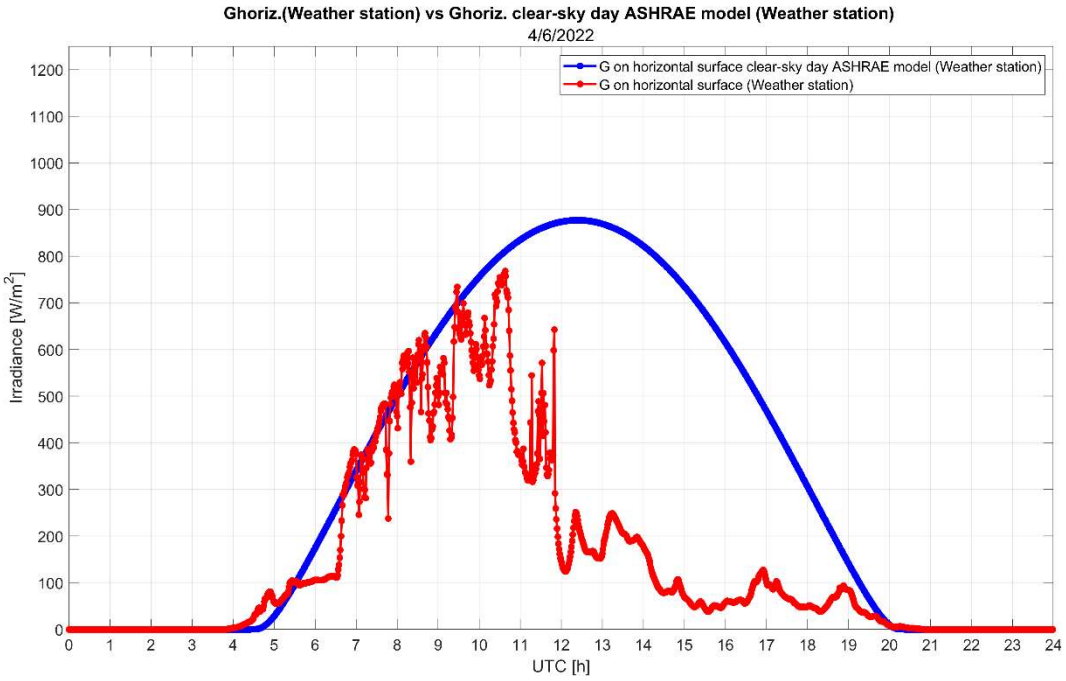

Figure 5-24 - $G_{horizontal}$ (from Włodawa weather station measurement system - red) vs $G_{horizontal}$ clear-sky day (ASHRAE model applied for a horizontal surface on the Włodawa weather station location - blue) 04/06/2022

The red line, representing the measured irradiance on the horizontal plane, does not show a bell-shaped curve but rather low values throughout the day. The K_c value for this day is 0.42 and it is shown in Figure 5-25.

The two graphs above illustrate examples of a sunny day and a cloudy day. The same calculation was performed for all days in June, except for 21th of June, 2022, which was excluded due to insufficient data. The K_c values for the analyzed days are presented in Figure 5-25.

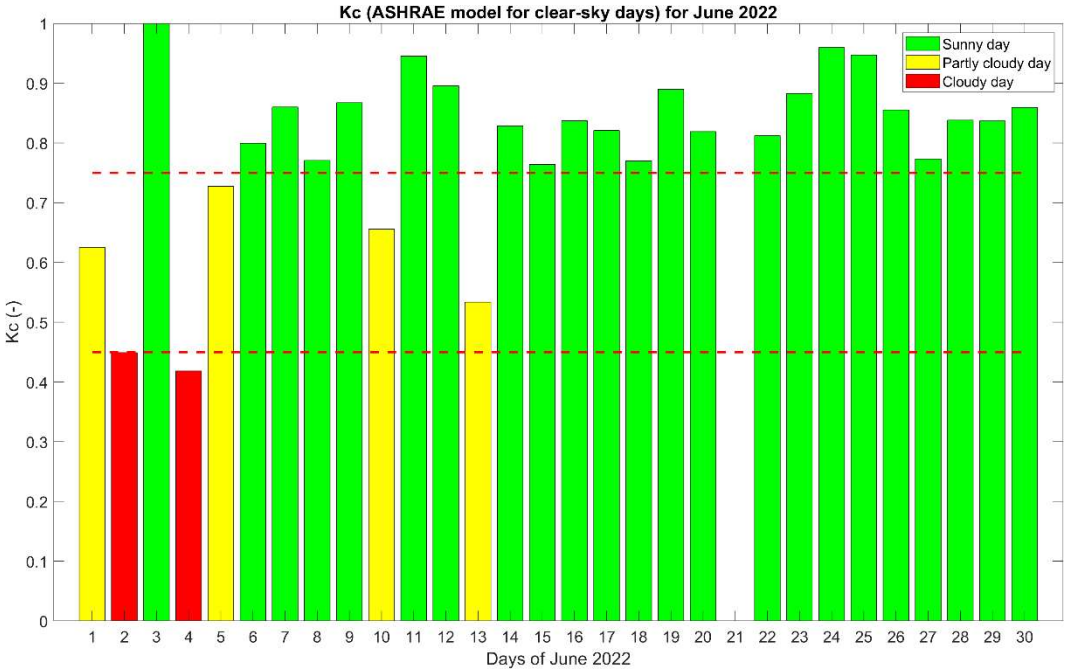

Figure 5-25 - days classification - K_c calculated with $G_{horizontal}$ clear-sky day (ASHRAE model applied for a horizontal surface on the Włodawa weather station location) for June 2022 – sunny day (green), partly cloudy day (yellow), cloudy day (red)

The histogram shows a mix of sunny, partially cloudy, and cloudy days in June. Specifically, there are 2 cloudy days (red bars), 4 partially cloudy days (yellow bars), and 23 sunny days (green bars). It is important to note that irradiance data measured at the Włodawa weather station on the horizontal plane sometimes show anomalous peaks during cloud passages (as discussed in Section 5.2.1 and visible in Figure 5-2), which could falsely increase the total calculated radiation, resulting in a K_c value above 0.75 and classifying the day as "sunny".

5.3.2 K_c according to SOLCAST clear-sky days data results

For this case, data from SOLCAST were used to obtain the solar irradiance trends during clear-sky days for June 2022. SOLCAST data have a five-minute timestep, representing the average irradiance over this period. Therefore, the measured irradiance data from the pyranometer, initially provided minute-by-minute, were averaged every five minutes to match this timestep.

In Figure 5-26, the irradiance trends for 19th of June, 2022, a sunny day, are shown. The blue line represents the clear-sky irradiance from SOLCAST, and the red line represents the measured irradiance from the pyranometer.

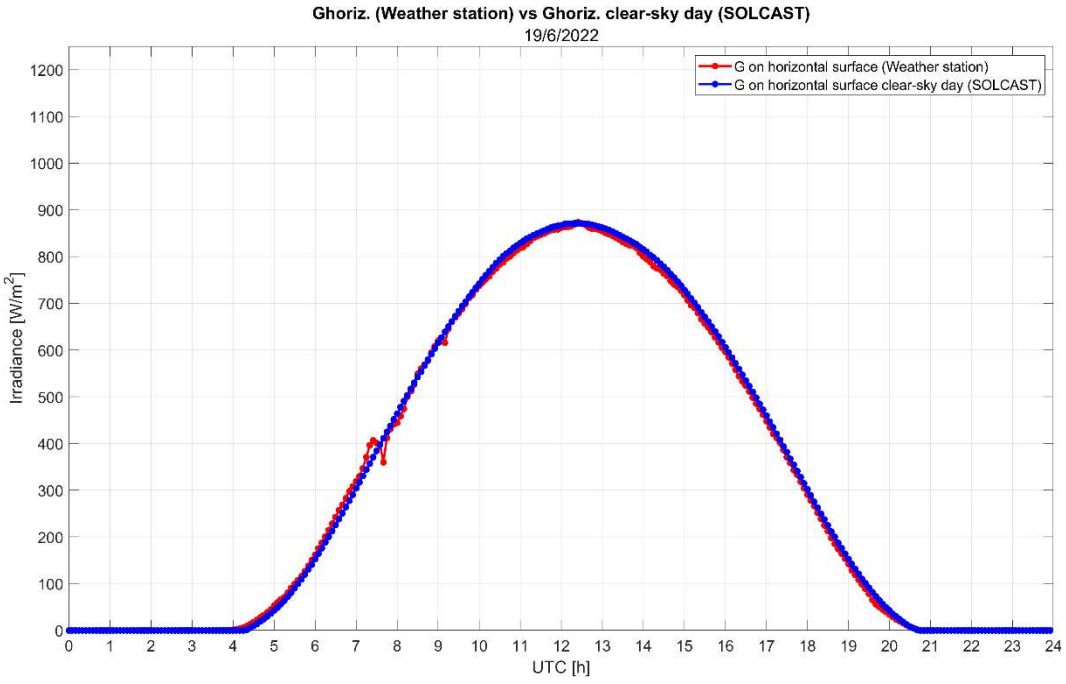

Figure 5-26 - $G_{horizontal}$ (from Włodawa weather station measurement system - red) vs $G_{horizontal}$ (SOLCAST horizontal irradiance source for the Włodawa weather station location - blue) 19/06/2022

As expected for a sunny day, both trends show a bell-shaped curve. By calculating the areas under the two curves through integral calculus and taking the

ratio of the red to the blue area, the K_c value is obtained and it is equal to 0.98, as shown in Figure 5-28.

In Figure 5-27, a similar graph is shown for 4th of June, 2022, a cloudy day.

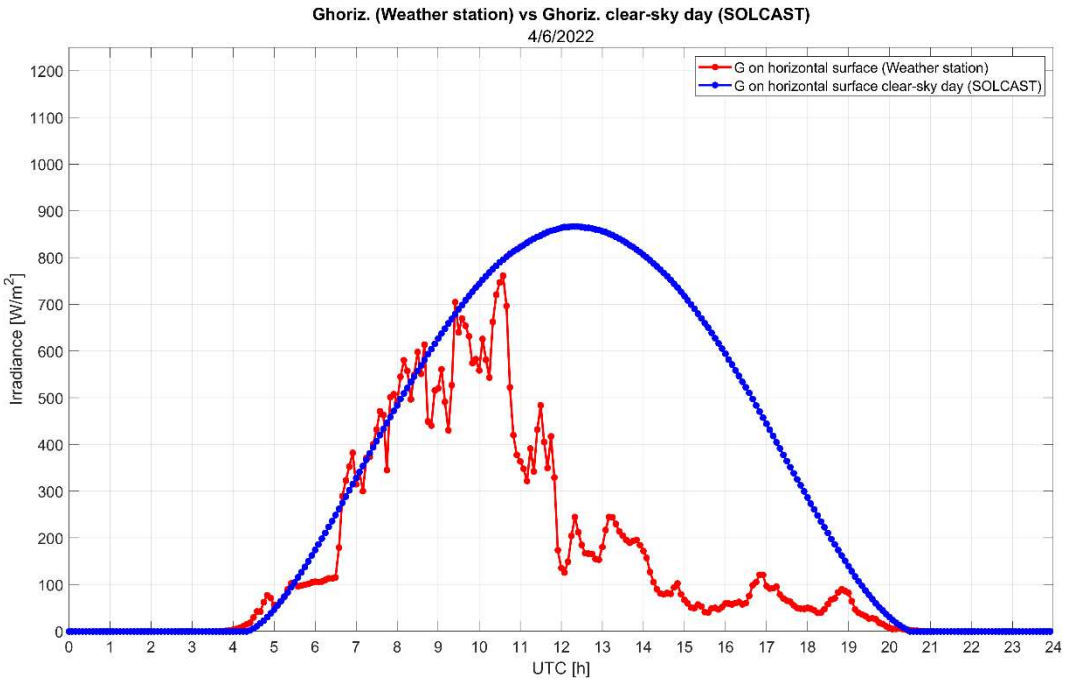

Figure 5-27 - $G_{horizontal}$ (from Włodawa weather station measurement system - red) vs $G_{horizonta}$ (SOLCAST horizontal irradiance source for the Włodawa weather station location - blue) 04/06/2022

The red line, representing the measured irradiance on the horizontal plane, shows low values throughout the day. The K_c value for this day is obtained (0.44) and shown in Figure 5-28.

The two graphs above illustrate examples of a sunny day and a cloudy day. The same calculation was performed for all days in June, except for 21st of June, 2022, which was excluded due to insufficient data. The K_c values for the analyzed days are presented in Figure 5-28.

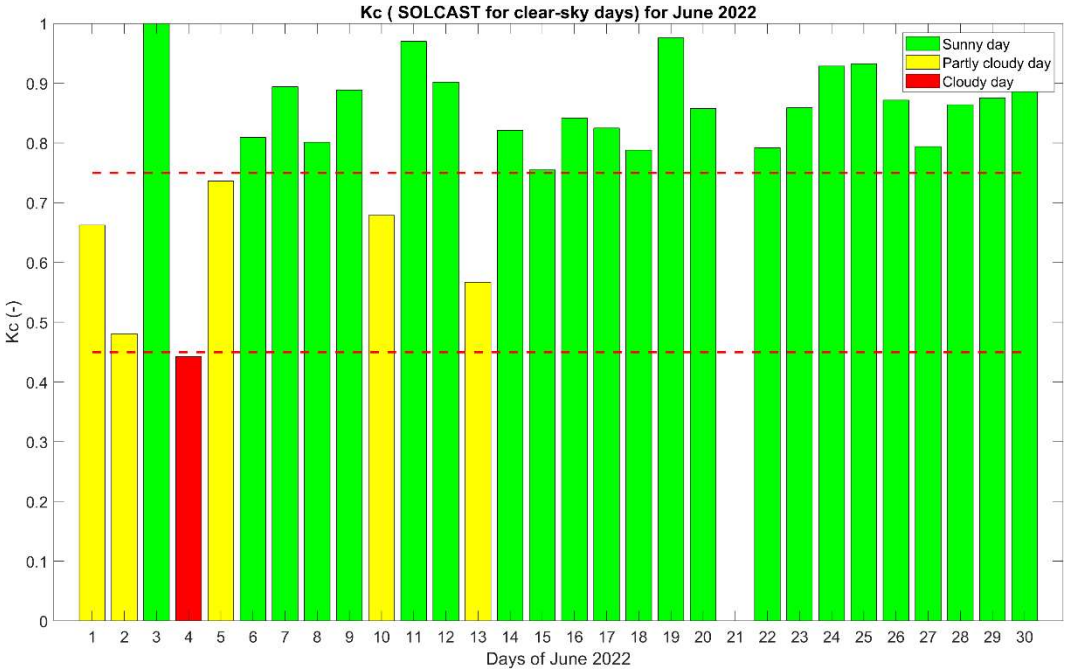

Figure 5-28 - days classification - K_c calculated with $G_{horizonta}$ clear-sky day (SOLCAST horizontal irradiance source for the Włodawa weather station location) for June 2022 – sunny day (green), partly cloudy day (yellow), cloudy day (red)

The histogram shows a mix of sunny, partially cloudy, and cloudy days in June. Specifically, there is 1 cloudy day (red bar), 5 partially cloudy days (yellow bars), and 22 sunny days (green bars). As with the ASHRAE method, care should be taken when analyzing the results due to potential anomalies in the measured irradiance data.

5.3.3 K_c according to PVGIS clear-sky days data results

For this case, data from PVGIS were used to obtain the solar irradiance trends during clear-sky days for June 2022. PVGIS data have a one-hour timestep, representing the average irradiance over this period. Therefore, the measured irradiance data from the pyranometer, initially provided minute-by-minute, were averaged every hour to match this timestep.

In Figure 5-29, the irradiance trends for 19th of June, 2022, a sunny day, are shown. The blue line represents the clear-sky irradiance from PVGIS, and the red line represents the measured irradiance from the pyranometer.

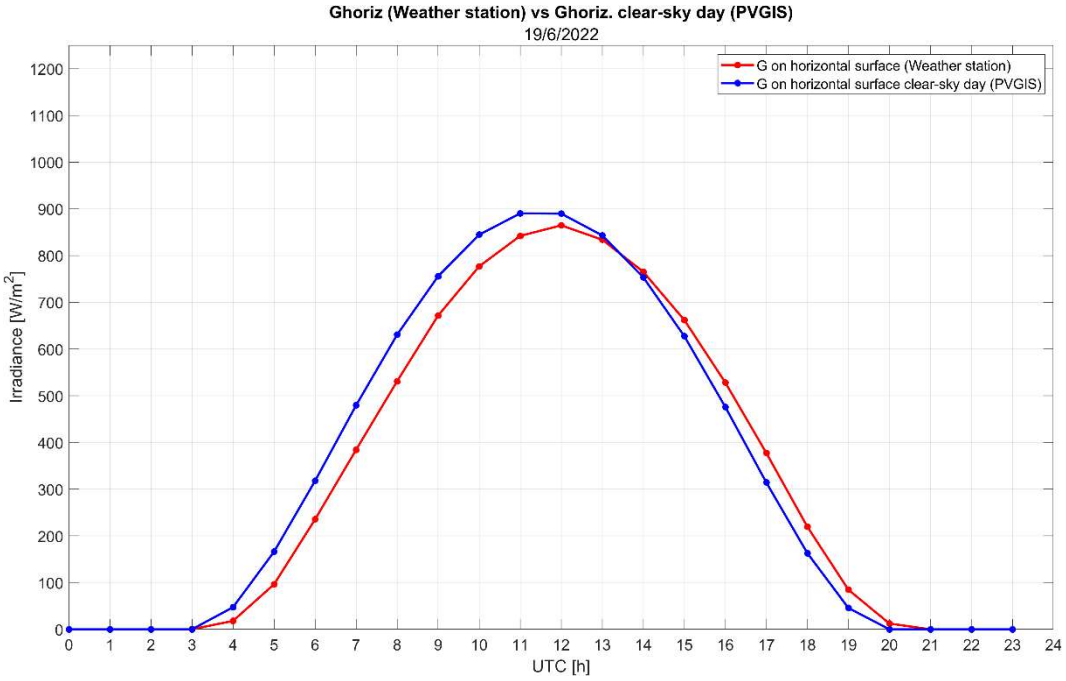

Figure 5-29 - $G_{horizontal}$ (from Włodawa weather station measurement system - red) vs $G_{horizontal}$ (PVGIS horizontal irradiance source for the Włodawa weather station location - blue) 19/06/2022

As expected for a sunny day, both trends show a bell-shaped curve. By calculating the areas under the two curves through integral calculus and taking the ratio of the red to the blue area, the K_c value is obtained and it is equal to 0.9, as shown in Figure 5-31.

In Figure 5-30, a similar graph is shown for 4th of June, 2022, a cloudy day.

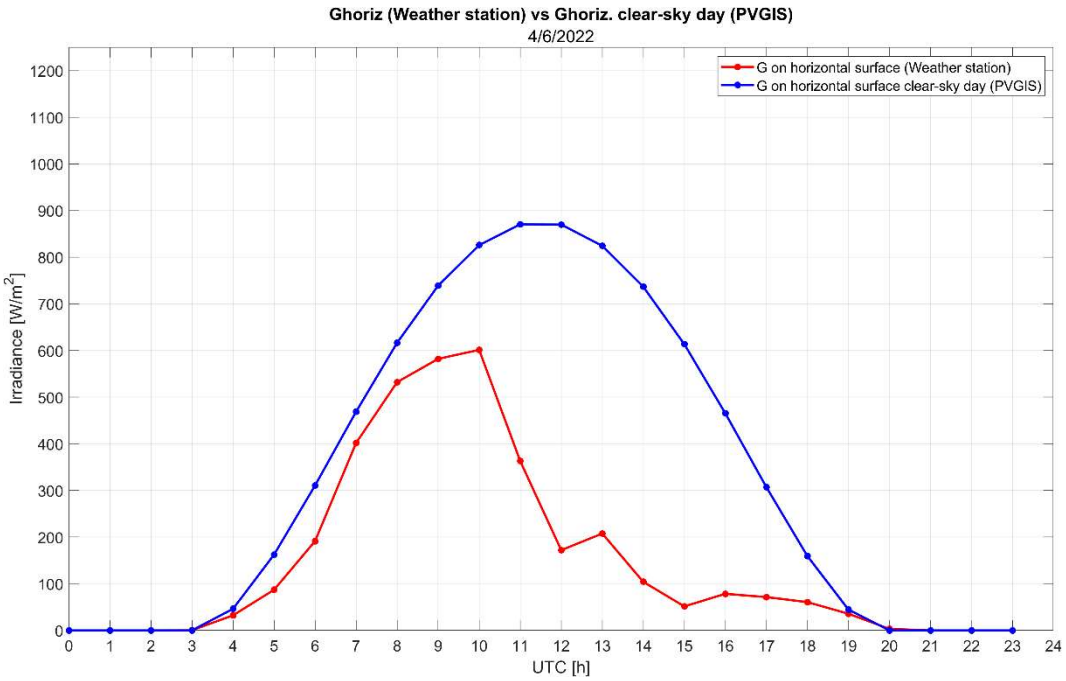

Figure 5-30 - $G_{horizontal}$ (from Włodawa weather station measurement system - red) vs $G_{horizontal}$ (PVGIS horizontal irradiance source for the Włodawa weather station location - blue) 04/06/2022

The red line, representing the measured irradiance on the horizontal plane, shows low values throughout the day. The K_c value for this day is obtained (0.41) similarly and shown in Figure 5-31.

The two graphs above illustrate examples of a sunny day and a cloudy day. The same calculation was performed for all days in June, except for 21st of June, 2022, which was excluded due to insufficient data. The K_c values for the analyzed days are presented in Figure 5-31.

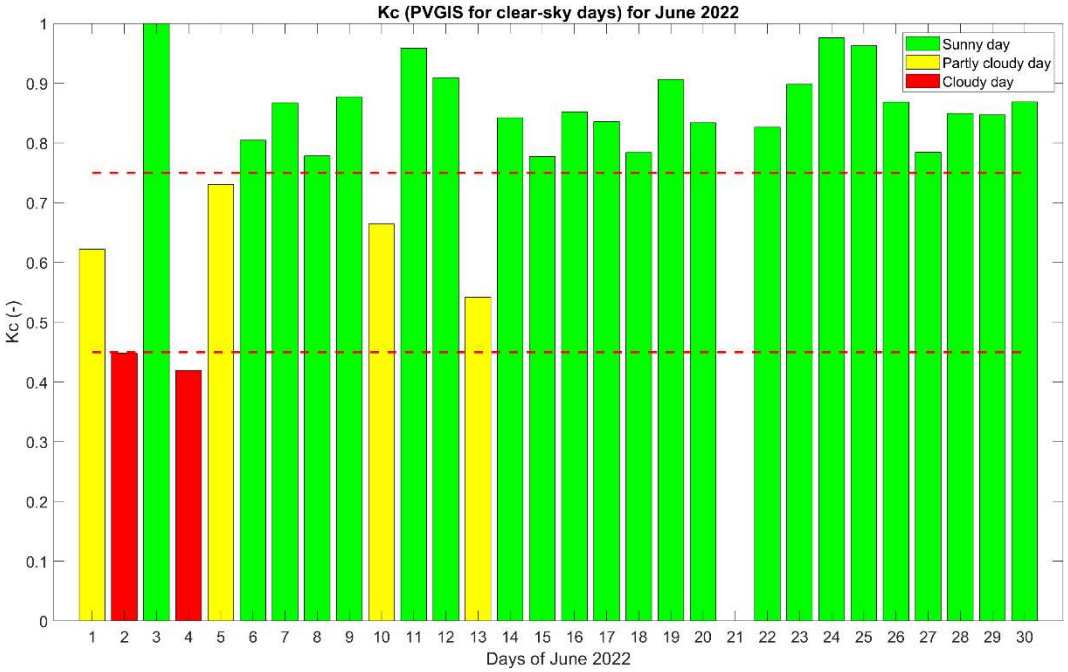

Figure 5-31 - days classification - K_c calculated with $G_{horizonta}$ clear-sky day (PVGIS horizontal irradiance source for the Włodawa weather station location) for June 2022 – sunny day (green), partly cloudy day (yellow), cloudy day (red)

The histogram shows a mix of sunny, partially cloudy, and cloudy days in June. Specifically, there are 2 cloudy days (red bars), 4 partially cloudy days (yellow bars), and 23 sunny days (green bars).

Comparison

Analyzing all three histograms obtained with different models, it is evident that the classification of days is consistent across the models, with minor differences. For instance, the day 2nd of June, 2022, 2022, was classified as partially cloudy in the SOLCAST model but cloudy in the other two models. This discrepancy arises because the SOLCAST clear-sky radiation values are slightly lower, increasing the K_c value.

Ultimately, the model using PVGIS data was chosen for the K_c values in the Olmo model with K_c (illustrated in Section 5.2.2) and for the energy production analysis. Despite minor differences, PVGIS was preferred due to its widespread use in the photovoltaic sector, lending greater reliability to its data.

5.4 Energy production analysis

This section presents the results of the energy production study. Specifically, the focus is on achieving the primary objective of comparing the energy produced by the photovoltaic system with the energy estimated using various models based on data collected from the Włodawa weather station. The aim is to evaluate whether the measured irradiance and air temperature data can, through the application of different models, provide an estimate of energy production that closely aligns with the actual energy measured on the DC side of the plant. The analysis includes a comparison of three distinct energy profiles:

- **Measured energy in the PV plant:** This represents the actual energy measured on the DC side of the inverter for the section of the plant considered in this study.

- **Model A: Estimated energy based on weather station data:** This model uses solar irradiance data measured on a horizontal plane at the weather station. The ASHRAE model (described in Section 4.3.1) is applied to transpose the irradiance onto an inclined plane. Subsequently, the Osterwald model (described in Section 4.5) is used to estimate the energy production by integrating the irradiance data with air temperature measurements from the weather station.

- **Model B: Estimated energy using PV plant data:** This model applies the Osterwald method (detailed in Section 4.5) using solar irradiance measured directly in the plant by the reference cell and cell temperature data. This approach evaluates the deviation between the energy calculated with the Osterwald model based on on-site data and the actual DC-side energy production measured in the plant.

As discussed in Section 5.2.3, after analyzing the ASHRAE model's performance for irradiance transposition across three types of days (cloudy, partially cloudy, and sunny), it was decided to proceed with the energy analysis without separating days by type. This decision was based on the observation that all three types exhibited similar deviations from the solar radiation measured in the plant, and no clear advantage was found in treating sunny days differently. Consequently, the study includes all days in June 2022, except June 21, 2022, which was excluded due to significant data gaps.

In Figure 5-32, the three energy profiles are compared. The x-axis represents the days in the selected period, while the y-axis indicates the energy produced [Wh]. For each day, three bars are displayed: the first (green) represents Model A, the second (blue) corresponds to the actual measured energy in the plant, and the third (light blue) depicts Model B.

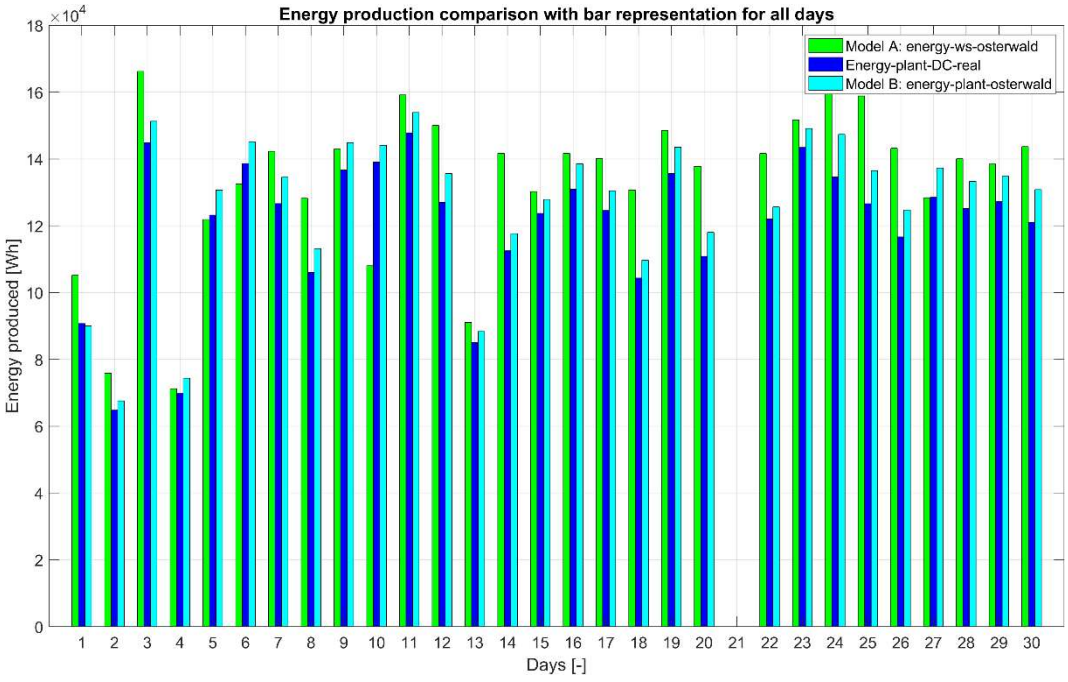

Figure 5-32 – Energy production comparison with bar-representation for all days – Measured energy in the PV plant (blue bar) - Model A: Estimated energy based on weather station data (green bar) - Model B: Estimated energy using PV plant data (light blue bar)

As shown in Figure 5-32, Model A (green bar)—which calculates energy production based on data from the Włodawa weather station—tends to overestimate the energy produced compared to the actual measured energy (blue bar) for most days. A similar trend is observed for Model B (light blue bar), although the magnitude of overestimation appears smaller on average than for Model A.

To further analyze the accuracy of the models, deviations between the modeled and measured energy were quantified. The Mean Absolute Percentage Error

(MAPE) and Mean Absolute Error (MAE) were calculated with respect to the actual measured energy (blue bar). For a detailed explanation of the calculation of MAE and MAPE, refer to Section 5.2.3. Table 5-2 summarizes the results.

	MAE (kWh)	MAPE (%)
MODEL A	17.25	14.07
MODEL B	7.33	5.81

Table 5-2 - MAE & MAPE for different models

From Table 5-2, it is evident that Model A has a significantly higher deviation, with an MAE of 17.25 kWh and a MAPE of 14.07%. In contrast, Model B shows a much smaller deviation, with an MAE of 7.33 kWh and a MAPE of 5.81%.

The MAPE of 5.81% for Model B suggests that even when using the Osterwald model with on-site irradiance and cell temperature data, discrepancies remain due to factors not accounted for by the model. These may include shading on parts of the panel array, dirt accumulation, and other environmental or system-specific inefficiencies. The primary objective of this thesis was to evaluate the feasibility of using data from the Włodawa weather station to estimate energy production reliably. The MAPE of 14.07% for Model A indicates a significant deviation, suggesting that these estimates are not sufficiently accurate for performance monitoring or as a reliable comparison metric without adjustments.

Given that Model A consistently overestimates energy production compared to the actual measured values, a corrective factor was introduced. The correction was derived by calculating the daily ratio of energy estimated by Model A (green bar) to the actual measured energy (blue bar). The arithmetic mean of these ratios across all days yielded a corrective factor of 1.115. This indicates that, on average, Model A overestimates energy production by 11.5%. By dividing the daily energy estimates of Model A by this factor, adjusted daily energy values were obtained. After applying the correction, the MAPE for Model A was recalculated, yielding a value of 7.31%. When compared to the MAPE of 5.81% for Model B, the corrected Model A results show a comparable level of deviation, suggesting that the adjusted

estimates can serve as a reasonable approximation of energy production, albeit with limitations.

Without the correction factor, the use of Model A for estimating energy production is not recommended due to the high deviation from actual values. However, applying the correction factor provides an acceptable level of accuracy for monthly energy estimates. It is important to note that while this approach improves the reliability of Model A, the inherent limitations of the Osterwald model and the quality of input data must be considered, and the corrected estimates should not be used for precise day-to-day energy performance assessments.

Chapter 6

6 Conclusion

The primary aim of this study was to develop an alternative method for evaluating whether the energy production of the PV plant aligns with predictions based on solar irradiance and temperature conditions. Data from the PV plant and a nearby weather station in Włodawa, 44.8 km away, were analyzed and compared. Additional datasets from PVGIS and SOLCAST were incorporated to fill data gaps and facilitate comparisons. This study was divided into two main analyses. The first one involved studying various models to obtain solar irradiance on an inclined plane. The second analysis focused on using these models to predict energy production and compare it with actual production data.

Given that the pyranometer at the weather station in Włodawa measures irradiance on a horizontal plane while the PV panels are inclined at 34°, models were applied to transpose irradiance data from the horizontal to the inclined plane to make these data comparable. Three models were evaluated for this transposition: the ASHRAE model, and two Olmo models (using K_t 'clearness index' and K_c 'clear sky index'). After analyzing the results obtained, as shown in Chapter 5, it was established that the ASHRAE model was the most effective for this purpose. In contrast, the two Olmo models produced significantly poorer transposition results and were therefore excluded from subsequent studies.

During the analysis of radiation conducted in Chapter 5.2.3, the goal of the calculation was to compare the radiation determined using irradiance transposition models with the actual radiation measured by the photovoltaic system on an inclined plane. Mean Absolute Error (MAE) and Mean Absolute Percentage Error (MAPE) metrics indicated that Model 1 and Model 2, which integrate irradiance on the inclined plane using data provided by SOLCAST (Model 1 through the transposition of horizontal irradiance via the ASHRAE model, and Model 2 using SOLCAST's inclined irradiance data for a 34° inclined plane), performed better than Model 3. The latter calculates radiation by integrating irradiance on the inclined plane obtained by applying the ASHRAE model to horizontal irradiance

data measured by the Włodawa weather station. This is significant as the primary aim of the study was to assess the feasibility of using weather station data to predict energy production and provide feedback on system performance. For Model 3, it was observed that MAPE values were high across all days, regardless of weather conditions, including cloudy, partially cloudy, and sunny days. This confirms that the primary issue lies in the measurement of horizontal irradiance by the pyranometer at the Włodawa weather station. Therefore, implementing the corrective actions described earlier for this location would be beneficial to improve measurement accuracy.

Additionally, the classification of days into sunny, partially cloudy, and cloudy was analyzed. This classification was carried out to evaluate whether the different models applied exhibited varying performance depending on the type of day. In such a case, different procedures could have been implemented for the final energy production analysis. Using the K_c index and data from three different sources (ASHRAE method, SOLCAST, and PVGIS for determining the $G_{clear-sk}$ value used in its calculation), days were categorized. The PVGIS model was selected to perform the final classification of the types of days due to its established reliability in the photovoltaic sector.

One of the primary objectives of the first part of this thesis was to assess whether irradiance data measured by the weather station in Włodawa, when processed through specific models, could be used for comparing and monitoring the actual energy production of the PV plant. The analysis revealed that the irradiance data measured on the horizontal plane by the weather station's pyranometer show some discrepancies on certain days. As shown in the graphs in Chapter 5, on cloudy and partially cloudy days, the irradiance data showed peaks that exceeded the maximum expected values for the Włodawa location. Given that the area is subject to frequent snowfalls, it was initially considered that snow might be causing measurement inaccuracies. However, since the analyzed month was June, a summer month with no snow, the issue was attributed to the pyranometer's malfunction. Proper maintenance, such as cleaning the sensors, or in extreme cases, replacing the pyranometer, is recommended.

Furthermore, it was considered that the significant distance of approximately 44.8 km between the weather station in Włodawa and the PV plant in Bordziłówka could potentially introduce discrepancies due to varying meteorological conditions at these locations. It was noted that such distance might result in noticeable

differences in irradiance measurements, as the meteorological conditions may vary between the two sites. To enhance the accuracy of future analyses, establishing a closer weather station or installing a new one near the PV plant would be advantageous.

The analysis of irradiance data on the inclined plane, measured by the monocrystalline silicon reference cell at the PV plant, also indicated some measurement irregularities on cloudy and partially cloudy days. The data occasionally showed peaks in irradiance that exceeded the expected maximum values, similar to the readings from the weather station. To ensure sustained accuracy in long-term energy production analysis, it is advisable to consider the maintenance or replacement of these sensors.

In the final part of the thesis, the focus was on comparing the energy produced by the photovoltaic system with the energy estimated using various models based on data from the Włodawa weather station. The goal was to determine whether irradiance and air temperature data could, through different models, provide an estimate of energy production that closely matched the actual energy measured on the DC side of the plant.

After analyzing the ASHRAE model's performance for irradiance transposition across cloudy, partially cloudy, and sunny days, it was decided to proceed with the energy analysis without separating days by type. This was because all day types showed similar deviations from the measured solar radiation at the plant, and no clear benefit was found in treating sunny days differently.

Model A (estimated energy based on weather station data) was compared to the actual energy produced and measured at the photovoltaic plant. The energy production for each day of the considered period was estimated using the Osterwald method with irradiance and air temperature data from the weather station. The MAE and MAPE were calculated to measure deviations from actual values. The MAPE for Model A was 14.07%, indicating significant inaccuracy for performance monitoring without adjustments. Since Model A consistently overestimated energy production, a corrective factor was applied, derived by calculating the daily ratio of estimated to measured energy. This factor was used to adjust the daily energy estimates.

After applying the correction, the MAPE for Model A decreased to 7.31%. Compared to Model B (energy estimated using PV plant data), which recorded a MAPE of 5.81%, the corrected Model A results showed a similar level of deviation. The MAPE of 5.81% for Model B highlights that even when using the Osterwald model with on-site irradiance and cell temperature data, discrepancies persist. These deviations can be attributed to factors not accounted for by the model, such as shading on parts of the panel array, dirt accumulation, and other environmental or system-specific inefficiencies, which can influence the accuracy of the estimated energy production. This makes the corrected estimates a viable solution for approximating energy production on a monthly basis, though they still have some limitations.

While the corrective factor improves the accuracy of Model A for monthly estimates, it is important to note that, due to the inherent limitations of the Osterwald model and the quality of input data, these estimates are not suitable for precise day-to-day energy performance assessments. However, on a monthly scale, they represent a feasible option.

7 References

[1] "Standard solar spectrum. | Download Scientific Diagram." https://www.researchgate.net/figure/Standard-solar-spectrum_fig2_280041456 (accessed Jun. 18, 2024).

[2] "PVEducation." https://www.pveducation.org/ (accessed Jun. 18, 2024).

[3] "Air-Mass-(AM)-bei-einem-Einfallswinkel-von-90°-und-41-8°_en.png (442×312)." https://www.itwissen.info/lex-images/Air-Mass-(AM)-bei-einem-Einfallswinkel-von-90°-und-41-8°_en.png (accessed Jun. 18, 2024).

[4] "AZIMUTH.gif (401×383)." https://www.pveducation.org/sites/default/files/PVCDROM/Properties-of-Sunlight/Images/AZIMUTH.gif (accessed Jun. 18, 2024).

[5] "electrons - What is energy band gap? - Physics Stack Exchange." https://physics.stackexchange.com/questions/467901/what-is-energy-band-gap (accessed Mar. 18, 2024).

[6] F. Spertino, "State of the art in photovoltaics," *(Politecnico di Torino Dip. di energia)*, 2017.

[7] "diode1.gif (450×254)." https://www.electronics-tutorials.ws/wp-content/uploads/2013/08/diode1.gif (accessed Jun. 18, 2024).

[8] F. Spertino, "F. Spertino PHOTOVOLTAIC POWER SYSTEMS Photovoltaic Power Systems," 2016.

[9] "Diode Physics." https://www.mks.com/n/diode-physics (accessed Jun. 18, 2024).

[10] "What is solar PV I-V curve tracing? | Solar FAQ's | Seaward." https://www.seaward.com/gb/support/solar/faqs/84179-what-is-solar-pv-i-v-curve-tracing/ (accessed Jun. 18, 2024).

[11] A. Calcabrini *et al.*, "Low-breakdown-voltage solar cells for shading-tolerant photovoltaic modules," *Cell Reports Phys. Sci.*, vol. 3, no. 12, p. 101155, 2022, doi: 10.1016/j.xcrp.2022.101155.

[12] LONGi, "LR5-72HBD 520-540M technical data sheet." [Online]. Available: https://www.ecorienergiasolar.com.br/assets/uploads/969be-4-18x-lr5-72hbd-520-540m-draft-v03.pdf.

[13] F. Spertino, “Series / Parallel Connections : Mismatch of Current-Voltage Characteristics and Shading Effect.”

[14] “structure_of_photovoltaic_module_2017.jpg (1830×1007).” https://ecoprogetti.com/wp-content/uploads/2017/02/structure_of_photovoltaic_module_2017.jpg (accessed Jun. 18, 2024).

[15] “Solar plant design guide: the basics - PVcase.” https://pvcase.com/blog/solar-plant-design-guide-the-basics/ (accessed Jun. 18, 2024).

[16] “Solar.” https://metapowersolutions.com/applications/solar/ (accessed Jun. 18, 2024).

[17] “Solar Combiner Box Introduction and Why Do You Need It.” https://igoyeenergy.com/what-is-a-solar-combiner-box/ (accessed Jun. 18, 2024).

[18] H. Yield and S. Investment, “SG3125HV-MV-30,” 2022.

[19] “Solar Power Inverters and EMI Filtering Elexana LLC.” https://www.elexana.com/solar-power-inverters-emi-filtering (accessed Jun. 18, 2024).

[20] D. S. Pillai and N. Rajasekar, “A comprehensive review on protection challenges and fault diagnosis in PV systems,” *Renew. Sustain. Energy Rev.*, vol. 91, no. July 2017, pp. 18–40, 2018, doi: 10.1016/j.rser.2018.03.082.

[21] P. C. Dongiovanni, “Data Acquisition Systems,” *Int. Geophys.*, vol. 9, no. C, pp. 23–56, 1966, doi: 10.1016/S0074-6142(08)60313-7.

[22] M. Ş. Kalay, B. Kılıç, and Ş. Sağlam, “Systematic review of the data acquisition and monitoring systems of photovoltaic panels and arrays,” *Sol. Energy*, vol. 244, no. February, pp. 47–64, 2022, doi: 10.1016/j.solener.2022.08.029.

[23] P. C. Dongiovanni, “Energy Systems Lab (Temperature Measurement),” 2020.

[24] E. ADIGÜZEL, K. GÜRKAN, and A. ERSOY, “Design and development of data acquisition system (DAS) for panel characterization in PV energy systems,” *Meas. J. Int. Meas. Confed.*, vol. 221, no. July, 2023, doi: 10.1016/j.measurement.2023.113425.

[25] F. Spertino, “Assessment of Energy Production from a Photovoltaic System.”

[26] F. Almonacid, C. Rus, P. Pérez-Higueras, and L. Hontoria, “Calculation of

the energy provided by a PV generator. Comparative study: Conventional methods vs. artificial neural networks," *Energy*, vol. 36, no. 1, pp. 375–384, 2011, doi: 10.1016/j.energy.2010.10.028.

[27] F. Spertino, S. Fichera, A. Ciocia, G. Malgaroli, P. Di Leo, and A. Ratclif, "Toward the complete self-sufficiency of an NZEBS microgrid by photovoltaic generators and heat pumps: Methods and applications," *IEEE Trans. Ind. Appl.*, vol. 55, no. 6, pp. 7028–7040, 2019, doi: 10.1109/TIA.2019.2914418.

[28] F. Spertino *et al.*, "Maintenance Activity , Reliability , Availability , and Related Energy Losses in Ten Operating Photovoltaic Systems up to 1 . 8 MW," vol. 57, no. 1, pp. 83–93, 2021, doi: 10.1109/TIA.2020.3031547.

[29] G.V. Fracastoro and M. Perino *et al.*, "Solar angles", *(Politecnico di Torino Dip. di energia).*

[30] "https://ars.els-cdn.com/content/image/3-s2.0-B9780128121498000028-f02-02-9780128121498.jpg" https://www.sciencedirect.com/topics/engineering/solar-altitude-angle (accessed Jun. 18, 2024).

[31] G.V. Fracastoro and M. Perino *et al.*, "Solar radiation", *(Politecnico di Torino Dip. di energia).*

[32] SamyA.Khalil, A.M.Shaffie, "A comparative study of total, direct and diffuse solar irradiance by using different models on horizontal and inclined surfaces for Cairo, Egypt" Renewable and Sustainable Energy Reviews 27 (2013) 853–863.

[33] Higor Miguel,Leticia Colombi Gomes,Cesar Turczyn Campos, Pablo Rodrigues Muniz, "ESTIMATION OF DAILY ENERGY GAIN OF SOLAR TRACKING SURFACES BASED ON GEOGRAPHIC POSITION", ISSN 2359-4799,Volume 7 / Número 1 / Ano 2021 – p. 01-14,DOI: 10.36524/ric.v7i1.940.

[34] Slawomir Gulkowski, "Modeling and Experimental Studies of the Photovoltaic System Performance in Climate Conditions of Poland", Energies 2023, 16(20), 7017; https://doi.org/10.3390/en16207017.

[35] Slawomir Gulkowski, Agata Zdyb, "Performance Assessment of Four Different Photovoltaic Technologies in Poland", Energies 2020, 13(1), 196; https://doi.org/10.3390/en13010196.

8 Appendix

ReneSola

156 Series Polycrystalline Solar Module

250W, 255W, 260W

Dimensions

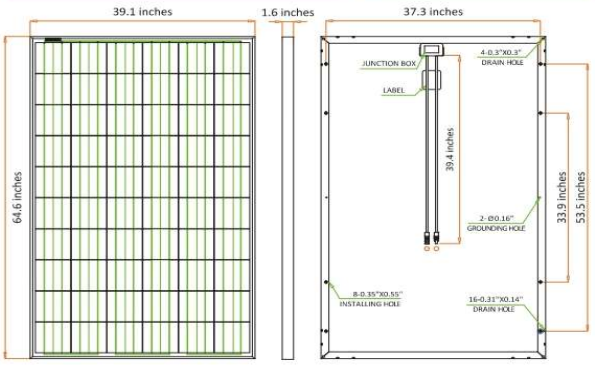

Drawing Only for Reference

I-V Curves

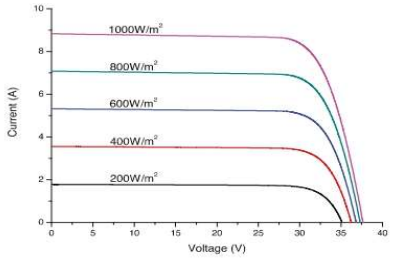

Varied Irradiation Efficiencies

Irradiance	200W/m²	400W/m²	600W/m²	800W/m²	1000W/m²
Efficiency	15.8%	16.2%	16.2%	16.1%	16.0%

Electrical Characteristics STC	JC250M-24/Bb	JC255M-24/Bb	JC260M-24/Bb
Maximum Power (Pmax)	250 W	255 W	260 W
Power Tolerance	0 ~ +5W	0 ~ +5W	0 ~ +5W
Module Efficiency	15.4%	15.7%	16.0%
Maximum Power Current (Imp)	8.31 A	8.39 A	8.53 A
Maximum Power Voltage (Vmp)	30.1 V	30.4 V	30.5 V
Short Circuit Current (Isc)	8.83 A	8.86 A	8.95 A
Open Circuit Voltage (Voc)	37.4 V	37.5 V	37.6 V

Values at Standard Test Conditions STC (Air Mass AM1.5, Irradiance 1000W/m² , Cell Temperature 25°C)

Electrical Characteristics NOCT	JC250M-24/Bb	JC255M-24/Bb	JC260M-24/Bb
Maximum Power (Pmax)	185 W	189 W	193 W
Maximum Power Current (Imp)	6.57 A	6.63 A	6.74 A
Maximum Power Voltage (Vmp)	28.2 V	28.5 V	28.6 V
Short Circuit Current (Isc)	7.12 A	7.20 A	7.27 A
Open Circuit Voltage (Voc)	35.0 V	35.1 V	35.2 V

Values at Normal Operating Cell Temperature, Irradiance of 800 W/m² , spectrum AM 1.5, ambient temperature 20°C, wind speed 1 m/s

Mechanical Characteristics

Cell Type	156 x156 mm Polycrystalline, 60 (6x10) pcs in series
Glass	High Transmission, Low Iron, Tempered Glass
Frame	Anodized Aluminum Alloy
Junction Box	IP65/IP67 rated, with bypass diodes
Dimension	*64.6 x 39.1 x 1.6 inches
Output Cable	12 AWG, 39.4 inches
Weight	41.9 lbs
Installation Hole Location	See Drawing Above

Characteristics

Temperature Coefficient of Voc	-0.30%/°C
Temperature Coefficient of Isc	0.04%/°C
Temperature Coefficient of Pmax	-0.40%/°C
Nominal Operating Cell Temperature (NOCT)	45°C±2°C

Packing Information

Container	20' GP	40' GP	40' HQ
Pallets per Container	12	28	28
Pieces per Container	300	700	770

Maximum Ratings

Operating Temperature	-40°F ~ + 185°F
Maximum System Voltage	1000VDC (EU) / 600VDC (US)
Maximum Series Fuse Rating	20A (EU) / 20A (US)

Rev No: JC/TDS/2013.02 *Contact Renesola for tolerance specification

CAUTION: All rights reserved. Design and specification are subject to change without prior notice.

Figure 8-1 - Renesola JC250M-24/Bb - polycrystalline silicon modules

20 kW transformerless solar inverters

Technical data SOLIVIA 20 TL

INPUT (DC)	SOLIVIA 20 EU G3 TL
Max. recommended PV power	25 kW_p
Nominal power	20.4 kW
Voltage range	250 ... 1000 V
Full power MPP range	350 ... 800 V
Max. current	60 A (30 A per MPP)
Max. number of MPP trackers	2

OUTPUT (AC)	
Nominal power	20 kW
Voltage range	3 x 400 V (± 20 %) (3 phases, 3 wires) [1]
Nominal current	29 A (per phase)
Nominal frequency	50 / 60 Hz
Frequency range	50 Hz: 47 ... 53 Hz; 60 Hz: 57 ... 63 Hz [1]
Power factor	> 0.99 @ nominal power
Total harmonic distortion (THD)	< 3 % @ nominal power

GENERAL SPECIFICATION	
Model name	SOLIVIA 20 EU G3 TL [2]
Part number Delta	EOE48010224
Max. efficiency	98.1 %
Efficiency EU	> 97.5 %
Operating temperature	-20 ... +60 °C
Full power without derating	-20 ... +40 °C
Storage temperature	-20 ... +80 °C
Humidity	0 ... 90 %
Max. operating altitude	2000 m (above sea level)

MECHANICAL DESIGN	
Size (L x W x D)	952 x 624.7 x 278 mm
Weight	65 kg
Cooling	Fan
AC connector	Amphenol C16/3
DC connector	4 pairs of Multi-Contact MC4
Communication interfaces	2 x RJ45 / RS485
DC disconnector	Integrated
Display	Black/white graphical LCD

STANDARDS / DIRECTIVES	SOLIVIA 20 EU G3 TL
Protection degree	IP65 / IP54 [3]
Safety class	I
Configurable trip parameters	Yes
Insulation monitoring	Yes
Overload behavior	Current limitation; power limitation
Anti-islanding protection / Grid regulation	DIN VDE 0126-1-1; RD 661/2007; UTE C15-712-1; EN 50438
EMC	EN61000-6-2; EN61000-6-3; EN61000-3-11; EN61000-3-12
Safety	EN 60950-1; EN 50178; IEC 62103; IEC 62109-1 / -2

1) AC voltage and frequency range will be programmed according to the individual country requirements.
2) An overview of our inverters that can be installed in your country can be found on our website www.solar-inverter.com.
3) IP65 for electronics / IP54 for cooling area

United Kingdom
Email: sales.uk@solar-inverter.com
Tel: 0800 051 4280 (Free Call)

International
Email: sales.europe@solar-inverter.com
Tel: +49 7641 455 547

Figure 8-2 – Delta SOLIVIA 20 TL – Solar inverter

3300 Watt solar inverters

Technical data SOLIVIA 3.3 TR

INPUT (DC)	SOLIVIA 3.3 EU G3 TR
Max. recommended PV power	4000 W_P
Nominal power	3630 W
Voltage range	125 ... 540 V
Full power MPP range	150 ... 450 V
Nominal current	13.3 A
Max. current	24 A

OUTPUT (AC)	
Nominal power	3300 W
Voltage range	184 ... 264 V [1]
Nominal current	14.4 A
Nominal frequency	50 Hz
Frequency range	47 ... 52 Hz [1]
Power factor	> 0.99 @ nominal power
Total harmonic distortion (THD)	< 3 % @ nominal power

GENERAL SPECIFICATION	
Model name	SOLIVIA 3.3 EU G3 TR [2]
Part number Delta	EOE46010190
Max. efficiency	96 %
Efficiency EU	94.8 %
Operating temperature	-25 ... +70 °C
Full power without derating	-25 ... +55 °C
Storage temperature	-25 ... +80 °C
Humidity	0 ... 98 %
Max. operating altitude	2000 m (above sea level)

MECHANICAL DESIGN	
Size (L x W x D)	410 x 410 x 180 mm
Weight	21.5 kg
Cooling	Convection
AC connector	Wieland RST25i3S
DC connector	3 pairs of Tyco Solarlok
Communication interfaces	2 x RJ45 / RS485
DC disconnector	Integrated
Display	3 LEDs, 2-line LCD

STANDARDS / DIRECTIVES	SOLIVIA 3.3 EU G3 TR
Protection degree	IP65
Safety class	I
Configurable trip parameters	Yes
Insulation monitoring	Yes
Overload behavior	Current limitation; power limitation
Anti-islanding protection / Grid regulation	DIN VDE 0126-1-1; UTE C15-712-1; France/Islands (60 Hz); RD 661/2007; EN 50438; G83/1-1; VDE-AR-N 4105
EMC	EN61000-6-2; EN61000-6-3; EN61000-3-2; EN61000-3-3
Safety	EN60950-1; EN50178; IEC62103; IEC62109-1 / -2

1) AC voltage and frequency range will be programmed according to the individual country requirements.
2) An overview of our inverters that can be installed in your country can be found on our website www.solar-inverter.com.

United Kingdom
Email: sales.uk@solar-inverter.com
Tel: 0800 051 4280 (Free Call)

International
Email: sales.europe@solar-inverter.com
Tel: +49 7641 455 547

Figure 8-3 - Delta SOLIVIA 3.3 Tr – Solar inverter

Technical Specifications

	CMP3	SMP3
Classification to ISO 9060:2018	Spectrally Flat Class C	Spectrally Flat Class C
Sensitivity	24 to 32 µV/W/m²	-
Impedance	80 to 140 Ω	-
Expected output range (0 to 1500 W/m²)	0 to 48 mV	-
Maximum operational irradiance	2000 W/m²	2000 W/m²
Analogue output • V-version	-	0 to 1 V
Analogue output range • V-version*	-	-200 to 2000 W/m²
Analogue output • A-version	-	4 to 20 mA
Analogue output range • A-version*	-	0 to 1600 W/m²
Serial output	-	RS-485 Modbus® RTU
Serial output range	-	-400 to 2000 W/m²
Response time (63 %)	< 6 s	< 1.5 s
Response time (95 %)	< 20 s	< 12 s
Spectral range (20 % points)	285 to 3000 nm	285 to 3000 nm
Spectral range (50 % points)	300 to 2800 nm	300 to 2800 nm
Zero offsets (unventilated)		
(a) thermal radiation (at 200 W/m²)	< ±15 W/m²	< ±15 W/m²
(b) temperature change (5 K/h)	< ±5 W/m²	< ±5 W/m²
Non-stability (change/year)	< ±1%	< ±1%
Non-linearity (100 to 1000 W/m²)	< ±3%	< ±3%
Directional response (up to 80° with 1000 W/m² beam)	< ±20 W/m²	< ±20 W/m²
Spectral selectivity (350 to 1500 nm)	< ±3%	< ±3%
Tilt response (0° to 180° at 1000 W/m²)	< ±1.5%	< ±1.5%
Temperature response	< ±4% (-10 °C to +40 °C)	< ±3% (-20 °C to +50 °C) < ±4% (-40 °C to +70 °C)
Field of view	180°	180°
Accuracy of bubble level	< ±0.2°	< ±0.2°
Power consumption (at 12 VDC)	-	V-version: 55 mW A-version: 100 mW
Supply voltage	-	5 to 30 VDC
Software, Windows™	-	SmartExplorer Software, for configuration, test and data logging
Detector type	Thermopile	Thermopile
Operating temperature range	-40 °C to +80 °C	-40 °C to +70 °C
Storage temperature range	-40 °C to +80 °C	-40 °C to +80 °C
Humidity range	0 to 100%	0 to 100%
MTBF (Mean Time Between Failures)	> 10 years	> 10 years
Ingress Protection (IP) rating	67	67
Recommended applications	Economical solution for routine measurements in weather stations, field testing, agriculture, horticulture and hydrology	Economical solution for efficiency and maintenance monitoring of PV power installations, routine measurements in weather stations

** adjustable with SmartExplorer Software | Note: The performance specifications quoted are worst-case and/or maximum values*

Dimensions

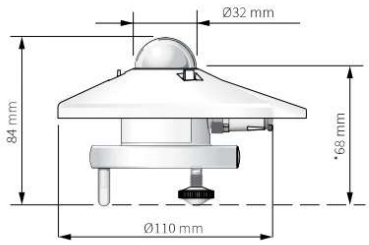

Figure 8-4 - Kipp and zonen cmp3 - Pyranometer